Ph.D. Thesis Dissertation

Experimental estimation of soil emissivity and its application to soil moisture retrieval in the SMOS mission

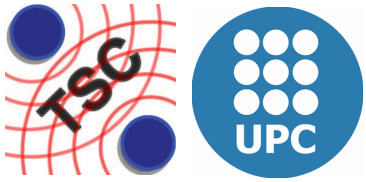

Alessandra Monerris i Belda

Remote Sensing Laboratory
Dept. Teoria del Senyal i Comunicacions
Universitat Politècnica de Catalunya

Ph.D. Thesis advisors

Dr. Adriano J. Camps Carmona & Dr. Mercè Vall-llossera Ferran

Barcelona, June 2009

Chapter 4

Field experiments over land

Emissivity of land surfaces depends upon the interaction of several soil and vegetation characteristics such as soil moisture, roughness, temperature, and topography, and vegetation optical thickness and albedo. This chapter describes the field campaigns over land carried out by the UPC as part of the SMOS pre-launch research activities. Field experiments have been carried out over vineyards (SMOS REFLEX), different types of flat bare smooth soils (MOUSE), fields with different plough but the same soil type (T-REX), and mountainous sites (TuRTLE) thus the impact of many of the parameters involved in land emission could be assessed. Measurements were done using the UPC L-band Automatic Radiometer (LAURA).

4.1 The L-band AUtomatic RAdiometer (LAURA)

Few L-band radiometers existed when the SMOS mission was selected by ESA in May 1999, among them the Passive-Active L- and S-band microwave sensor (PALS) Wilson *et al.* [2001] from JPL, and the L-band radiometer from the University of Massachusetts. The approval of SMOS promoted the development of other radiometers such as ELBARA [Mätzler *et al.*, 2003], LEWIS [Lemaître *et al.*, 2004], and LAURA [Camps *et al.*, 2001, Villarino, 2004], which were to be used in SMOS preparatory science campaigns.

The L-band AUtomatic RAdiometer (LAURA) was designed and implemented by the Remote Sensing Laboratory from the Universitat Politècnica de Catalunya (UPC) in 2000. A picture of the instrument is shown in Fig. 4.1(a). Since then, LAURA has been used in experiments over sea water such as WISE 2000/2001 [Camps *et al.*, 2004], FROG 2003 [Camps *et al.*, 2005a], and ALBATROSS 2008/2009, and in land field campaigns which are presented in the next sections, and which have provided the experimental data used in this Thesis. LAURA's main characteristics and the updates carried out during these years are presented in hereafter.

4.1.1 The instrument

LAURA is a fully-polarimetric radiometer working at a frequency of 1.4135 GHz, the same as SMOS' payload MIRAS. The instrument is composed of two Dicke radiometers, one for the

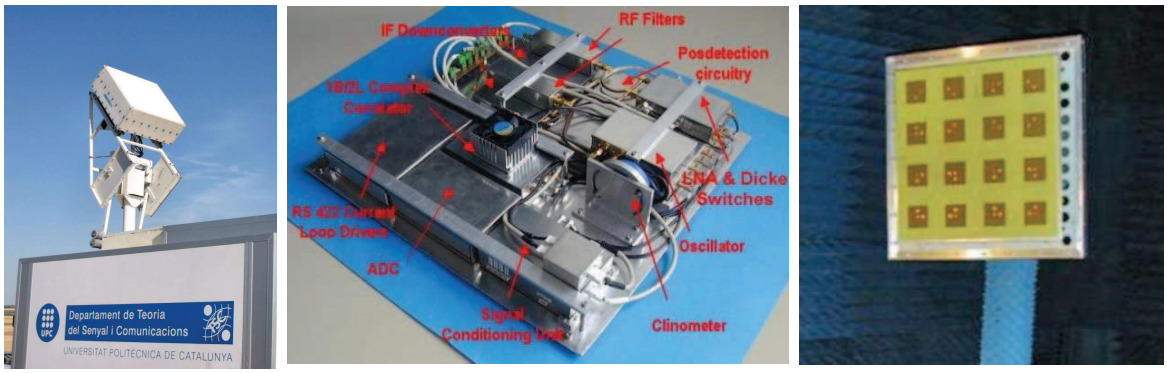

(a) (b) (c)

Fig. 4.1: (a) View of the fully-polarimetric L-band AUtomatic RAdiometer (LAURA). (b) Interior of LAURA radiometer, and (c) LAURA's patch antenna images taken from [Villarino, 2004]

horizontal and the other for the vertical polarisation (first and second Stokes parameters), plus a digital correlator unit for the third and fourth Stokes parameters. A picture of the radiometer hardware is shown in Fig. 4.1(b).

The antenna is a 4×4 array of dual-polarisation microstrip patches (see Fig. 4.1(c)) with 20° half-power beamwidth , 95.2% main beam efficiency , a side lobe level of -18 dB in the E-plane and -26 dB in the H-plane, and a cross-polarisation level better than -35 dB in the whole pattern, and better than -40 dB in the main beam. LAURA is placed inside of a polythene box which has been covered with a metal film to prevent radio frequency interferences (RFI). Moreover, layers of polystyrene have been placed in the interior to isolate the radiometer from external temperature changes, and from humidity. A complete description of LAURA may be found in Villarino [2004, Ch. 2].

The instrument is mounted on a pedestal which allows an automatic motion in elevation and azimuth. The almost 60 kg weight of LAURA are counter-weighted as shown in Fig. 4.1(a). Two step-motors control the radiometer motion: one for the elevation movement, and the other for the azimuth movement. Data acquired by LAURA are sent to a control unit composed by a PC running a software developed by UPC in Matlab, a frequency synthesiser, the step-motor controllers, a thermal control unit, a fans unit, and an uninterruptible power supply (UPS), see Fig. 4.2.

4.1.2 LAURA's update

Control rack

The first version of the radiometer's control rack is shown in Fig. 4.2(a). This was the configuration used in WISE 2000/2001, FROG 2003, SMOS REFLEX 2003, and T-REX 2004 experiments. During 2005, a new industrial PC and monitor were installed, and the motor drivers were substituted by MicroLYNX 4/7 devices. The rack shown in Fig. 4.2 was used during the T-REX 2006, SMOS REFLEX 2006, and TuRTLE 2006 experiments. The update of the PC forced an update of the operative system, which changed from Windows 95 to Windows

(a) (b)

Fig. 4.2: View of the LAURA radiometer control rack, (a) before, and (b) after the update.

XP. The Matlab version was updated from 5.3 to 7.0, so some of the code for controlling the radiometer had to be rewritten and recompiled.

Trailer

The rack in Fig. 4.2(a), and the radiometer without the pedestal were used in the two first experiments over land: SMOS REFLEX 2003, and MOUSE 2004. Then, LAURA and its pedestal, the control rack, the microwave absorber used as hot load target, and a power generator were mounted on the trailer in Fig. 4.3. This set-up was only used during the T-REX 2004 experiment. In 2005 the trailer was rebuilt: its structure was closed leaving an opening on the top for the radiometer to exit, and two doors, one at the front to access the control rack, and other at the rear through which to access the interior of the trailer. This new trailer, which has been used since 2005 till present, has also external power connections so that power for the instrumentation might be provided by a power line (particularly useful when the radiometer is left unattended during long-term experiments).

4.2 Instrumentation for ground-truth measurements

4.2.1 Soil moisture sensors and data loggers

Thetaprobe ML2x

The ThetaProbe ML2x sensor from Delta-T Devices Ltd. is a time domain reflectometer consisting of four 60 mm long per 3 mm diameter stainless steel rods (see Fig. 4.4(e)). The Thetaprobe generates a 100 MHz sinusoidal signal which is applied to the rods, three of them

(a) (b)

Fig. 4.3: Trailer containing the LAURA radiometer, its control rack, a power generator, and the microwave absorber for hot load calibrations. (a) First configuration and (b) present configuration.

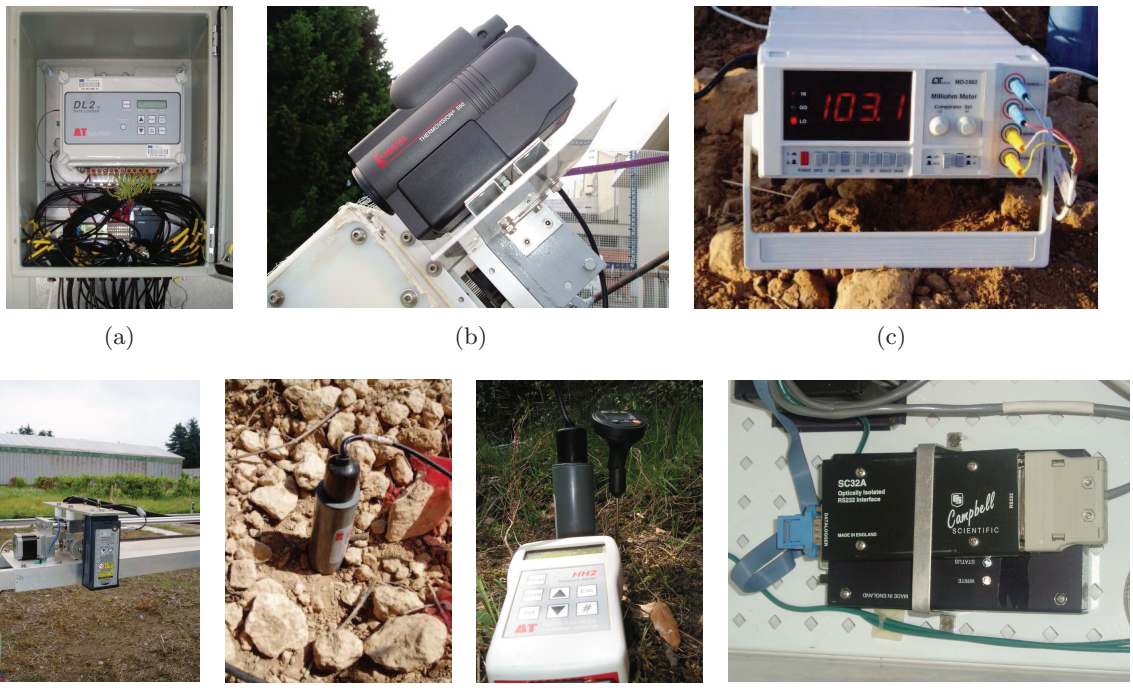

(a) (b) (c)

(d) (e) (f) (g)

Fig. 4.4: Instrumentation used during different experiments for ground-truth measurements. (a) DL2e data logger, (b) Infra-red camera, (c) Milliohm metre, (d) Leica Disto Pro 4a, (e) Thetaprobe ML2x, (f) HH2 moisture metre, and (g) SC32A data logger.

acting as shield for the central signal rod. The impedance of the array of rods varies with the impedance of the soil, and affects the reflection of the sinusoidal signal. The output of the probe varies from 0 to 1 V for a range of soil dielectric constant between 1 and 32 (which corresponds to approximately 50% volumetric soil moisture content). Its accuracy is 1% in soil moisture from 0 to 40 °C after calibration for a specific soil type, and 5% from 0 to 70 °C using the general calibration supplied by the manufacturer. The sensor can operate in the range −10 °C to 70 °C without damage, and may be buried up to 5 m in soil. The probe can be fed with a voltage between 5 V and 15 V. For further details refer to Miller & Gaskin [1999].

HH2 moisture metre

Figure 4.4(f) shows the hand-held moisture metre HH2 from Delta-T Devices Ltd. which reads the measurements from the ML2x probes (see Section 4.2.1). The HH2 moisture metre has an accuracy of 0.13% of mV and a resolution of 1 mV, and can operate at temperatures from 0 to 40 °C . Soil water content output is expressed either in $m^3 \cdot m^{-3}$ or % of volume, water deficit (mm), or voltage (mV). Readings are displayed on a LCD and can also be stored to memory for later download to a PC using a RS-232 cable.

DL2e data logger

Figure 4.4(a) shows the DL2e data logger from Delta-T Devices Ltd. Up to 60 sensors can be connected to a numbered screw terminal connector block. Instantaneous output from any sensor, battery and memory status, and report on any sensor malfunctions are shown in its LCD. The logging interval may vary from seconds to hours, and can be different for each channel. Data are transferred to a PC by a RS-232 serial cable.

ECH_20 EC-5 sensor

The EC-5 is a volumetric water content sensor which measures the dielectric constant of soils using capacitance/frequency domain technology. Its range of soil moisture goes from 0 to 100% volumetric water content, with a resolution of 0.1% in mineral soils and 0.25% in rockwool. The accuracy goes from 4% if the generic calibration for mineral soils is used, down to 2% is a soil specific calibration is performed. The accuracy stated by the manufacturer in rockwool is 3%. The EC-5 sensor can operate in the range −40 °C to 50 °C without damage.

4.2.2 Soil roughness profile metre

The soil surface height profile was measured using a Disto Pro 4 distance laser metre by Leica. A picture of this device is shown in Fig. 4.4(d). The Disto Pro 4a contains a laser operating at the 635 nm. The measuring accuracy is of 1.5 mm in the range of distance from 0.3 m to 100 m. The acquisition can be single or continuous, providing a distance value every 0.5 to 4 s. Measurements are shown in a graphic displayed and up to 800 values can be stored in memory and then transferred to a PC. The temperature range of operation goes from -40 °C to 70 °C .

4.2.3 IR camera

A Thermovision 550 IR camera by Agema Infrared Systems was mounted by the LAURA radiometer during the MOUSE 2004 experiment (see Fig. 4.4(b)). This IR camera works in the 3.6 to 5 um spectral range and is able to measure the IR emission of targets whose temperature is within the -20 °C to 250 °C range with a ±2 °C accuracy and a thermal sensitivity better than 0.1 °C . The Thermovision 550 camera has a field of view of 20° ×15° which is well matched to the antenna beamwidth and uses a detector of the type focal plane array with 320×240 pixels.

4.3 Field experiments over land

4.4 Soil texture: The MOUSE experiment

Soil emissivity is related to the soil water content by the dielectric constant, which also depends on soil physical properties such as texture. The Monitoring Underground Soil Experiment (MOUSE) was carried out to assess the variability in the soil moisture retrieval due to the selected dielectric mixing model and soil type. L-band radiometric data of six different soil types were acquired under different observation angles and soil moisture conditions. The data were processed using laboratory measurements, and two widely used semi-empirical dielectric constant models: Wang & Schmugge [1980] and Dobson *et al.* [1985]. The retrieved soil moisture was compared to ground-truth values at different depths to estimate the goodness of each model for each soil type, and the depth of the emitting soil layer. The experimental setup is described hereafter.

4.4.1 Experiment site

MOUSE was carried out at the ESA Joint Research Centre (JRC) outdoor test facility in Ispra, Italy (45° 48′ N, 8° 37′ E, altitude = 213 m), from June 7 to July 1, 2004 (day of year, DOY, 159 to 184). The site had been previously used as a mine detection experiment site and soils had been carefully selected with this purpose. There were six 6 m × 6 m smooth bare plots of different soil type, labelled as follows: (LO) loamy soil, (SA) homogeneous natural sandy terrain, (RS) sieved sand used in the construction industry, (CL) natural terrain taken from rice fields, (OR) mixture of LO and of commercial products for gardening, (FE) ferromagnetic crushed volcanic soil. Their texture Lewis & Logreco [2002] and roughness are shown in Table 4.1. The six plots were distributed along a lane as shown in Fig. 4.6(a). Six ThetaProbes (see Section 4.2.1) and six thermistors are permanently installed in each plot at surface level and at 5, 10, and 15 cm depth according to Fig. 4.7.

4.4.2 Microwave measurements

Radiometric observations of the six plots were acquired using LAURA at incidence angles from 25° to 65° from nadir in 10° step. As shown in Fig. 4.6(b) the radiometer and the control rack were mounted on a metallic gantry, guided by a rail on one side and freely rolling on the

Fig. 4.5: Location of the experiments sites

(a) (b)

Fig. 4.6: (a) View of the MOUSE 2004 experimental site. The tent was used to protect the field 3 from water (it was kept dry during all the experiment. (b) The LAURA radiometer and the control rack were mounted on a 3 m high moving gantry used to position the antenna above the plot to be measured. The metallic shield was used to reduce RF interferences

Table 4.1: Characteristics of the Six Field Plots

Field	Label	Roughness (mm) height (std. dev)	Roughness (mm) corr. length	Soil texture (%)	
		σ_s	l_c	Sand	Clay
1	LO	6.16	72.1	78	2
2	SA	6.02	168.9	95	0
3	RS	8.46	105.01	96	0.5
4	CL	4.94	280.4	15	40
5	OR	8.32	65.52	78	2
6	FE	4.13	47.16	82.5	2.5

other. Due to the orientation of the lane, the observation direction of the radiometer was West so measurements were done after dawn to avoid Sun emission. The position of the gantry along the test lane changed with the field and also with the incidence angle so that the radiometer was always pointing at the centre of each plot.

In general, microwave measurements at V-pol were affected by some kind of interference, probably coming from a TV broadcasting station. To have enough measurements to discard the contaminated ones, the observation time at each plot and for every incidence angle was five minutes. This means 300 acquisitions per position, since the radiometer takes one measure per second. Unfortunately, the interference was too high for incidence angles larger than 45° and many of the data had to be discarded at V-pol, and some at H-pol.

Hot- and cold-load calibrations, as well as the correlated and uncorrelated noise injection calibrations for the polarimetric channels, were performed hourly. Microwave absorber and the cold sky measurements through reflection on a metallic plate were used as hot and cold load targets, respectively.

4.4.3 Ground-truth data

Soil moisture data

Different soil moisture values were obtained by irrigating the plots and then letting them dry out. This procedure was repeated three times in all the plots except plot number 3, which was kept dry and protected from water by a sliding tent (see Fig. 4.6(a)). As expected, soil texture affects the water percolation and drying and, as shown in Fig. 4.8, different soil moisture profiles were measured at each plot. As expected, water rapidly penetrates through sandy soils, which consequently have the shortest drying period. On the other side, soils with high clay content dry slowly. Some anomalies in the soils drying period are because of rainfall events registered in the area between irrigations.

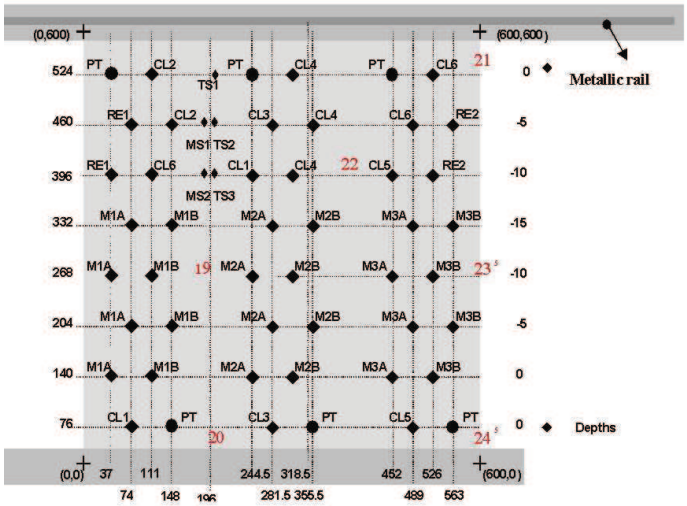

(a)

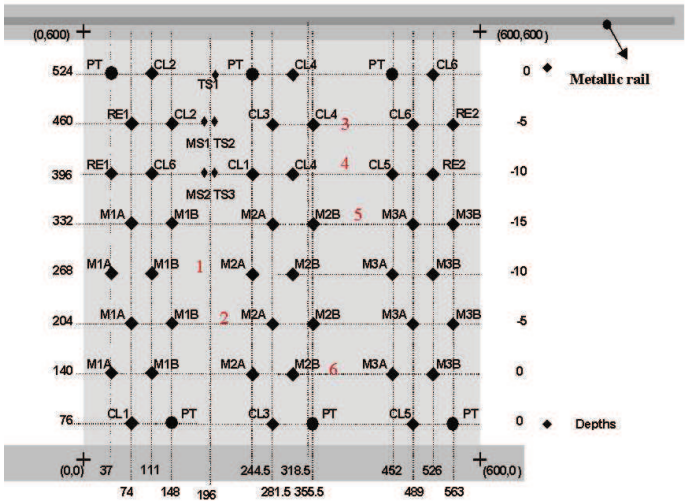

(b)

Fig. 4.7: Soil moisture and temperature sensors were buried at different depths at each plot (from [Lewis & Logreco, 2002])

Soil temperature data

Soil temperature, moisture and roughness data were acquired concurrently with the radiometric measurements. Soil temperature was measured using three thermistors per plot located just below the surface, at 5 cm and at 10 cm depth. An infrared (IR) video camera was mounted by the LAURA radiometer to take soil surface temperature images and observe the impact of litter on the IR-derived surface temperature. IR soil temperature value was found to be in very good agreement with the thermistors at 0 and 5 cm depth, but it was detected that the image had a peak-to-peak deviation of 3 K mostly due to the presence of organic debris. This suggests that the effective soil temperature could also be left as a free parameter in the soil moisture retrieval procedure when IR data is used as an auxiliary parameter in the retrieval process. The probes were connected to a CS21X Campbell Scientific data logger, which averaged the measurements taken every 10 s to give half hourly values.

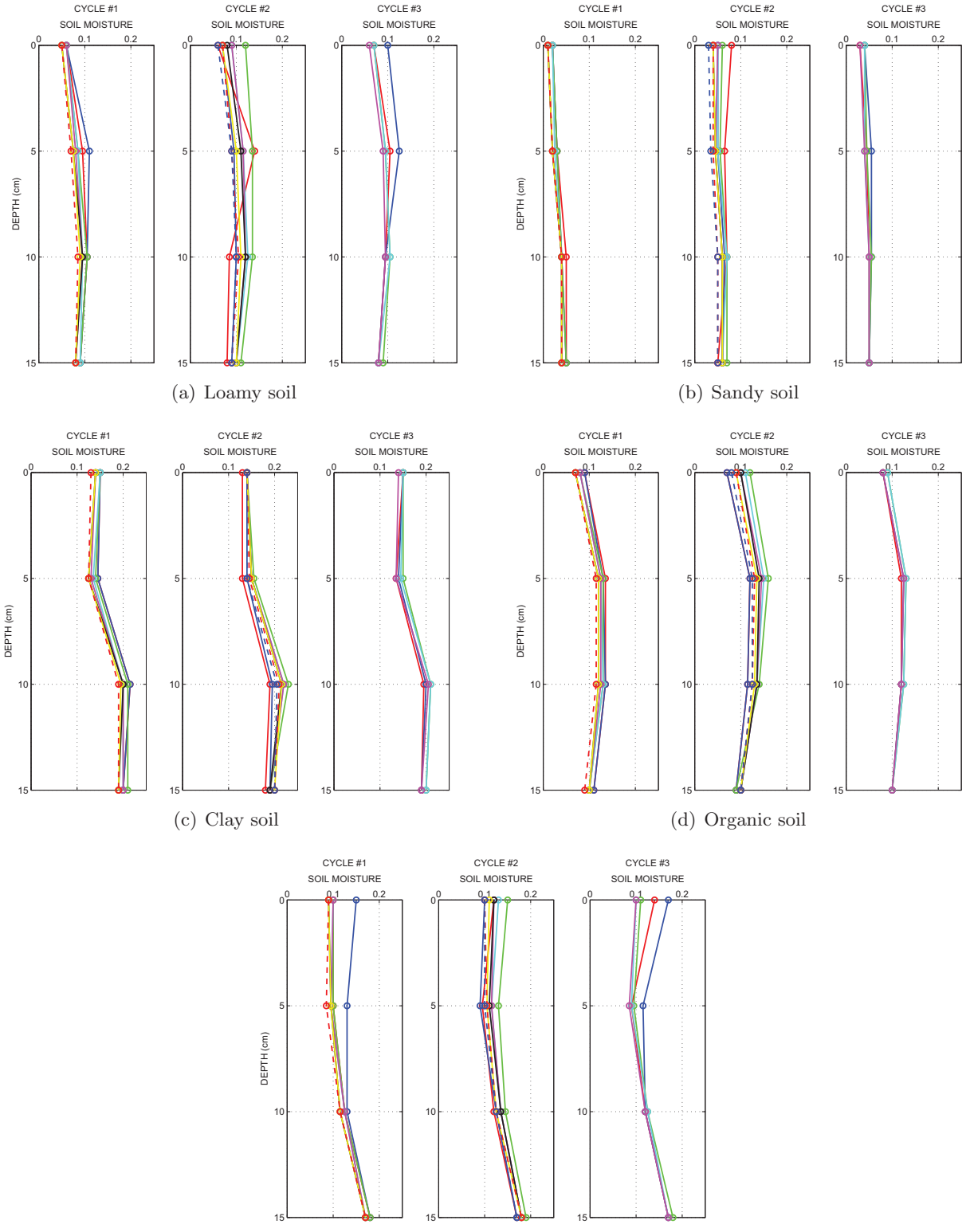

(a) Loamy soil

(b) Sandy soil

(c) Clay soil

(d) Organic soil

(e) Ferromagnetic soil

Fig. 4.8: Soil moisture profiles acquired during the MOUSE 2004 experiment. The three measurement cycles, from irrigation to dryness, for each soil type are shown. Different soil moisture profiles can be seen depending on soil texture. Lines with different colors correspond to different days of experiment (DoE): – blue DoE1,– red DoE2, – green DoE3, – cyan DoE4, – magenta DoE5,– black DoE6, – yellow DoE7, – – red DoE8, – – blue DoE9.

Soil roughness data

The soil surface height was measured by means of a laser profiler developed and implemented at UPC using a Leica Disto Pro4a laser distance metre. One profile per soil type was recorded after each irrigation with a sampling interval of 5 mm along a 1.5 m transect. The standard deviation of the height σ_S and the correlation length L_c for the six plots were computed from the measured soil profiles and are presented in Table 4.1.

4.4.4 Soil dielectric constant measurements

One of the goals of the MOUSE 2004 experiment was to assess the impact of soil dielectric constant ε_S on the retrieved soil moisture. At present, the dielectric mixing models by Wang & Schmugge [1980] and Dobson *et al.* [1985] are widely used, but it has not been determined whether they can be applied to any soil type without distinction or not. With this purpose, a sample of the six soils at the experimental site was collected, and their dielectric constant measured at the UPC laboratories. The setup and the measurement strategy is fully described by Vall-llossera *et al.* [2005a]. The coefficients of the best-fit polynomial for the dielectric constant of each soil type as a function of the water content are summarised in Table 4.2, and represented in Fig. 4.9. Rather high differences between the dielectric constant curves is appreciated for high water content values. Figure 4.9 was compared in Vall-llossera *et al.* [2005a] to the curves obtained using the expressions by Wang & Schmugge [1980] and Dobson *et al.* [1985]. In general, permittivity curves are more in line with Wang & Schmugge [1980] except for clay soils, where they are very similar. Laboratory-measured imaginary part of ε_S tends to increase faster than that computed with the other two models. Loamy soil experimental data are in excellent agreement with Wang & Schmugge [1980] while discrepancies increase for organic and ferromagnetic soils. For sandy soils, the drier the soil is the more similar to Wang & Schmugge [1980], but as the wetness increase the experimental curve tends to be closer to Dobson *et al.* [1985].

Table 4.2: Coefficients of the best-fit polynomial for the measured dielectric constant of soils as a function of the water content w_s ($\varepsilon_s = \varepsilon'_S + j\varepsilon''_s$, $\varepsilon'_s = a_1 w_s^2 + b_1 w_s + c_1$ and $\varepsilon''_s = a_2 w_s^2 + b_2 w_s + c_2$)

Label	ε'_s			ε''_s		
	a_1	b_1	c_1	a_2	b_2	c_2
LO	98.328	13.848	2.39	2.09	7.67	- 0.093
SA-RS	149.113	- 4.157	2.448	3.068	4.945	0.019
CL	149.183	- 0.084	3.536	9.538	4.526	0.546
OR	125.73	5.05	1.143	8.73	4.39	- 0.108
FE	124.02	17.51	3.163	12.99	2.96	0.112

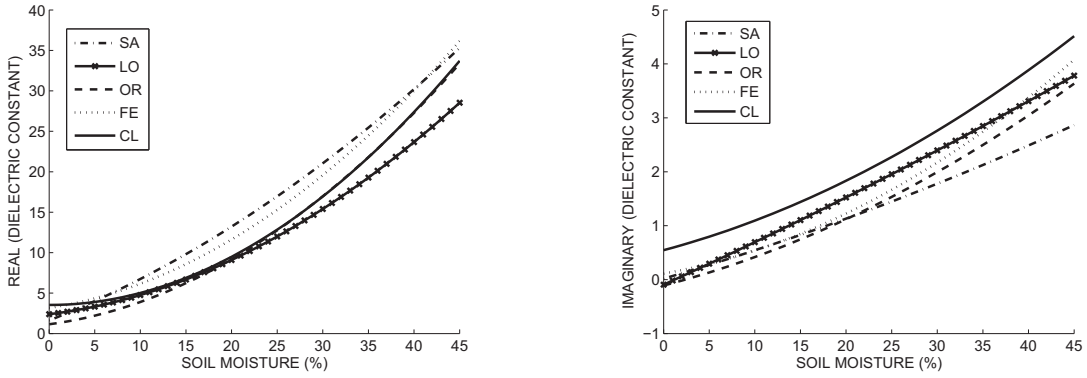

(a) (b)

Fig. 4.9: Variability in the measured soil dielectric constant due to soil type and water content. (a) Real part. (b) Imaginary part.

4.5 Soil roughness: The Terrain-Roughness Experiments (T-REX)

How soil roughness effects should be modelled at L-band has not been established so far. Some approaches take into account "effective" best-fit roughness parameters, whereas other approaches use statistics of the soil height profile such as the standard deviation or the correlation length. With the aim of studying the effect of roughness on the radiometric measurements,the T-REX experiments were carried out in Agramunt, Spain, in collaboration with the Universitat de Lleida-Institut de Recerca i Tecnologia Agroalimentàries (UdLl-IRTA).

4.5.1 Experiments site

The Terrain-Roughness EXperiments (T-REX) were carried out in Agramunt, Spain (41° 48′ N latitude, 1° 7′ W longitude, 356 m altitude) from DOY 333 to DOY 337, 2004, and then again from DOY 143 to DOY 160, 2006. The sites consisted of bare soil plots with four different ploughing, but the same textural composition (21% clay, 21.3% sand, 0.25 m^3/m^3 field capacity). Each parcel was 6 m wide × 50 m long in T-REX 2004, and 6 m wide × 15 m long in T-REX 2006. The same ploughing was applied to two different plots to observe spatial diversity effects. Pictures of the ploughs at the T-REX 2006 site may be seen in Fig. 4.10. LAURA was installed on a trailer towed by a car. As it can be seen in Fig. 4.11, the trailer's configuration changed between one experiment and the other. Table 4.3 shows the roughness parameters of each plough.

4.5.2 Radiometric measurements

As in previous campaigns, the radiometric observations were acquired with the UPC L-band Automatic Radiometer (LAURA). Radiometric measurements were acquired at incidence angles of 30° , 35° , 40° , 45° , 50° , 55° , 60° , and 65° in T-REX 2004, and of 40° , 45° , 50° , 55° , 60° , and 65° in T-REX 2006. Every plough type was measured twice each day of experiment. Measurements of the cold sky and of a microwave absorber were acquired at the beginning and

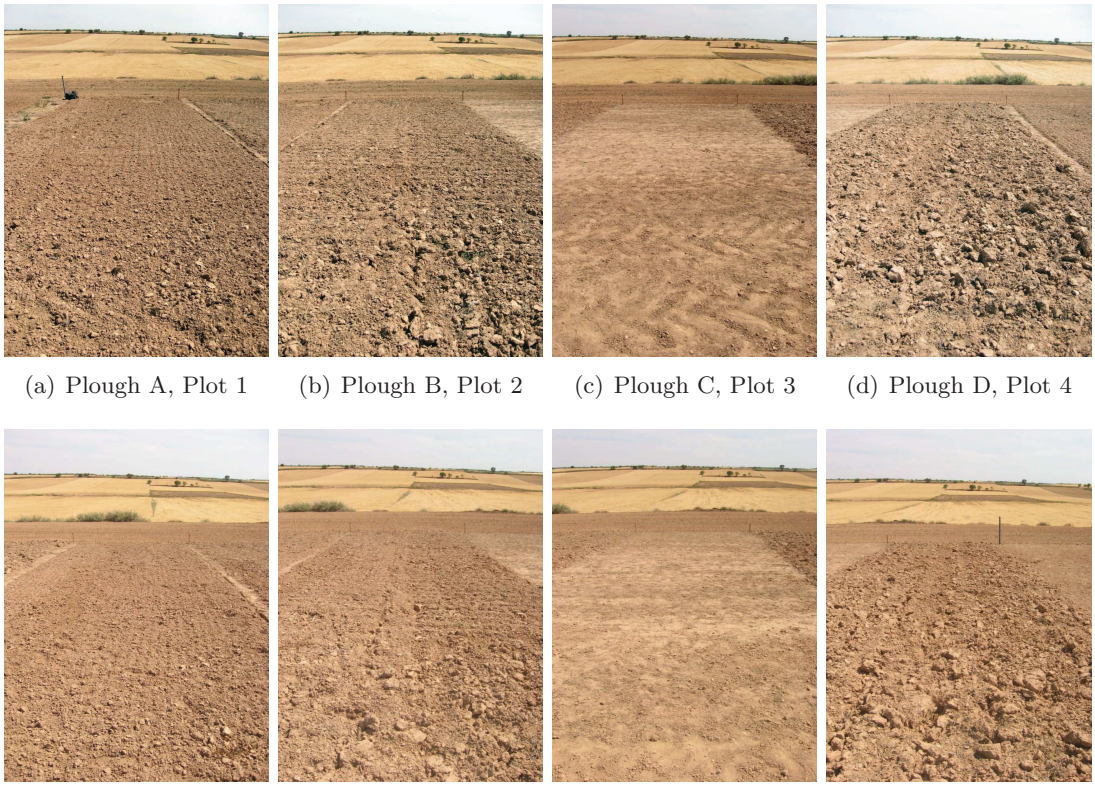

(a) Plough A, Plot 1 (b) Plough B, Plot 2 (c) Plough C, Plot 3 (d) Plough D, Plot 4

(e) Plough A, Plot 5 (f) Plough B, Plot 6 (g) Plough C, Plot 7 (h) Plough D, Plot 8

Fig. 4.10: View of the eight plots with four different ploughs measured during T-REX 2006

Table 4.3: Roughness characteristics of the measured ploughs. Symbols indicate tillage direction with respect to the antenna reference system: $\parallel$ parallel; $\perp$ perpendicular.

Experiment	Plough	$l_c \parallel$ (mm)	$l_c \perp$ (mm)	rms l_c (mm)	$\sigma_s \parallel$ (mm)	$\sigma_s \perp$ (mm)	rms σ_s (mm)
T-REX 2004	H	29.64	15.24	33.33	23.38	16.68	28.72
	E	51.12	98.23	110.74	7.48	13.84	15.73
	F	108.24	42.72	116.36	15.10	13.17	20.03
	G	158.54	34.30	162.21	8.66	12.12	14.90
T-REX 2006	A	100.72	51.58	113,74	9.63	11.07	14.75
	B	85.52	37.61	96.53	12.43	10.16	16.40
	C	198.8	92.68	230.65	3.02	6.78	7.45
	D	91.35	63.00	111.21	30.23	15.27	33.89

(a) T-REX 2004

(b) T-REX 2006

Fig. 4.11: View of the T-REX experiments measurements site.

end of each measurement sequence, and used as cold and hot load calibrations, respectively. Raw radiometric data from one day of experiment and for both experiments is represented in Fig. 4.12.

4.5.3 Ground-truth measurements

The soil surface height was measured by a laser profiler implemented at the UPC using a Leica Disto Pro4a laser mounted on a rolling structure whose position is controlled from a laptop. Two profiles per soil plot were acquired with a sampling interval of 5 mm along a 1.5 m transect: one parallel and the other perpendicular to the antenna reference frame. The standard deviation of height (σ_s) and the correlation length (l_c) of the six field plots were computed from the measured soil profiles and are given in Table 4.3.

Soil temperature was measured using three PT-100 thermistors located just below the surface, at 5 cm, and at 10 cm depth during T-REX 2004, and at 0, 5, 10, 15, and 20 cm depth using thermometers during T-REX 2006. Very low soil surface temperatures, from 3 °C to 9 °C , were measured during the winter experiment T-REX 2004. In contrast, soil temperature during the T-REX 2006 reached up to 35 °C . Since the purpose of the experiment was to assess the impact of the soil roughness on the L-band emission, the soil was not irrigated. However, soil moisture varied significantly during T-REX 2004 due to the heavy dew and rainstorms. At-

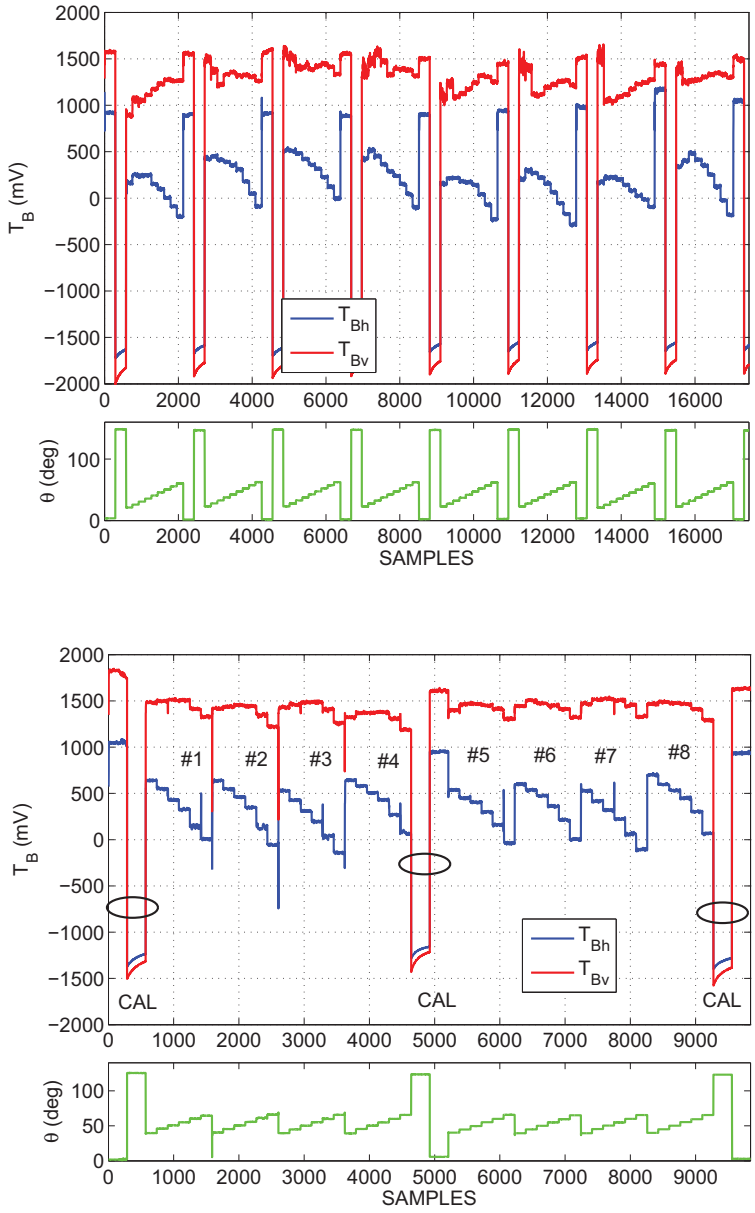

Fig. 4.12: Raw radiometric measurements acquired during (a) T-REX 2004, DOE 4, and (b) T-REX 2006, DOE 12.

mospheric temperature, relative pressure, and accumulated rainfall data were acquired from a meteorological station located 18 km far from the sites.

4.6 Vine canopy: SMOS REFerence pixel L-band EXperiments

A six month CalVal phase is scheduled after SMOS launch. During this period a number of field campaigns will be conducted in various sites around Europe. The Valencia Anchor Station (VAS) in the Requena-Utiel region in Spain [López-Baeza *et al.*, 2001] has already been selected as a CalVal site because its large area (approximately the size of a SMOS pixel, 50 km × 50 km) and its homogeneity (it is covered mostly by vineyards, and in lower fractions,

by other Mediterranean ecosystems). Since the CalVal will last half a year, vines at the VAS will be measured at different growth stages and thus a previous radiometric characterisation of vines development would be important for the calibration activities. This was the purpose of the SMOS REFLEX experiments. The SMOS REFLEX 2003 experiment is described hereafter, while the SMOS REFLEX 2006 experiment is presented in Section 4.7.

4.6.1 Experiment site

SMOS REFLEX 2003 took place at the València Anchor Station (VAS, 39° 33′ N, 1° 17′ W, h = 876 m), València, Spain, from June 30 to July 10, 2003 [Vall-llossera *et al.*, 2005b, López-Baeza *et al.*, 2001], some time before it was selected as a SMOS cal/val site. During the experiment period, the weather was very dry and hot. In order to get a wide range of soil moisture values, the field was irrigated twice (on July 1st and again on July 4th, that is, the second and fifth days of the experiment) and it was then left to dry out. Hence, two complete measurement cycles (from saturated wet soil to completely dry soil) were performed. The first of them was shorter than the second (3 days in front of 7 days) because the high temperatures and strong winds recorded at the beginning of the experiment dried the land much faster. Concurrently with the radiometric measurements, the gravimetric soil moisture, the temperature and the roughness were measured and the vines were fully characterised (water content, grapevine size, branches distribution, etc.). This section presents a description of all the tasks performed during the field campaign [Vall-llossera *et al.*, 2005b].

4.6.2 Radiometric measurements

During SMOS REFLEX 2003, LAURA was mounted on the top of a crane placed on a path between vineyards as shown in Fig. 4.13(a). The antenna was oriented to the West and its look direction was perpendicular to the tillage direction of the plot. Figure 4.13(b) schematically shows the settlement of the site under study. The vines, represented by a green asterisk, are distributed along rows parallel to the path, and are separated 1.5 m; in each row plants are separated 2.5 m and located at x(m) = 12.5, 10, 7.5, 5, 2.5, 0, 2.5, 5, 7.5, 10, 12.5, 15.

Radiometric observations at nine incidence angles θ, from 25° to 65° in 5° steps, and seven azimuth angles φ, from -45° to 45° in 15° steps (being $\varphi = 0$ the direction perpendicular to the tillage) were carried out daily. Ellipses in Fig. 4.13(b) show the 63 footprints at half-power for each sequence (each footprint corresponds to a direction of observation). Note that ellipses are not all of the same shape and size; the major axis increases with the incidence angle, while the minor axis is kept constant by changing the radiometer height for each incidence angle.

During the experiment, a set of measurements were taken so as to calibrate the instrument: (i) hot and cold load calibrations, to obtain the first and second Stokes' parameters, and (ii) correlated and uncorrelated noise injection calibration, to compensate the correlator errors and determine the third and fourth Stokes' parameters. Eccosorb slabs placed just in front of the antenna at ambient temperature were used as hot targets. The cold target was obtained by measuring the sky radiation through reflection on a metallic plate.

(a)

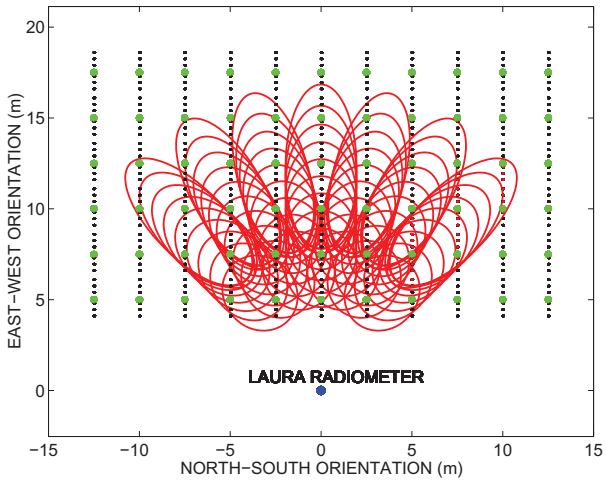

(b)

Fig. 4.13: (a) Picture of the SMOS REFLEX 2003 experiment site. The crane with the LAURA radiometer was placed on a path between two vineyards. (b) Schematic of the REFLEX 2003 test site. The vines (green dots) were distributed in rows and columns separated 2.5 m. Six soil moisture samples were measured in the nearby of each vine (black dots). Red ellipses indicate the observed pixel at each observation position.

Raw data for two days of experiment, one with dry soil and the other with wet soil, have been represented in Fig. 4.14. Small emissivity variations with the incidence angle at both polarisations are noticed, specially if the soil is dry. Emissivity variations with the azimuth angle are only observed in the case of wet soil, when the contribution to the emission coming from the soil is more significative and changes in the percentage of soil within the radiometer's FOV are more noticeable.

4.6.3 Ground-truth measurements

When SMOS REFLEX 2003 began, the soil was completely dry because neither rain nor irrigation had moistened the area for three months. Dots in Fig. 4.13(b) represent the soil moisture sampling points: 1 sample under each grapevine and 5 samples between them (from row to row). These measurements were taken with Delta-T ThetaProbe sensors (see Section 4.2.1), which were previously calibrated. Even though the field was irrigated until saturation, different values of moisture were measured at different locations within the site because of

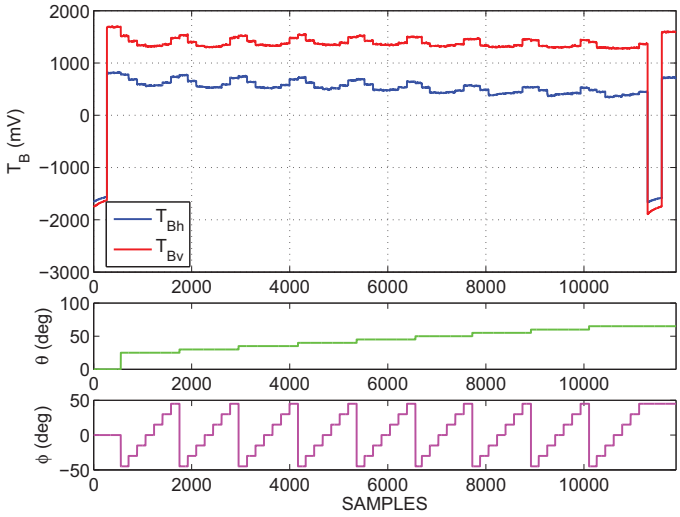

(a) Wet soil

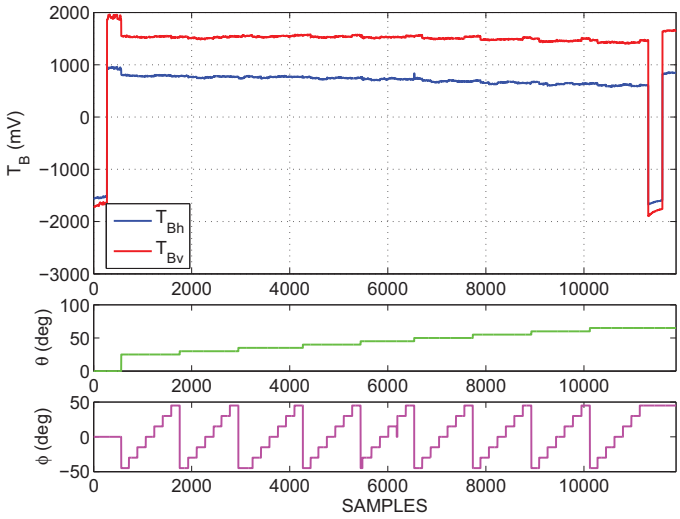

(b) Dry soil

Fig. 4.14: Radiometric measurements acquired during SMOS REFLEX 2003 for (a) wet and (b) dry soil.

surface inhomogeneities and variations on the compactness of the terrain due to plough and roots distribution.

Sensors were buried in the field to measure the soil temperature at the surface and at 5, 10, 15, 20 and 40 cm depth. Due to technical problems, there were no soil temperature data available for sequences DOE 7 and 8, and the data at 5 cm depth was only acquired the first four days of experiment.

The atmospheric temperature, pressure and relative humidity were registered by the VAS meteorological station. Large atmospheric temperature gradients are registered in this area and for this time of the year. This fact was especially important in July 1st, when the atmospheric temperature reached 38 ° C at day-time and 14 °C at night. The difference between the atmospheric and the soil surface temperatures was larger when the soil was wet (up to 3 °C within

a measurement period) than when the soil was dry. The deep soil temperature keeps almost constant with time during the experiment.

Vines at the site were of *tempranillo* variety. The canopy was parameterised by measuring different parts of eleven test-vines. The water content (WC) per compartment of a full plant per unit area was found to be 9–10 kg/m^2. Vines characteristics are summarised in Table 4.4 and Fig. 4.15. These values make evident that these vines are taller than others in the Mediterranean region (medium height of 1.63 m and medium width of 1.45 m). The leaf area index (LAI) was measured in different locations of the plot using a LAI-LICOR2000 sensor. Figure 4.15(b) shows the mean value and the standard deviation of the LAI for twelve plants randomly selected. The LAI of each selected plant was measured in two directions: one parallel to the rows of vines (circles/continuous lines) and the other perpendicular to them (asterisks/dashed lines). Their values for each sample are compared in Fig. 4.15. A mean value of 1.5 m^2/m^2 was obtained for the LAI of the vineyard. This fact will strongly influence the brightness temperature because of the great amount of water contained in the leaves and fruits.

(a)

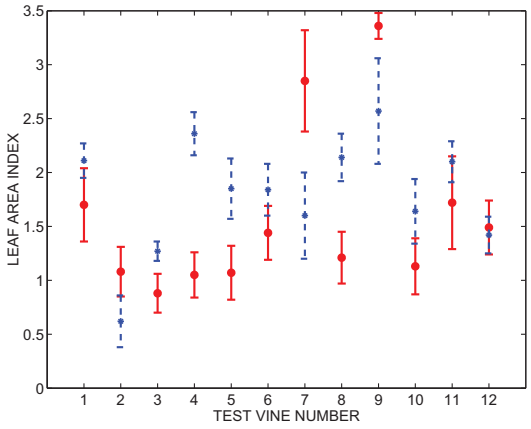

(b)

Fig. 4.15: (a) Twelve plants were randomly selected as samples and fully characterised during the SMOS REFLEX 2003 experiment. (b) Mean value (circles and asterisk) and standard deviation (continuous and dashed lines) of the measured LAI. The circles with continuous lines represent the LAI of each sample plant in the direction parallel to the rows of vines, and asterisks with dashed lines represent the LAI value of each sample plant in the perpendicular direction.

Table 4.4: Grapevine characterisation

Vineyard	Size (cm)		WC (%)
Plant	AX	110 to 200, mean = 145	
	AY	70 to 170, mean = 116	
	AZ	140 to 180, mean = 162	
Stem	Height	37 to 60, mean = 46.5	31.5
	Base diameter	5.4 to 8.1, mean = 6.6	
	Knot diameter	5.4 to 7.7, mean 6.9	
Primary branches	Diameter	3.7 to 4.5, mean = 4.1	10.5
	Length	40 to 78, mean = 55.5	
Secondary branches	Number	15 to 21, mean = 18	2.5
	Length	24 to 26, mean = 24.8	
	Diameter	0.6 to 1.2, mean = 0.9	
Tertiary branches	Diameter	0.1 to 0.4, mean = 0.2,	2.5
Leaves	Large	18×17 to 29×27	16.4
	Small	12×11 to 16×16	
Grapes	14×5 to 17×9		39.2

A video camera was mounted by LAURA pointing to the radiometer boresight and was used to determine the fraction of soil covered by vegetation at each FOV. Figure 4.16 shows three pictures taken at three different positions. As it can be appreciated, vegetation coverage depends on the direction of observation.

(a) (b) (c)

Fig. 4.16: Video camera shots at three different radiometer's positions: (a) $(\theta, \phi) = (25^\circ , 0^\circ)$, (b) $(\theta, \phi) = (35^\circ , -45^\circ)$, and (c) $(\theta, \phi) = (60^\circ , -45^\circ)$

4.7 Rock fraction: The SMOS REFerence pixel L-band EXperiment 2006

The SMOS Reference Pixel L-band Experiment (SMOS REFLEX) 2006 was planned to monitor changes in the L-band (1.400-1.427 GHz) emission of vineyards for varying growth stages of plants. The experiment was carried out from July 3 to November 10, 2006, which correspond to DOY (day of year) 184 to 314. The vineyard was harvested from DOY 260 to

262.

4.7.1 Experiment site

The experiment site was a different vineyard at the Valencia Anchor Station site, Spain (VAS, 39.6° N lat, 1.25° W long, 780 m altitude), located close to a wine cellar so that power for the instrumentation was available all the time and instrumentation could be left unattended. The site had a sandy clay loam soil with a 63% sand and 22% clay by volume. Trickle irrigation was used in the vineyard. Rocks were kept in half the vineyard (from 40% to 80% of rocks) and were partially removed in the other half (from 6% to 30% of rocks) as shown in Fig. 4.17. A picture of the site the first and last days of experiment are shown in Fig. 4.18(d) and Fig. 4.18(e). Vines are in full maturity and there is no litter in Fig. 4.18(d) while, in contrast, in Fig. 4.18(e) vines are withering and have no fruits, and plants litter and/or grass is present in some areas within the site (especially in the half with few rocks).

4.7.2 Radiometric measurements

LAURA, the control rack, and the microwave absorber were installed on a trailer as shown in Fig. 4.18(c). The radiometer was remotely controlled via Internet using an Hispasat link.

Automatic observations were continuously acquired at incidence angles from 40° to 65° in 5° steps. Varying the incidence angle implied the increase of the canopy percentage within the FOV so its impact on the emission was more noticeable. The scan in incidence angles was performed for two azimuth angles φ which were selected so that the rocks-side was observed at φ_1 and the few-rocks-side was observed at φ_2. Measurements were calibrated using a microwave absorber and the sky as hot and cold load targets, respectively. Raw data acquired during one day of experiment are represented in Fig. 4.19.

4.7.3 Ground-truth measurements

Ground-truth soil moisture and temperature were registered every 15 minutes at 0, 5, 10, 15, 20, and 40 cm depth using EC-5 sensors by Decagon (see Section 4.2.1) and thermometers, respectively. Moreover, ML2x probes (see Section 4.2.1) were installed to measure every 10 minutes the soil moisture in the 0-5 cm layer under vines, between vines, and between rows of vines (bare soil). Time series of soil moisture and temperature are shown in Fig. 4.20. Since rocks protect soil from direct solar radiation, the soil water content W_c in the rocks half vineyard was larger than in the other half. Since, apart from trickle irrigations, various rainfall events were registered during the experiment, a wide range of soil moisture values was measured: 6.7% to 26% in the space between rows of vines, 15% to 43% under vines, and 21% to 40% between two vines.

A meteorological station from the Spanish National Meteorological Centre, located 20 m far from the experiment site, registered the atmospheric temperature at 2 m height, and the wind direction and intensity (every 15 min.), and the accumulated precipitation (hourly).

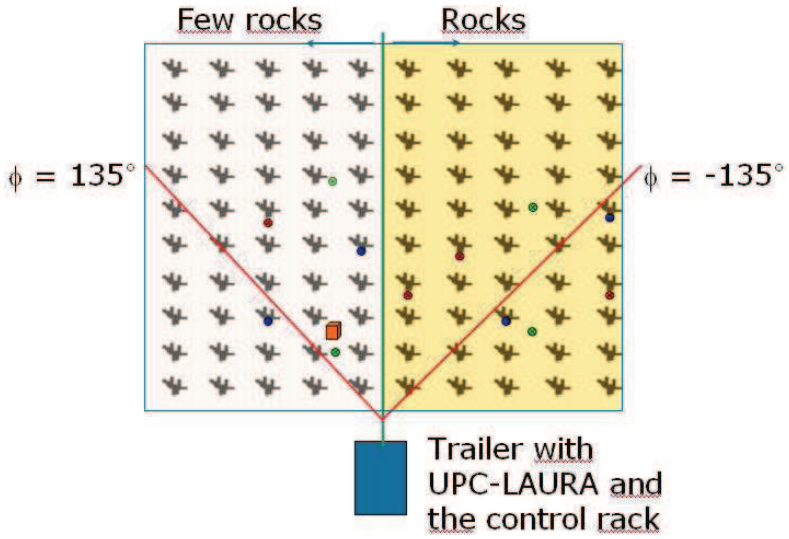

Fig. 4.17: Diagram of the REFLEX 2006 site. Dots indicate the position of the soil moisture sensors: under vines(blue), between vines (red), and between rows of vines (green). The orange box indicates the position of the soil temperature sensors and dataloggers.

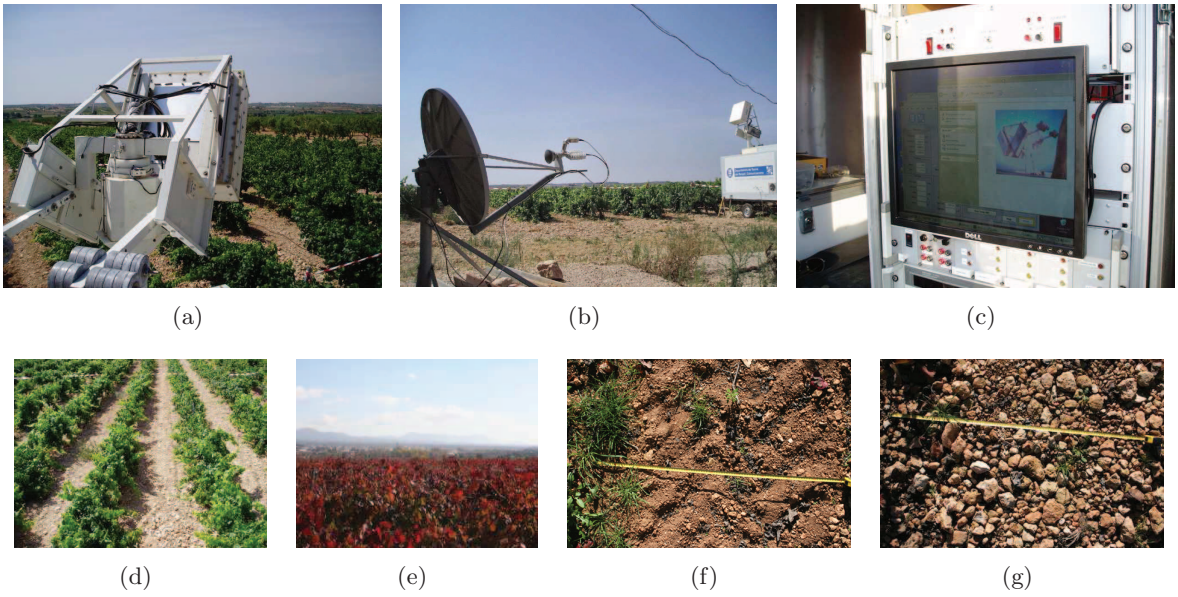

Fig. 4.18: (a) and (b) The trailer with the LAURA radiometer, its control rack, and the microwave absorber was installed on a vineyard. The Internet was accessed via Hispasat. (c) A camera pointing LAURA was used to visually check the correct position of the radiometer. (d) Experiment site on DOY 184. Vines are fully developed while fruits are still growing. (e) Experiment site on DOY 314. Leaves are withering and there are no fruits. (f) and (g) Pictures of the soil surface taken at the few-rocks and rocks half of the vineyard, respectively.

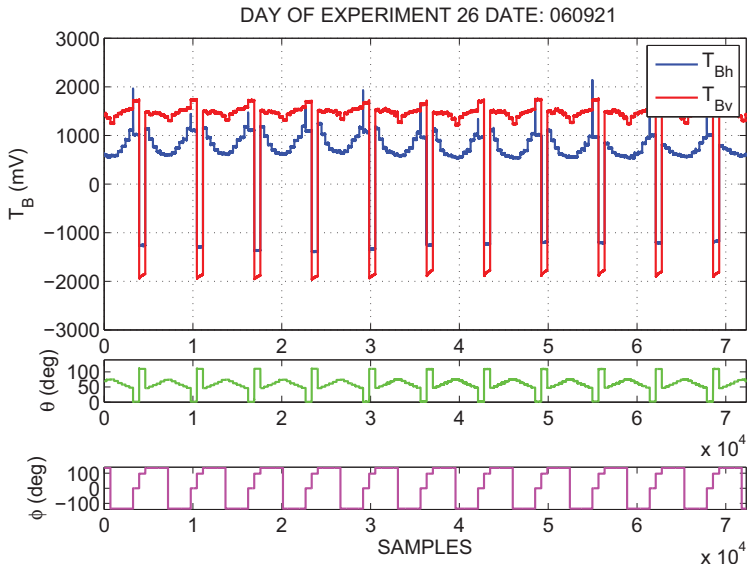

Fig. 4.19: Radiometric measurements acquired during REFLEX 2006.

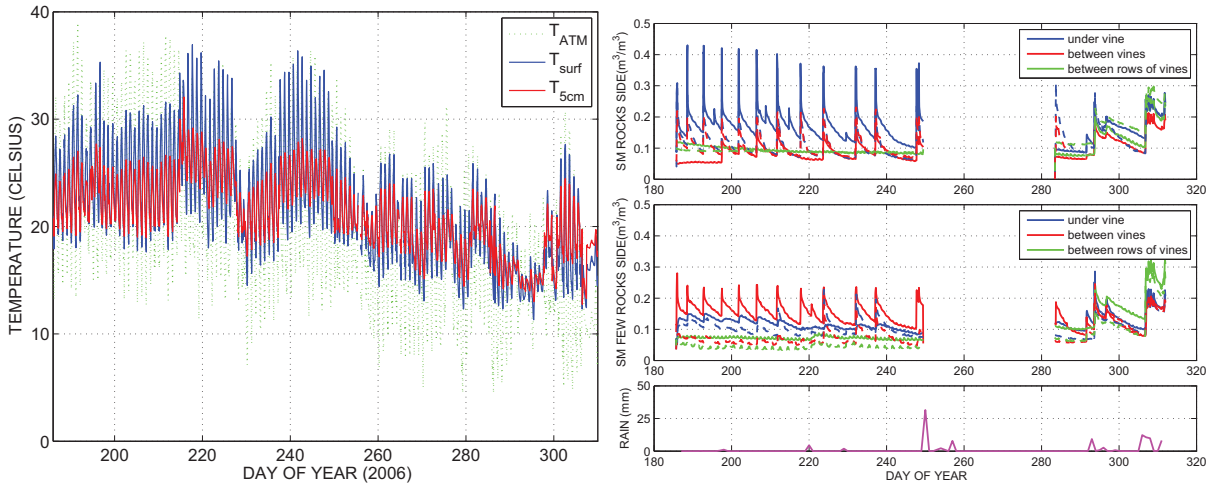

(a) (b)

Fig. 4.20: Ground-truth data acquired during the REFLEX 2006 experiment. (a) Atmospheric temperature, and soil temperature at surface and 5 cm depth, and (b) soil moisture under vines, between vines, and between rows of vines, and daily precipitation.

The soil surface height profile was measured every 5 mm along a 1.5 m transect using a Leica Disto4a laser distance metre. The correlation length and standard deviation of the roughness profiles before (after) harvest are 10.1 cm (8.7 cm) and 1.2 cm (1.3 cm), respectively.

Finally, pictures at every look direction were taken to estimate the percentage of FOV covered by plants. At incidence angles lower than 55° the percentage of FOV occupied by bare soil is up to 40%, so the contribution of soil to the measured radiation is important.

4.8 Topography: The topography effects on RadiomeTry at L-band Experiment

Up to now, few studies have investigated the effects of topography on the microwave radiometric signal Mätlzler & Standley [2000]-Talone *et al.* [2007], and very few experimental data is available Berger *et al.* [2002]. As a contribution to fill this lack of information, the Topography effects on RadiomeTry at L-band Experiment (TuRTLE) was conducted [Monerris *et al.*, 2007]. TuRTLE 2006 is a first approach to the topography issue from a ground-based point of view, and in a future airbone experiments will be carried out. This will increase the existing data set and, besides, will provide observations of larger pixels, closer to the SMOS acquisitions.

The Topography effects on RadiomeTry at L-band Experiment (TuRTLE) 2006 was carried out at the Parc Natural del Montseny, 50 km north of Barcelona, Spain, in May 2006. The trailer containing the L-band AUtomatic RAdiometer (LAURA), its control rack, and a microwave absorber used as hot load calibration target was installed on a valley at (41°48′ N, 2°19′ E) and 898 m altitude. A digital elevation model and a picture of the experiment site are shown in Fig. Fig. 4.21 and Fig. 4.22, respectively. The location of the radiometer, at a medium altitude and looking at the valley, allowed the observation of descending and ascending mountain slopes, as well as the observation of the transition between the mountain top and the sky. Measurements strategy is described hereafter.

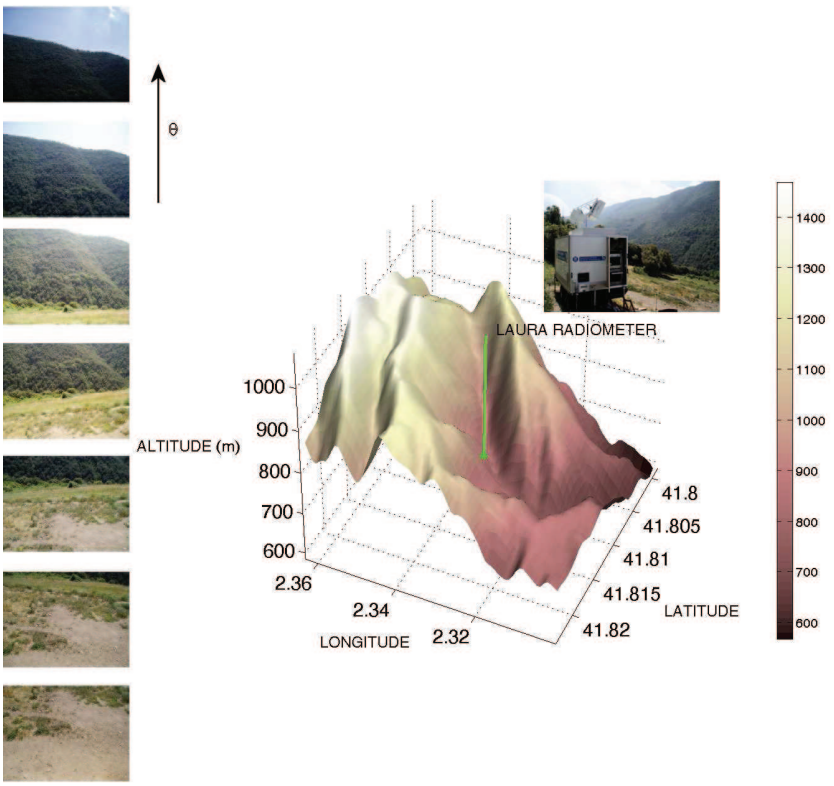

Fig. 4.21: Digital elevation model of the TuRTLE 2006 experiment site at El Brull, Montseny mountain, north of Barcelona, Spain. The position of the LAURA radiometer is indicated with a green dot. A picture of the pixel observed by the radiometer at a fixed azimuth angle and varying antenna elevation angle is shown.

4.8.1 Radiometric measurements

The site was observed using LAURA at seven antenna elevation angles (θ_A), which are not equal to incidence angle at the observed pixel (θ_{local}) due to topography. The antenna elevation angle with respect to nadir varied from 45° to 105°, in 10° steps, so that the descending slope of the valley, the mountain ascending slope, and the mountain-to-sky transition were observed during a complete scan in elevation. For every θ_A, the antenna azimuth angle (φ_A) varied between 50° and 130° from the radiometer trailer's orientation, in 10° steps. Figure 4.22(a) shows a picture of the experiment site. The position of the radiometer and the portion of site observed by LAURA during a complete scan in elevation and azimuth have been highlighted in red. To illustrate the nature of the pixels observed at each radiometer position, a picture taken at every combination of (θ_A, φ_A) is represented in Fig. 4.22(b). As it can be seen, various land covers, from almost bare soil to thicket and mixed forest (mainly oaks), were observed.

The radiometer kept looking at each position during three minutes with a sampling interval of 1 s. The average value of measurements was used to estimate the antenna temperature. Hot and cold load calibrations were performed every 2 hours as in Camps *et al.* [2004], using microwave absorbers and the sky as hot and cold load targets, respectively. Raw radiometric data acquired during one complete scan are represented in Fig. 4.23.

4.8.2 Ground-truth measurements

Soil samples of three different locations within the experiment site were collected to obtain the soil texture. The composition of soil was very homogeneous: sand content from 54.5% to 57.4%, and clay content from 12.1% to 12.6%. Therefore, the mean value (57.2% sand and 12.5% clay) was assumed as unique value for the whole site.

The average volumetric water content in the top 6 cm of soil was measured using a hand-held ThetaProbe (see Sections 4.2.1 and 4.2.1). Very low soil moisture values were measured (from 1% to 7% at most), since no rainfall events had been registered in the area in the previous three months. Soil temperature was measured at 0, 5, 10 and 15 cm depth using thermometers.

Atmospheric temperature at 2 m height, relative pressure, and accumulated rainfall data (0 mm during the experiment) were acquired by a weather station 15 km far from the site. The vegetation temperature was assumed to be equal to the atmospheric temperature at 2 m, while the vegetation water content (VWC) was obtained from the Montseny Natural Park database.

4.9 Conclusions

This Chapter summarises the six field experiments over land performed during the present Ph.D. Thesis:

- MOUSE 2004, which studies the impact of soil texture on soil moisture and temperature profiles, soil emissivity, and the impact on the soil moisture retrieval using multi-angular dual-polarization radiometric observations.

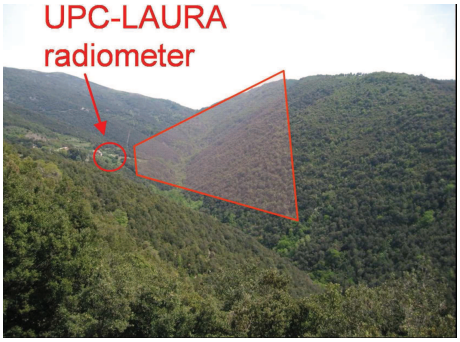

(a)

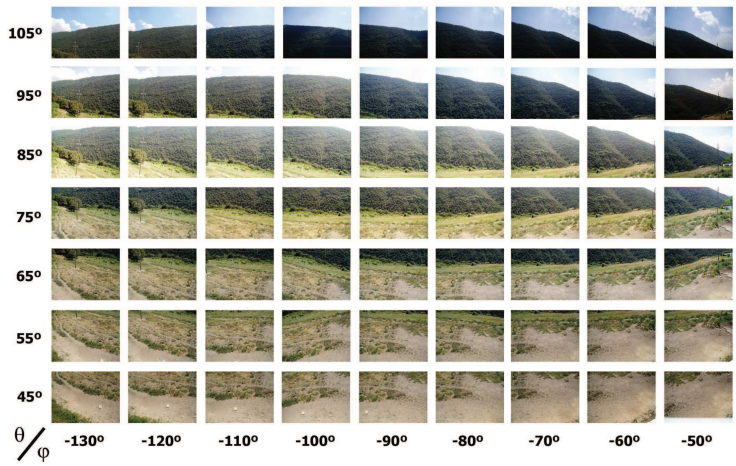

(b)

Fig. 4.22: (a) Picture of the experiment site. The position of the radiometer and the area observed during measurements are indicated in red. (b) A digital photo camera was mounted by the radiometer to take pictures of the pixel seen by the radiometer at every observation position. A picture per observation position is shown.

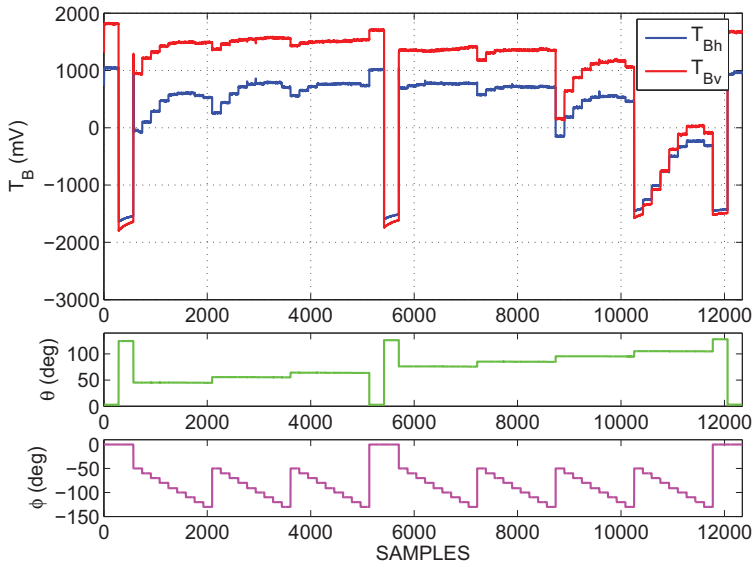

Fig. 4.23: Radiometric measurements acquired during TuRTLE 2006, DOE 6.

- T-REX 2004/2006, which aim to assess the impact of soil roughness on the brightness temperature.
- SMOS REFLEX 2003/2006, which study the effects of rock-fraction and vines. The brightness temperature dependence on soil moisture and observation angle was studied, and soil moisture retrieval was discussed. The experiment site in Valencia has already been selected as a SMOS calibration and validation site.
- TuRTLE 2006, which studies the impact of topography on soil emissivity at L-band.

The execution of these experiments, the data processing, and the physical interpretation of measurements constitutes the core of this Ph D Thesis. Next chapters analyse all these measurements, which will be compared to existing theoretical and semi-empirical land emission models.

Chapter 5

Texture effects on the L-band emissivity of bare soils

Soil emission at microwave frequencies is related to soil water content by the dielectric constant. The dielectric constant is a measure of the soil response to an electromagnetic wave and may be estimated with a dielectric mixing model. It is frequency dependent and principally determined by the soil water content, but also dependent on factors such as soil texture, salinity and temperature [Schmugge, 1980, Wang, 1983, Rouse, 1983]. This chapter presents some results of the Monitoring Underground Soil Experiment (MOUSE) which was carried out to study the impact of texture on the soil moisture and temperature profiles, and on the soil emission and soil moisture retrieval.

5.1 Overview of the MOUSE 2004 experiment

The Monitoring Underground Soil Experiment (MOUSE) 2004 was performed from DoY 159 to 184, 2004, at the Joint Research Centre (JRC) complex of the European Union in Ispra, north of Italy (45° 48′ N, 8° 37′ E, 213 m altitude; Fig. 5.1). This site was originally built for antipersonnel land mine detection studies and, therefore, it was fully instrumented. The test lane consisted of six 6 m long by 6 m wide by 1 m depth flat bare plots of different soil types which are distributed along a lane with West-East orientation. Five of the plots were open to the sky and separated from each other by textile membranes, whereas the sixth one was kept dry by using a sliding tent. The LAURA radiometer, an infra-red video-camera (3.6–5 μm), and the control rack were installed on a metallic gantry guided by a rail on one side and freely rolling on the other. The gantry was used to position LAURA at any point of the test lane. The site had a permanent ground installation which included thermocouples and moisture sensors buried at various depths and connected to automatic data-loggers, and a meteorological station [Lewis & Logreco, 2002]. For pictures, diagrams, and further information refer to Chapter 4, Section 3.

(a) (b)

Fig. 5.1: (a) Google-Earth image of the MOUSE 2004 experiment site at the ESA's Joint Research Centre, Ispra, Italy. (b) The LAURA radiometer mounted on a rolling gantry during MOUSE 2004.

5.1.1 Ground measurements of soil temperature and moisture

Soil temperature was measured using 107 probes from Campbell Scientific installed just below the surface, and at 5 cm and 10 cm depth. The nominal accuracy is ±0.4 °C over the range -20 °C to 4 °C , while the measured accuracy was verified found to be better than ± 0.3 °C . An infra-red video camera was mounted by LAURA to acquire soil surface temperature images concurrently with the radiometric measurements. Most probably, satellite-borne radiometers will have to rely on this kind of auxiliary sensors to estimate soil moisture from radiometric observations. The mean value of the IR soil temperature images agreed well with surface thermistors, but had a peak-to-peak deviation of 3 K caused by the sparse vegetation litter which was not sensed by the buried probes. Figure 5.2 represents the ground soil temperature measurements acquired during MOUSE 2004. Colours stand for the depth at which the sensors were installed: blue (soil surface), red (5 cm), and green (10 cm). Since the experiment was performed during June and the weather was warm at the site, strong daily gradients of surface soil temperature (up to 25 °C) are observed, specially for the sandy (SA) and ferromagnetic (FE) plots. Note that although the RS plot was also sand, the soil did not heat so much as SA since RS was covered by a tent and was not exposed to Sun radiation. The same occurred for clay which, although being exposed to Sun radiation, did not heat as much as other soil types because its mean water content was on the order of 10% during the experiment.

On the other hand, soil moisture profiles were automatically acquired every 30 min by seven ML2x Thetaprobes per plot installed with the rods inclined 20° down below the surface (×2), and at 5 cm (×2), 10 cm (×2), and 15 cm (×1) depth. Sensors had been calibrated by JRC personnel according to the probes user manual [Miller & Gaskin, 1999, pp. 10–11]. A third order polynomial,

$$\sqrt{\varepsilon_s} = 1.07 + 6.4V - 6.4V^2 + 4.7V^3, \tag{5.1}$$

was found to fit the relationship between the voltage measured by the probe, V (in mV), and the square root of the soil dielectric constant, $\sqrt{\varepsilon_s}$, for all soils. The conversion from $\sqrt{\varepsilon_s}$ to

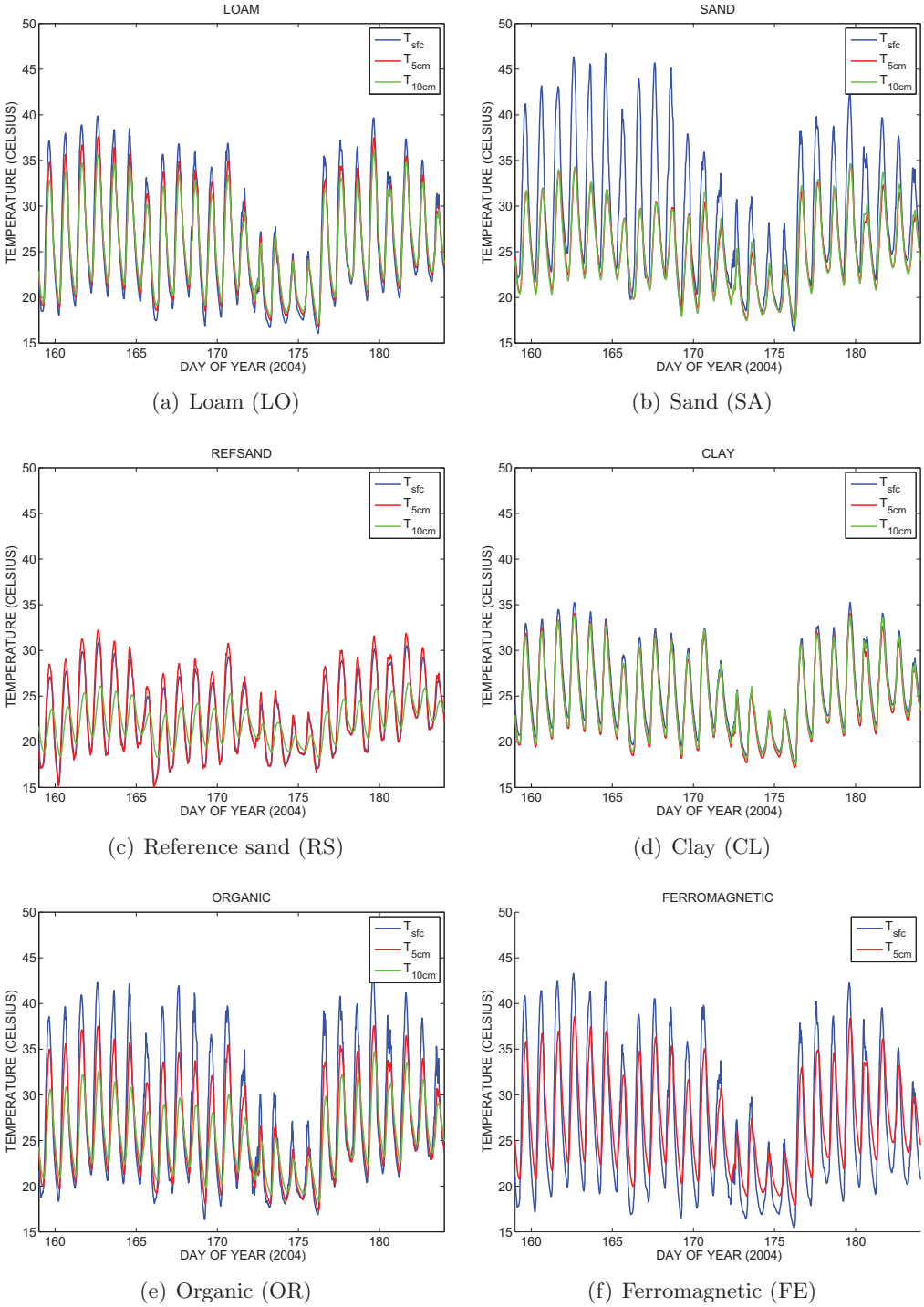

(a) Loam (LO)

(b) Sand (SA)

(c) Reference sand (RS)

(d) Clay (CL)

(e) Organic (OR)

(f) Ferromagnetic (FE)

Fig. 5.2: Ground-truth soil temperature measurements acquired during MOUSE 2004 experiment. Colours indicate the depth at which the sensors were installed: blue (surface), red (5 cm), and green (10 cm).

soil water content w_s was done according to Miller & Gaskin [1999, p. 11], which conveys with the linear relationship proposed in Topp *et al.* [1980] and White *et al.* [1994],

$$\sqrt{\varepsilon_s} = a_0 + a_1 w_s, \tag{5.2}$$

where the variables a_0 and a_1 are soil-dependent. Dirksen & Dasberg [1993] noted that expressions in Topp *et al.* [1980] are only valid for soils with low clay content and typical bulk densities. However, (5.2) was found adequate for all the soils at the experiment site, but FE. An extra free parameter had to be added to the fitting curve for FE. Further information on the sensors calibration may be found in Lewis & Logreco [2002].

Plots were irrigated three times during the experiment, except RS which was kept dry and protected from water by a sliding tent. The soil moisture profiles acquired during some days after the first irrigation, which was done on DoY 160, are shown in Fig. 5.3. It is noted that soil texture affects the moisture profile: soils with high sand content dry faster than other soils, whereas clays hold much more water and dry slowly. Water rapidly penetrates through sandy soils, which consequently have the shortest drying period.

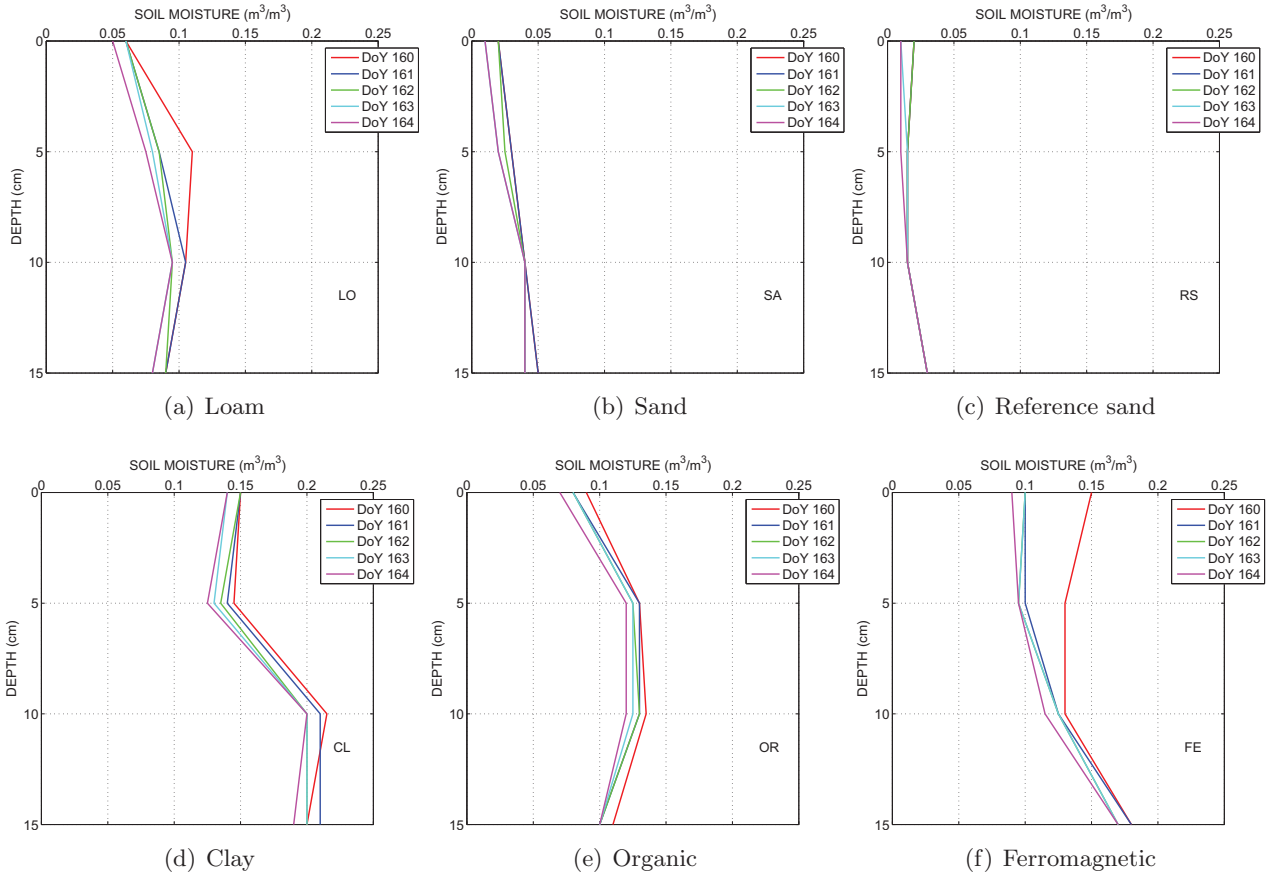

(a) Loam (b) Sand (c) Reference sand

(d) Clay (e) Organic (f) Ferromagnetic

Fig. 5.3: Soil moisture profiles acquired during the first week of MOUSE 2004 experiment. Colours indicate the DoY, being DoY 160 the date of irrigation.

5.1.2 Ground measurements of soil roughness and texture

Soils at the experiment site were loam (LO), natural sand (SA), sieved sand used in the construction industry (RS), clay from rice fields (CL), a mixture of loam and of commercial products for gardening (OR), and ferromagnetic crushed volcanic soil from Naples (FE). Their label, textural composition, bulk density, wilting point, transition moisture, and roughness standard deviation and correlation length are indicated in Table 5.1. Soil roughness was measured three times per plot during the experiment, taking a sample every 5 mm along a 1.5 m long transect. Figure 5.4 represents the roughness profiles of each of the plots. The ratio between the standard deviation of height and the wavelength at L-band (21.43 cm) remains much smaller than one which indicates that soils are electromagnetically smooth at this frequency [Ulaby *et al.*, 1986, Fung, 1994].

5.2 Dielectric constant of soils

5.2.1 Laboratory measurement of the dielectric constant of soils

Samples of the soils at the experiment site were collected and their dielectric constant was measured at the laboratory. The measurement setup was the same as in Blanch & Aguasca [2004], and has been shown in Fig. 5.5. The technique is based on a strip-line structure where a cylindrical conductor (270 mm length and 3 mm diameter) is placed between two parallel plates (100 mm × 270 mm) separated 10 mm. Samples of the soils were positioned between the plates, and the strip-line was connected to a Vector Network Analyser (VNA) through coaxial cables to obtain the S-parameters of the structure and, from them, its complex dielectric constant for different moisture contents. Almost no dependence of the dielectric constant on frequency was appreciated within the range of measurements (1.2–2.5 GHz). Soils were carefully manipulated to minimise the variation of their properties. Measurements procedure is summarised hereafter:

1. Soil samples are dried inside an oven at 100 °C to obtain a 0% reference humidity.
2. Samples are introduced between the plates. The structure is weighted.

Table 5.1: Soil characteristics of the six plots at the MOUSE 2004 experiment site

Label	Roughness (mm)		Soil texture (%)		Bulk density (g/cm^3)	Wilting point (%)	Trans. moist. (%)
	std. dev.	corr. length					
	σ_s	l_c	Sand	Clay	ρ_b	WP	w_t
LO	5.9	57.4	78	2	1.45	2.7	17.84
SA	4.2	34.1	95	0	1.46	0.7	16.84
RS	7.02	63.2	96	0.5	1.61	0.9	16.93
CL	2.5	81.3	15	40	1.56	24.9	28.72
OR	8.1	68.7	78	2	1.28	2.7	17.84
FE	4.1	39.4	82.5	2.5	1.72	2.7	17.82

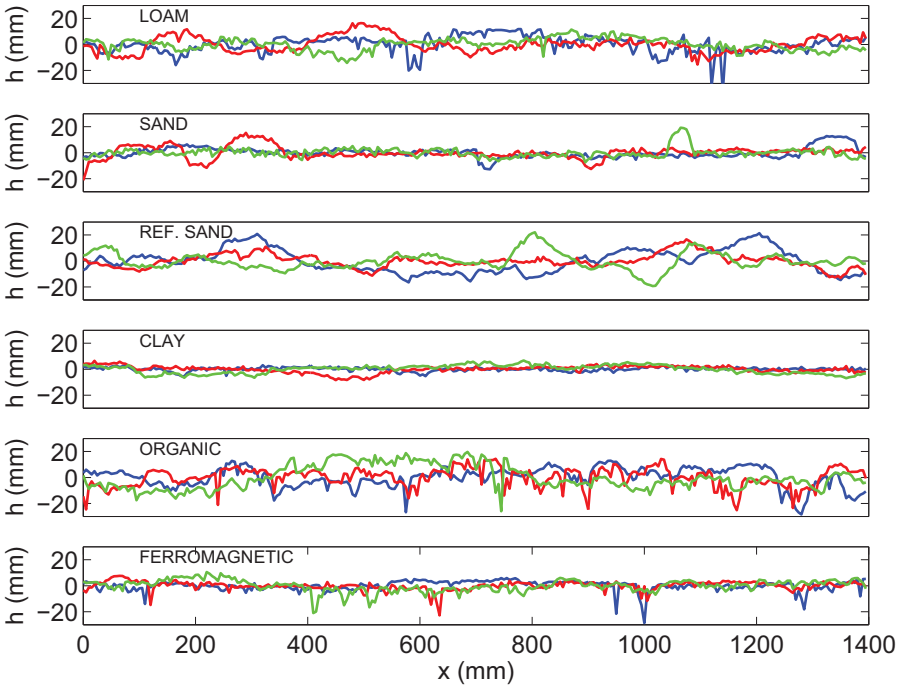

Fig. 5.4: Soil height profiles of each of the six plots measured during MOUSE 2004 experiment. Each colour indicates a different roughness measurement.

3. The VNA is calibrated.

4. S-parameters from the soil sample are measured and, from them, the dielectric constant is estimated.

5. 27 ml of water, which corresponds to a 10% increment in soil moisture, are uniformly distributed in the cavity.

6. The new sample is weighted again, and S-parameters are measured using the VNA.

7. Steps 5 and 6 are repeated by introducing controlled amounts of water to obtain increasing levels of moisture contents.

More information on the dielectric constant measurements can be found in the Master Thesis by Cardona [2005].

Coefficients of the best-fit second order polynomials derived from measurements as a function of the soil water content are indicated in Table 5.2. These coefficients are valid only for these data and can not be generalised, but they are useful in the context of this experiment for interpreting results. If the soil brightness temperature at nadir is simulated using the expressions derived from laboratory measurements and an effective soil temperature of 15 °C , differences in brightness temperature can be up to 28 K for dry soils, slowly decreasing as soil moisture increases (see Fig. 5.6). This fact suggests, as other authors pointed in the past [Schmugge, 1980, Wang, 1983], that the effect of texture on the brightness temperature and, thus, on the retrieval of geophysical parameters cannot be neglected.

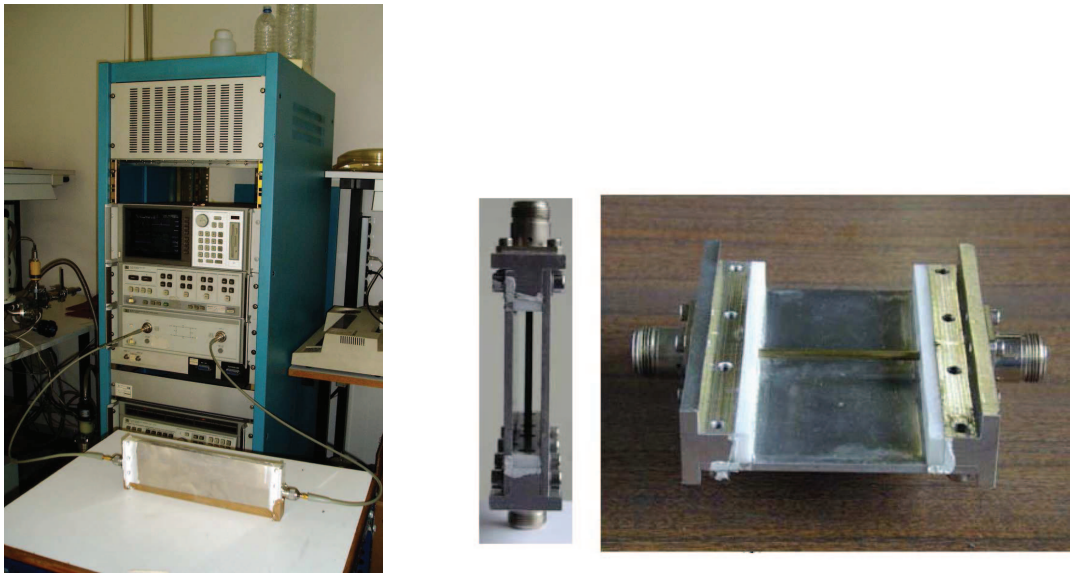

(a) (b)

Fig. 5.5: (a) Laboratory setup for measuring the dielectric constant of the experiment site soils. (b) Detail of the strip-line structure used to measure the dielectric constant. Top outer conductor has been removed.

Table 5.2: Coefficients of the best-fit polynomial for the measured dielectric constant of soils as a function of the water content w_s ($\varepsilon_s = \varepsilon'_S + j\varepsilon''_s$, $\varepsilon'_s = a_1 w_s^2 + b_1 w_s + c_1$ and $\varepsilon''_S = a_2 w_s^2 + b_2 w_s + c_2$)

Label	ε'_S			ε''_S		
	a_1	b_1	c_1	a_2	b_2	c_2
LO	98.328	13.848	2.39	2.09	7.67	- 0.093
SA-RS	149.113	- 4.157	2.448	3.068	4.945	0.019
CL	149.183	- 0.084	3.536	9.538	4.526	0.546
OR	125.73	5.05	1.143	8.73	4.39	- 0.108
FE	124.02	17.51	3.163	12.99	2.96	0.112

5.2.2 Comparison of different dielectric constant approaches

Figure 5.7 shows the dielectric constant of the site soils as a function of soil moisture. Dielectric constant values have been estimated from the laboratory measurements reported in Section 5.2.1, and from the semi-empirical models in Wang & Schmugge [1980] and Dobson *et al.* [1985]. Both models take into account the soil texture, but Wang & Schmugge [1980] has the particularity of also distinguishing between bound water and free water fractions by including the transition moisture term, w_t. The transition moisture refers to the soil moisture content at which the free water phase begins to dominate the soil hydraulics, and is estimated from the wilting point, WP (see Chapter 3). Values of these two parameters for the MOUSE 2004 site soils have been indicated in Table 5.1.

The effect of bound water is clear in Fig. 5.7(a), which shows results for the Wang &

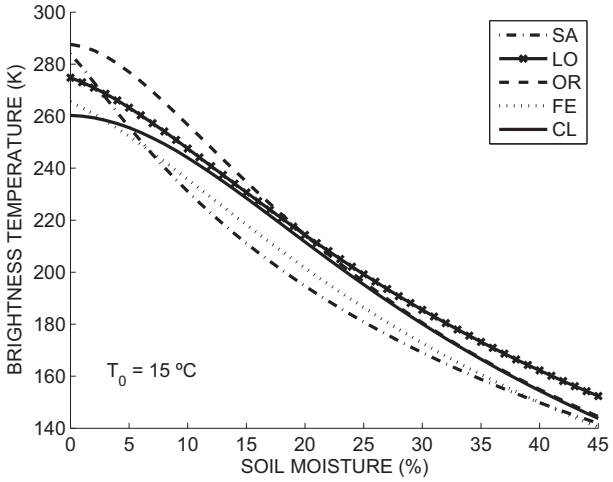

Fig. 5.6: Soil brightness temperature dependence on soil type and moisture at nadir, $T_0 = 15\,^{\circ}\mathrm{C}$. Values for each of the six soils at the MOUSE experiment site are represented.

Schmugge [1980] model. For soil moisture values above the transition moisture the dielectric constant rises faster and has an almost linear trend. This occurs at $w_s \simeq 0.17$ m^3/m^3 for all soils at the MOUSE 2004 site, but CL that has a $w_t = 0.29$ m^3/m^3. So, for a given soil moisture, clays' dielectric constant will be lower than sands' or loams'. On the other hand, the Dobson *et al.* [1985] model predicts almost the same dielectric constant as Wang & Schmugge [1980] for CL in the lower moisture range (up to 0.25 m^3/m^3), but much higher dielectric constants for all other soils (see Fig. 5.7(b)).

Dielectric constant curves in Fig. 5.7(c) are similar to those in Fig. 5.7(a) for $w_s < 0.3$ m^3/m^3. Above this moisture predictions have an intermediate value between those from Wang & Schmugge [1980] and Dobson *et al.* [1985]. However, since laboratory measurements were done until a maximum moisture content of 0.4 m^3/m^3, predictions for higher moisture may not be correct. These observations were also noted in the work by Owe & de Griend [1998], who found out that the Wang & Schmugge [1980] model agreed better with laboratory dielectric constant measurements than Dobson *et al.* [1985].

5.3 Temporal variation of the emissivity

Figure 5.8 represents the emissivity variation with time for all fields and two incidence angles. Blue lines stand for V-pol while red lines stand for H-pol measurements. There are some missing data in some plots due to technical problems or interferences.

Soils were irrigated on DOY 160, 169, and 173, and rainstorms were registered on DOY 180. A decrease in the measured emission is observed on these dates at each plot, but RS which, as was said previously, was protected from water and kept dry.

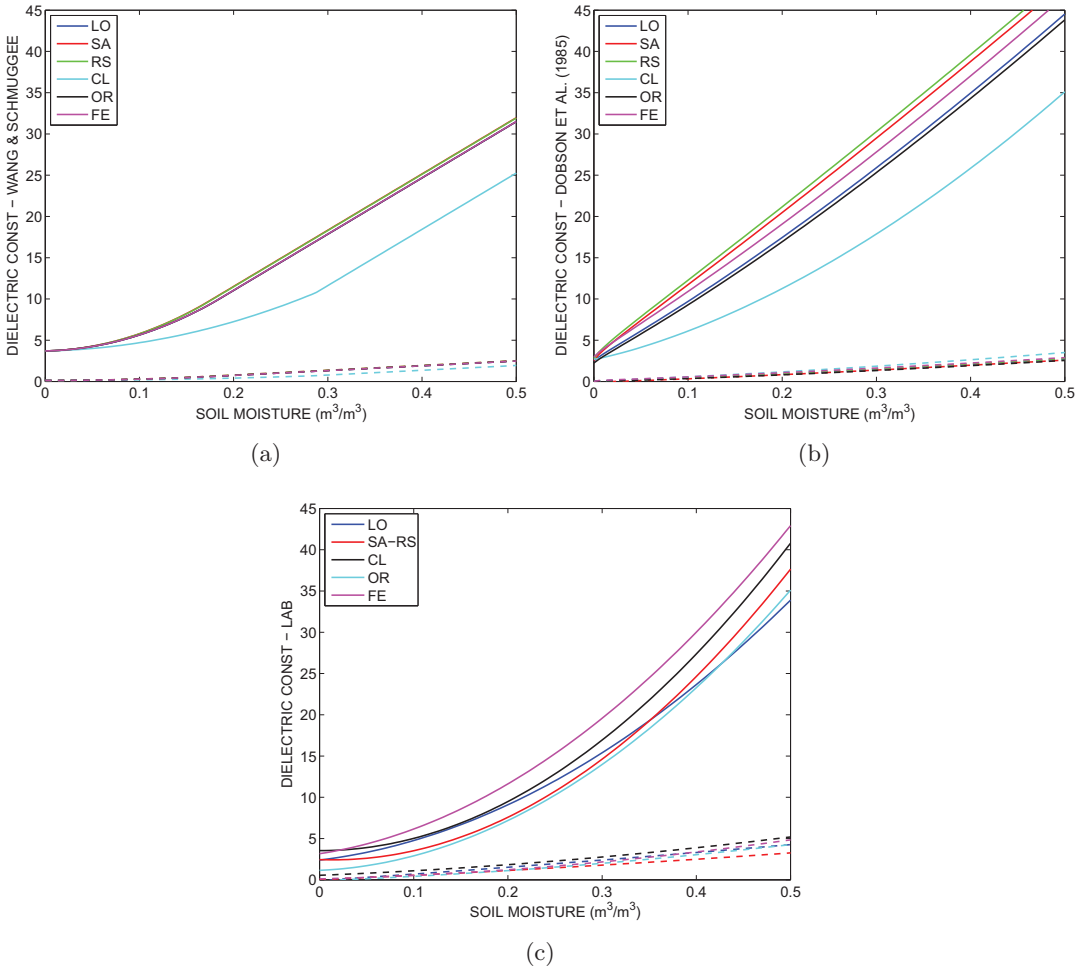

Fig. 5.7: Variation of the dielectric constant with soil water content. Values for the six soils at the experiment site and for the (a) Wang & Schmugge [1980], (b) Dobson *et al.* [1985], and (c) laboratory measurements have been represented.

5.4 Variation of the emissivity with soil moisture and texture

The variation of the measured emissivity at H- (left) and V-polarisation (right) with the ground-truth soil moisture in the 0-6 cm layer is represented in Fig. 5.9. Measurements for three incidence angles (θ=25° , 35° , and 45°) and all fields have been plotted. Measurements for the other two incidence angles have been discarded because unfortunately measurements were very much affected by interferences. As expected, the highest the soil moisture the lowest the measured emission at both polarisations, which also decreases with increasing incidence angle.

Sands and clay registered the lowest and highest soil moisture during the experiment, respectively. Although plots were irrigated three times until saturation, a look at Fig. 5.9 shows that the range of moisture values is rather low, which could be in part explained by a rapid water percolation to deeper soil layers during daytime before radiometric measurements began at night.

Table 5.3 indicates the goodness of a linear fitting between soil emission and soil moisture. A perfect fit would lead to $R^2 = 100\%$. Measurements of the loam and ferromagnetic soils show

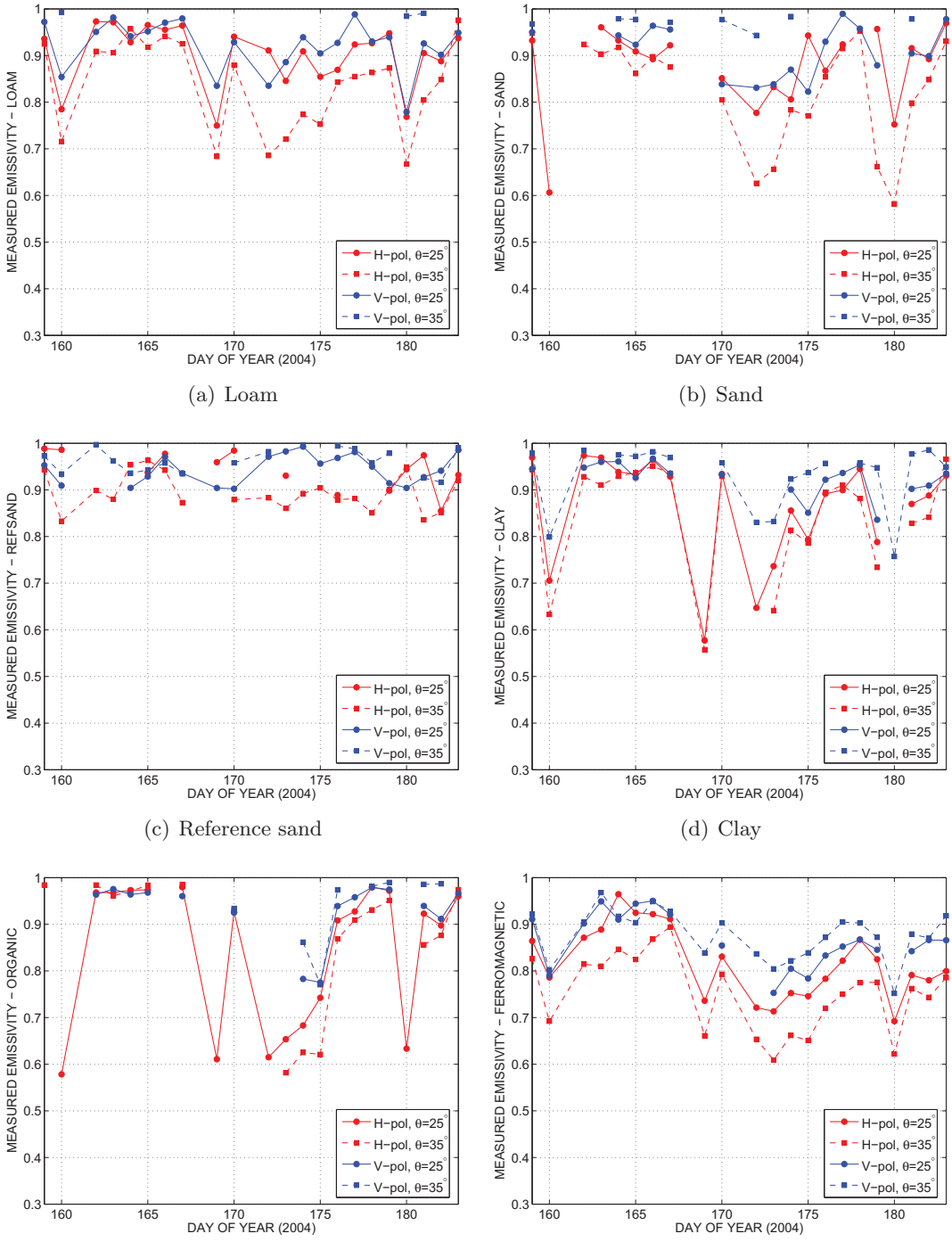

(a) Loam (b) Sand

(c) Reference sand (d) Clay

(e) Organic (f) Ferromagnetic

Fig. 5.8: Temporal variation of the measured emissivity for each soil type and two incidence angles.

an almost perfect linear relationship with soil moisture. The R-squared estimator for LO is up to 73% (88%) while for FE is up to 87% (95%) at H-(V-pol) and θ=35° . Clay has the worst fitting due to the large scattering observed in the measurements. In this case, R^2 is lower than 25% and, thus, the linear regression does not model the trend of the data.

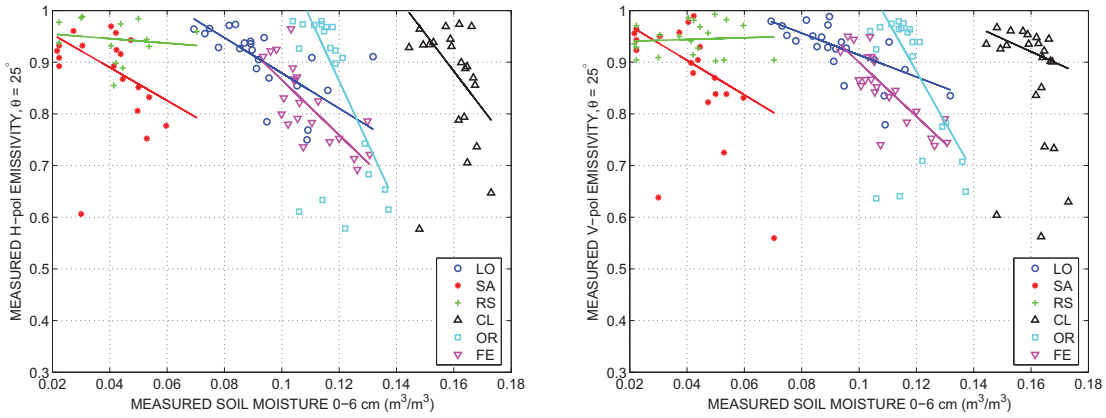

(a) θ=25°

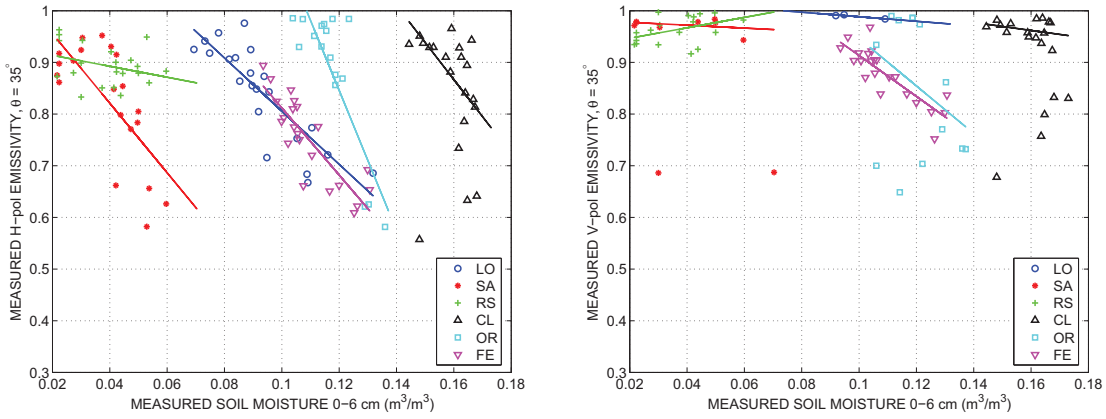

(b) θ=35°

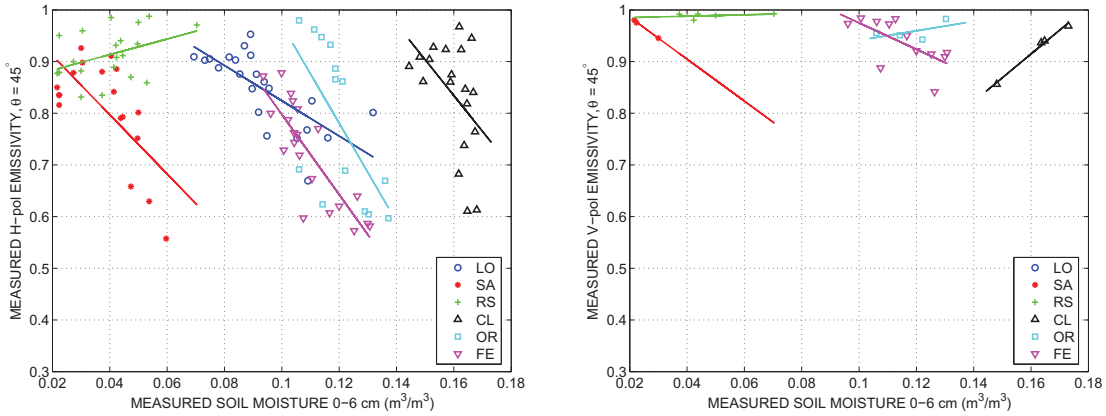

(c) θ=45°

Fig. 5.9: Variation of the measured emissivity at H- (left) and V-polarisation (right) with ground-truth soil moisture at an incidence angle of (a) θ=25° , (b) θ=35° , and (c) θ=45° . Each plot is represented with a different icon.

Table 5.3: R^2 (%) estimator of the goodness of the linear relationship between emissivity and soil moisture

Label	V-pol			H-pol		
	θ=25°	θ=35°	θ=45°	θ=25°	θ=35°	θ=45°
LO	49.25	88.34	-	31.55	72.95	57.01
SA	34.03	15.40	99.86	12.88	54.29	46.76
RS	44.78	63.07	98.71	68.61	66.10	82.76
CL	5.37	25.64	99.07	13.02	3.44	23.17
OR	20.53	58.93	44.38	26.00	69.16	44.08
FE	84.72	95.11	48.43	81.05	87.09	85.47

5.5 Variation of the emissivity with the field capacity

Figure 5.10 represents the sensitivity of the emissivity to the percentage of field capacity, which depends on soil texture. Measurements at vertical (top) and horizontal (bottom) polarisations have been plotted for three incidence angles: $\theta = 25°$ (blue), $\theta = 35°$ (red), and $\theta = 45°$ (green). The R^2 statistics of the linear regression between both variables has also been indicated to show the goodness of the fitting. Measurements of LO, RS, and FE have a linear dependence on field capacity, especially at H-polarisation. The R-squared estimator at θ=35° for LO at H-pol is 71%, for RS 70%, and for FE is 85%. As in the previous section, the clay has the worst linear fit, R^2 is lower than 20%.

5.6 Estimation of the soil moisture content from radiometric measurements

5.6.1 Cost function

Soil moisture is retrieved from measurements by an iterative least squares minimisation algorithm. The cost function F is a simplification of that in Camps *et al.* [2004], which accounts for the multi-angular and polarisation observation capabilities of SMOS and, thus, includes covariance matrixes which increase the computation time:

$$F = \sum_{\theta} \frac{(T_{Bh} - T_{Bh}^{\mathrm{meas}})^2 + (T_{Bv} - T_{Bv}^{\mathrm{meas}})^2}{\sigma_{T_B^2}} + \sum_{n} \frac{(P_n^{\mathrm{ini}} - P_n)^2}{\sigma_{P_n}^2}. \tag{5.3}$$

In the forward model, three soil dielectric constant predictions have been computed to estimate the brightness temperature at p-polarisation, T_{Bp}: the models by Wang & Schmugge [1980] and the Dobson *et al.* [1985], and the formulation derived from measurements of samples taken from the soils of the experiment site. The measured brightness temperature T_{Bp}^{meas} was derived from LAURA measurements. The symbol Σ indicates the summation of T_{Bp} for observation

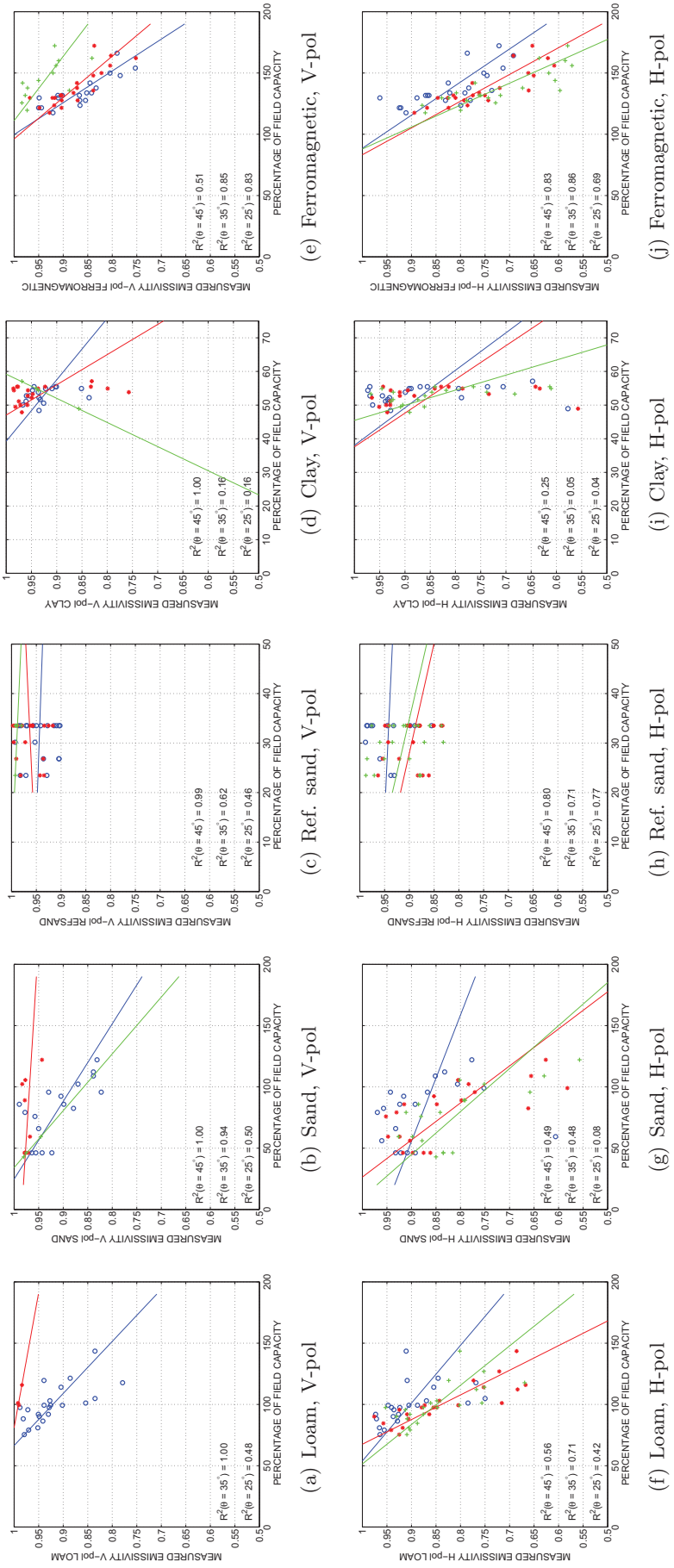

(a) Loam, V-pol (b) Sand, V-pol (c) Ref. sand, V-pol (d) Clay, V-pol (e) Ferromagnetic, V-pol

(f) Loam, H-pol (g) Sand, H-pol (h) Ref. sand, H-pol (i) Clay, H-pol (j) Ferromagnetic, H-pol

Fig. 5.10: Variation of the emissivity with the field capacity at vertical (top) and horizontal (bottom) polarisations. Colours indicate the incidence angle: $\theta = 25°$ (blue), $\theta = 35°$ (red), and $\theta = 45°$ (green).

angles between 25° and 45°, and P_n is any of the parameters on which T_{Bp} depends, namely soil moisture, soil temperature, and the roughness parameter. Although measurements at 55° and 65° were also acquired, they were discarded in the soil moisture retrieval because the interference level was too high for most of the plots.

An *a priori* estimate of the parameter P_n (P_n^{ini}) with associated standard deviation σ_{P_n} has been used. Estimates can be constrained to be close to the initial value by choosing low σ_{P_n} values, or they can be left as a free parameter by selecting $\sigma_{P_n} \gg 1$. Constraints, initial values, and boundaries of P_n are indicated in Table 5.4. The standard deviation of the brightness temperature σ_{T_B} was fixed to 0.5 K. The adequate selection of σ_{P_n} was found to be important for the convergence of the algorithm. Various tests using different combinations of the constraints and standard deviations in Table 5.4 were performed. Best results were obtained when the soil temperature T_s was left as a free parameter (large σ_{T_s} values) and h_s was constrained to be close 1 (small σ_{h_s} values) which is the value for smooth soils.

Table 5.4: Constraints and boundaries of the retrieved parameters. (LB, UB): Lower- and Upper-boundaries. k_λ: wave number. σ_s: standard deviation of soil roughness

P_n	P_n^{ini}	σ_{P_n}	LB	UB
T_s	$T_{\text{s,mean}}$	10^{-3},0.1,1,10	$T_{\text{s,mean}}$ - 3	$T_{\text{s,mean}}$ + 3
h_s	$4k_\lambda^2\sigma_s^2$,0	10^{-3},0.1,1,10	0	0.4
SM	-	-	0	0.4 m^3/m^3

5.6.2 Dependence on the dielectric constant model and texture

The estimated values for soil moisture have been compared with the measured soil moisture at different depths and the root mean square error (RMSE) has been obtained. Figure 5.11 shows the minimum soil moisture RMSE obtained considering different depths as ground-truth data and the three dielectric constant models. The depth of the soil layer whose emission is being sensed can be determined by comparing the retrieved soil moisture with the moisture profiles in Fig. 5.3):

1. Loam (LO) and Ferromagnetic (FE): Best results are achieved for the soil moisture in the 0–5 cm layer, but few discrepancies between RMSE values at different depths can be found out. This is in agreement with the assumption in the MOUSE 2004 preliminary study [Monerris *et al.*, 2006b] and is mainly due to the almost linear SM profile.

2. Sand (SA): Best results are obtained for the soil moisture in the 0–15 cm layer (as sandy soils dry faster, the penetration depth is higher).

3. Reference sand (RS): As this plot was kept dry throughout the experiment, no significative differences in the RMSE have been found in the comparison.

4. Clay (CL): This plot has high water content at 10 cm (~ 0.22 m^3/m^3) and hence the main signal contribution comes from the first 10 cm of soil.

5. Organic (OR): Similar RMSE values have been found considering either the 0–5 cm layer or the 0–10 cm layer as ground-truth. Similarities are because the water content at 5 cm and 10 cm depth is almost the same during the experiment.

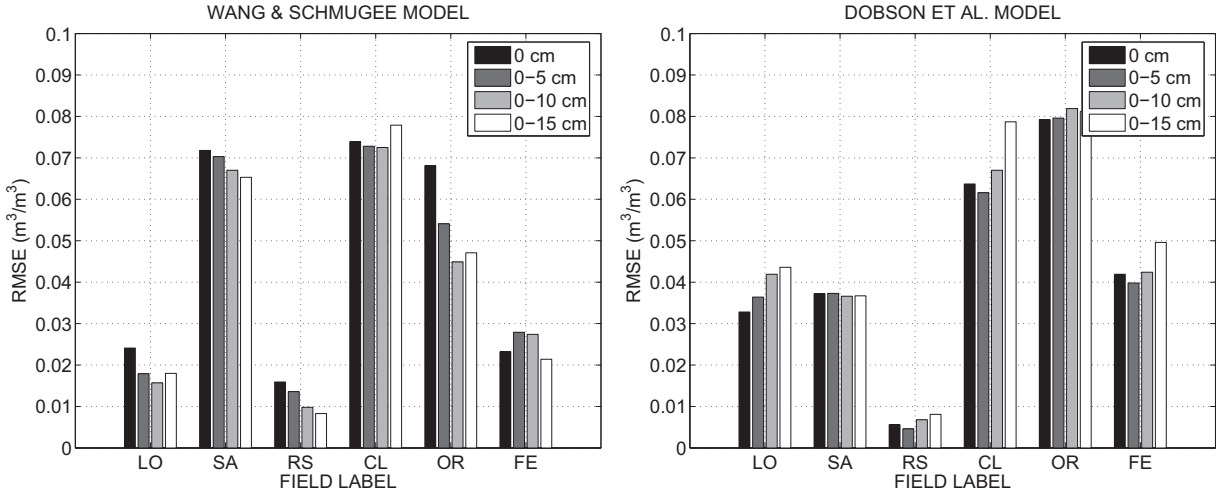

(a) Wang-Schmugge (b) Dobson et al.

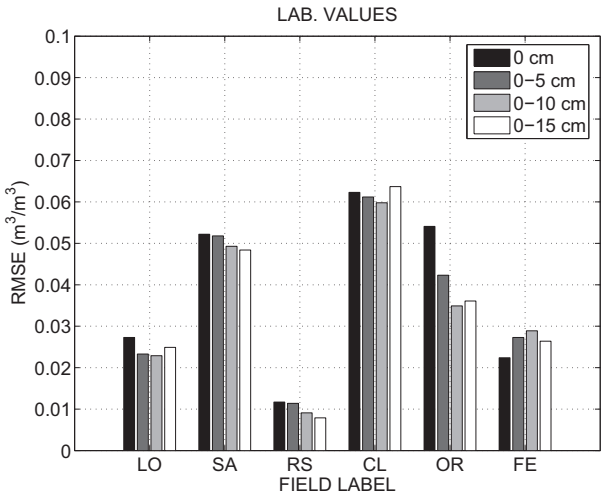

(c) Laboratory

Fig. 5.11: Minimum root mean square error of the soil moisture retrieval. Each plot depicts the results for a soil dielectric constant model while colours indicate the depth of soil moisture ground-truth data.

On the other side, in Fig. 5.11 it can be noted the performance of each dielectric constant models for each soil type. Results for Wang & Schmugge [1980] model are good for loamy and ferromagnetic soils, but their performance for sandy soils is worse than Dobson *et al.* [1985] and *Vall-llossera et al.* [2005b]. The model in Dobson *et al.* [1985] offers best results for sandy soils (SA and RS) which registered lower soil moisture values and dried faster than the others. The expressions derived from UPC laboratory experiments show good performance for most of the

soils. These facts confirm that the selected ε_S model has an impact on soil moisture estimation error and can increase it between 3 to 5% depending on the soil type.

5.7 Conclusion

The MOUSE 2004 experiment took place during the spring of 2004 at the Joint Research Centre outdoor test facility in Ispra, Italy. Six plots of different types of bare soil were measured under five incidence angles and moisture conditions. Concurrently with the radiometric measurements, the soil moisture, temperature, and roughness were measured.

The technique proposed by Blanch & Aguasca [2004] has been used to measure the dielectric constant ε_s of the soil types measured in MOUSE 2004. No variation of ε_s with frequency in the range 1.2-2.5 GHz was appreciated for any soil type and moisture content. As expected, both real and imaginary parts of the dielectric constant increase with water content. The real part of the dielectric constant measured using the Blanch & Aguasca [2004] technique is in better agreement with predictions from the Wang & Schmugge [1980] model. Errors in the estimation of the dielectric constant can lead to brightness temperature errors at nadir as high as 28 K for a soil surface temperature of 15 °C , which is an important uncertainty term in the retrieval of soil moisture values.

Soil emissivity has been derived from the radiometric measurements and then soil water content has been retrieved using three different soil dielectric constant models. Best results were obtained when the soil temperature T_s was left as a free parameter (high σ_{T_s} values) and h_s was constrained to be near 1 (low σ_{h_s} values). Results have been compared with the measured soil moisture at different depths and the RMSE has been obtained. For loamy and ferromagnetic soils best results are achieved considering as ground-truth data the soil moisture in the 0–5 cm layer, 0–15 cm layer for sandy soils, 0–10 cm layer for clay soils and 0–10 cm layer for organic soils. On the other side, retrieval results for Wang & Schmugge [1980] model are good for loamy and ferromagnetic soils, Dobson *et al.* [1985] model offers best results for sandy soils, and the expressions derived from UPC laboratory experiments show good performance for most of the soils. The development of improved soil emission models should be a priority in view of the upcoming missions devoted to the measurement of soil moisture from space. These must include a better parametrisation of the soil texture variability, the soil surface roughness, and the soil moisture and temperature profiles.

Chapter 6

Characterising the L-band emission from bare rough soils

Several experiments have been performed in the past years to study the L-band emission from bare soils, both at small and large scales. Although small scale measurements are not representative of onboard sensor data, they can be useful to evaluate the various approaches to the land emission modelling. This chapter presents the results from the T-REX 2004/2006 field experiments, which were conducted to characterise the emissivity of bare soils with different surface height profiles. Measured emissivity was compared to simulations using semi-empirical and numerical approaches as an exercise to determine which option describes the best the roughness impact on the soil emission.

6.1 Overview of the T-REX experiments

The Terrain-Roughness EXperiments (T-REX) were carried out in Agramunt, Spain (41° 48′ N latitude, 1° 7′ W longitude, 356 m altitude) from DOY 333 to DOY 337, 2004, and then again from DOY 143 to DOY 160, 2006. The sites consisted of bare soil plots with four different ploughing, but the same textural composition (21% clay, 21.3% sand, 0.25 m^3/m^3 field capacity). Each parcel was 6 m wide × 50 m long in T-REX 2004, and 6 m wide × 15 m long in T-REX 2006. The same ploughing was applied to two different plots to observe spatial diversity effects. LAURA was installed on a trailer towed by a car. As it can be seen in Fig. 6.1, the trailer's configuration changed between one experiment and the other.

Radiometric measurements were acquired at incidence angles of 30° , 35° , 40° , 45° , 50° , 55° , 60° , and 65° in T-REX 2004, and of 40° , 45° , 50° , 55° , 60° , and 65° in T-REX 2006. Every plough type was measured twice each day of experiment. Measurements of the cold sky and of a microwave absorber were acquired at the beginning and end of each measurement sequence, and used as cold and hot load calibrations, respectively.

(a) (b)

Fig. 6.1: View of the (a) T-REX 2004 and (b) T-REX 2006 experiment sites

6.1.1 Ground measurements of soil roughness

Roughness measurements were performed in the along and across directions of LAURA's field of view. The soil roughness profile was measured every 5 mm along a 1.5 m transect using a Leica Disto Pro4a distance meter controlled by a laptop computer. Results from these measurements showed no correlation with the direction of measurements and thus the roughness properties have been considered to be randomly distributed, and the average value of all replications has been considered. The standard deviation of height (σ_s) and the correlation length (l_c) of the ploughing at both experiment sites are summarised in Table 6.1. Two additional parameters have also been included: (i) $h_{\text{air-soil}}$, which is the transition layer thickness used to evaluate the small-scale soil roughness in the model proposed in Schneeberger *et al.* [2004], and (ii) σ_λ, which is the standard deviation of height assuming a windowing of length λ.

Table 6.1: Roughness characteristics of the T-REX ploughing

Parameter	T-REX 2006 labels				T-REX 2004 labels		
(mm)	A	B	C	D	E	F	G
l_c	126	100	190	96	110.73	116.36	162.21
σ_s	17	16.6	8	33	16	20	15
σ_λ	7	6.8	2.5	17	7.8	9.32	8.17
$h_{\text{air-soil}}$	31	26	13	46	30	35	28

6.1.2 Ground measurements of soil temperature and moisture

Soil temperature was measured using three PT-100 thermistors located just below the surface, at 5 cm, and at 10 cm depth during T-REX 2004, and at 0, 5, 10, 15, and 20 cm depth using thermometers during T-REX 2006. Very low soil surface temperatures, from 3 °C to 9 °C , were measured during the winter experiment T-REX 2004. In contrast, soil temperature during the T-REX 2006 reached up to 35 °C as shown in Fig. 6.2. The atmospheric temperature has been represented together with the soil temperature at surface level and down to 20 cm depth for all eight plots at the experiment site. Note that graphics in the left hand side of Fig. 6.2, which have higher soil temperatures, correspond to the ploughs which were measured first, right after sunset.

On the other hand, soil moisture was measured with ML2x ThetaProbe sensors at various positions within the radiometer's field of view. As the purpose of this experiment was to study the impact of soil roughness, the site was not irrigated to keep as constant a value of soil moisture as possible. The mean soil moisture during T-REX 2006 was of 4% to 6%. However, soil moisture changed during T-REX 2004 due to the persistent fog and precipitation. In this chapter, measurements of the first and last days of experiment are shown, which correspond to the soil moisture lower and upper values. These limits vary from 7% to 13.5% for plough E, 9.5% to 17.4% for plough F, and 6.8% to 14% for plough G.

Meteorological data of atmospheric temperature, relative pressure, and accumulated rainfall were obtained from a weather station located 18 km from the experiment site.

6.2 Reflectivity of bare rough soils

Natural soils have a certain roughness which is known to influence soil reflectivity. Several experiments have been performed to study the L-band emission from bare soils, both at small [Schneeberger *et al.*, 2004, de Rosnay *et al.*, 2006, Monerris *et al.*, 2006a,b, Paloscia *et al.*, 1993, Wigneron *et al.*, 2001] and large scales [Jackson *et al.*, 1999]. All of them show an increase in the measured emission with increasing soil roughness due to the increase in the soil area interacting with the atmosphere. Some of the existing approaches to model the roughness effects on the radiometric measurements were summarised in Chapter 3. They are divided into two approaches. The first one correspond to numerical methods based on the integration of the surface bistatic scattering coefficients [Fung, 1994, Ulaby *et al.*, 1986]. The second approach is based on semi-empirical models derived from experimental data and physical properties of the surface [Wang & Choudhury, 1981, Wegmüller & Mätzler, 1999, Wigneron *et al.*, 2001, Escorihuela *et al.*, 2007]. These last models are simpler and suitable to be used in soil moisture retrieval algorithms. In most cases, the soil reflectivity is estimated from the Fresnel reflectivity as $\Gamma_{op}(\theta)\exp(-h_s)$. The parameter h_s is usually empirically determined by best fit or from other roughness characteristics, but it is not well established yet.

In this chapter, measurements from the T-REX experiments are compared to soil emission predicted with both numerical [Ferrazzoli *et al.*, 2002, Fung, 1994] and semi-empirical approaches [Wang & Choudhury, 1981, Escorihuela *et al.*, 2007, Schneeberger *et al.*, 2004, Mo & Schmugge,

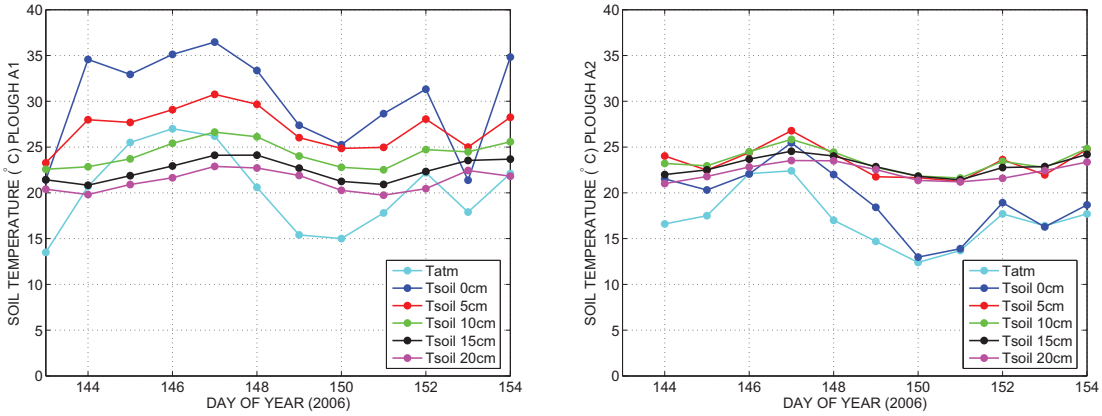

(a) Plough A

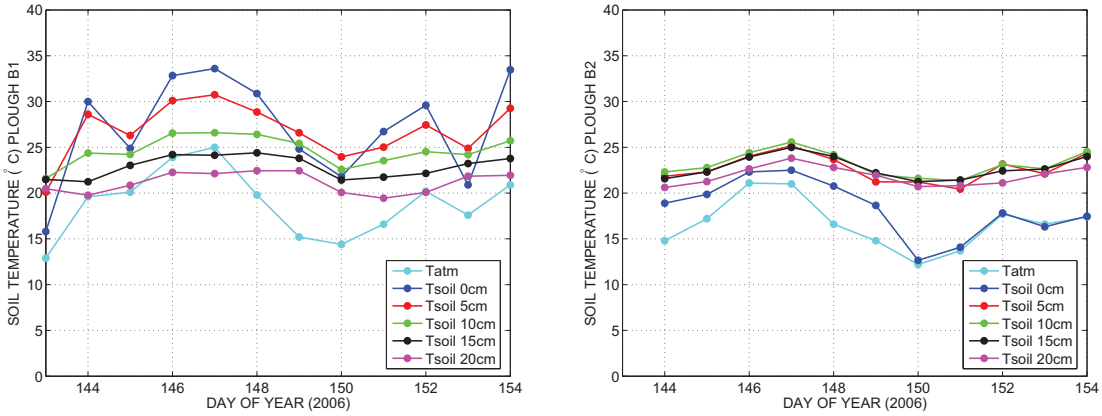

(b) Plough B

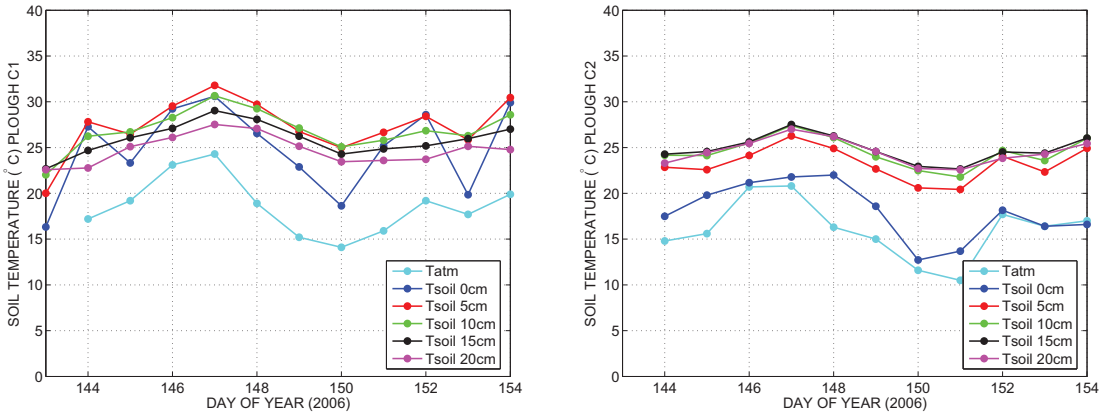

(c) Plough C

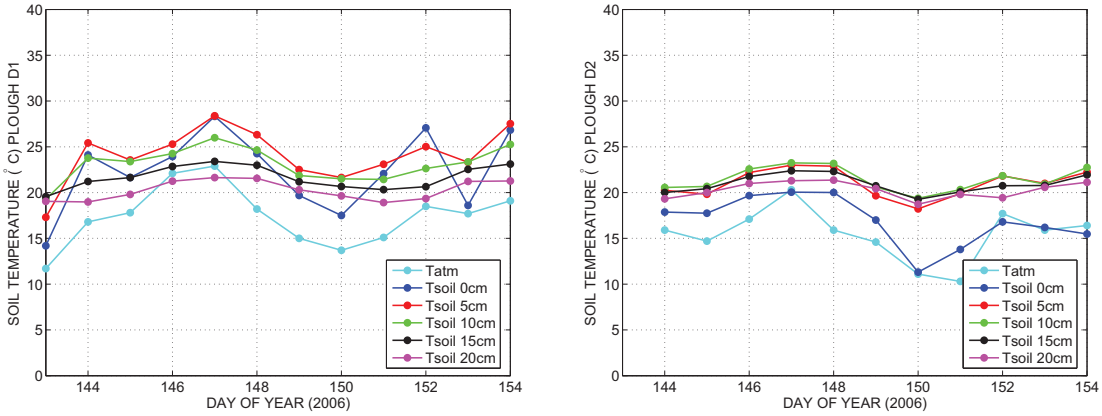

(d) Plough D

Fig. 6.2: Atmospheric and soil temperature during T-REX 2006 for every plot.

1987]. Expressions for the semi-empirical models have been summarised in Table 6.2 for completeness.

6.3 Variation of the measured emissivity with time

Figure 6.3 represents the variation with time of the emissivity measured during the T-REX 2006 experiment, at H- (red) and V-polarisation (blue). Values for the two plots with the same plough have been plotted together and are distinguished by the line style. Icons represent values for two incidence angles: circles indicate $\theta = 45°$ while squares indicate $\theta = 65°$. The mean and standard deviation of the soil emissivity for each plot during all the experiment at both incidence angles have also been plotted. Since the fields were not irrigated, and it did not rain during the experiment, radiometric measurements should be similar.

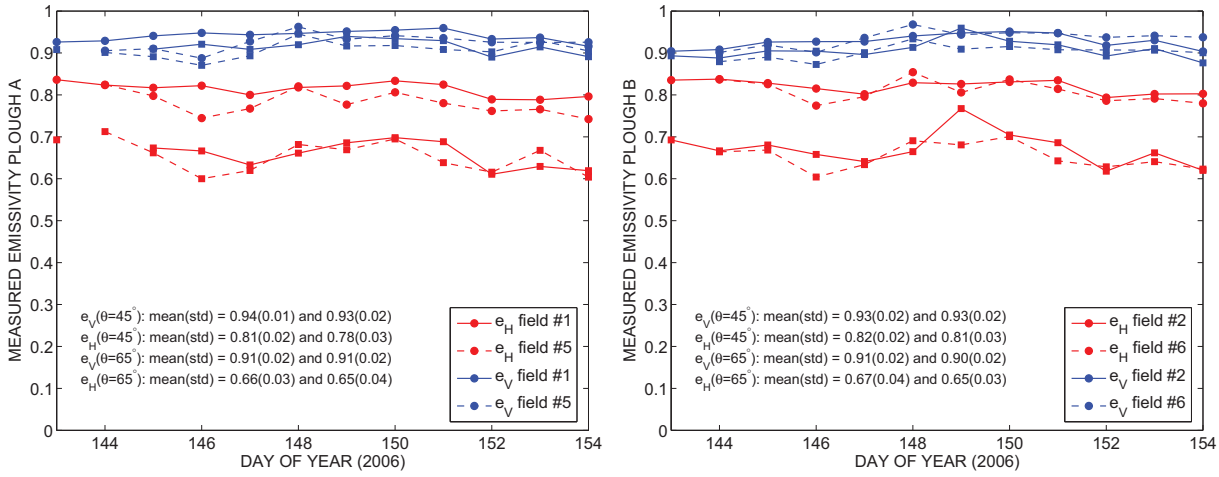

(a) Plough A

(b) Plough B

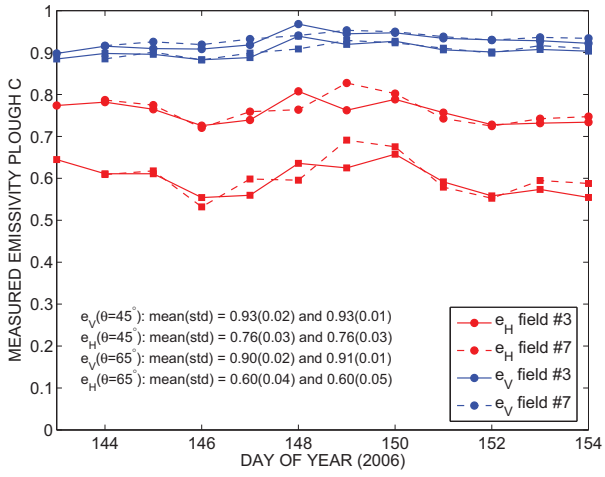

(c) Plough C

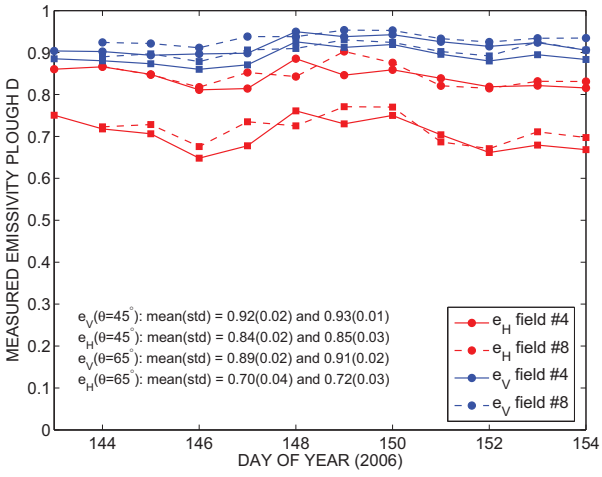

(d) Plough D

Fig. 6.3: Variation with time of the emissivity measured during the T-REX 2006 experiment, at H- (red) and V-polarisation (blue). Values for the two plots with the same plough have been plotted together and are distinguished by the line style. Icons represent values for two incidence angles: circles indicate $\theta = 45°$ while squares indicate $\theta = 65°$.

Table 6.2: Different formulations for semi-empirical estimation of the soil reflectivity $\Gamma_p(\theta)$

Model	$\Gamma_p^{coh}(\theta)$
Wang & Choudhury [1981]	$[(1-Q_s)\Gamma_{op}(\theta)+Q_s\Gamma_{oq}(\theta)]\exp(-4k_\lambda^2\sigma_s^2\cos^2\theta)$
Mo & Schmugge [1987]	$\Gamma_{op}(\theta)\exp\left[0.5761w_s^{-0.3475}(\frac{\sigma_s}{l_c})^{0.423}\right]$ $\Gamma_{op}(\theta)\exp\left[1.3972(\frac{\sigma_s}{l_c})^{0.5879}\right]$
Escorihuela *et al.* [2007]	$\Gamma_{ov}(\theta)\exp\left[-(4k_\lambda^2\sigma_s^2-4.4(w_s-0.3))/\cos^2\theta\right]$ $\Gamma_{oh}(\theta)\exp\left[-(4k_\lambda^2\sigma_s^2-4.4(w_s-0.3))\cos^2\theta\right]$

The vertical polarisation of dry soils seems to be almost independent on the incidence angle and soil roughness. Its mean value is in the order of 0.93 (0.91) at $\theta = 45^\circ$ (65°), and no significative variations with ploughing are found out. Radiometric measurements at horizontal polarisation are more sensitive to roughness, which is in accordance with results in the literature. It ranges from 0.76 for plough C (the smoothest) to 0.85 for plough D (the roughest) at $\theta = 45^\circ$. From Fig. 6.3 it is noted that the mean offset between H-pol measurements at $\theta = 45^\circ$ and $\theta = 65^\circ$ is equal to 0.16 ($\sim$ 47 K) and does not depend on the ploughing.

6.4 Variation of the measured emissivity with the incidence angle

Figure 6.4 represents the variation of the emissivity measured during the T-REX 2004 as a function of the incidence angle. Line style distinguishes between dry soil (solid line) and wet soil (dashed lines), while icons distinguish two plot with the same ploughing.

As expected, dry soil emissivity at horizontal polarisation decreases as the incidence angle increases, and the decrement is inversely proportional to the roughness. Similar emissivity values are observed for low incidence angles ($e_h(\theta = 35^\circ) \sim 0.9$), but, as the incidence angle increases, emissivity decreases slowly for rougher soils [plough E, $e_h(\theta = 65^\circ) = 0.7$] than for smoother soils [plough G, $e_h(\theta = 65^\circ) = 0.62$]. The same trend is observed for wet soils. However, the spatial variability is more noticeable since plots with the same plough had different soil moisture when they were measured. It is observed that the emissivity decreases faster above $\theta = 50^\circ$.

Roughness effect over emission at vertical polarisation is not as significant as over horizontal polarisation. When the soil is wet, e_v increases as the incidence angle increases, which is in accordance with most model predictions. However, the trend for dry soils is decreasing with increasing incidence angle and roughness, but the dynamic range is less than 0.1.

In Fig. 6.5 the variation of the emissivity measured during the T-REX 2004 as a function of the incidence angle for the three ploughs has been represented. Icons represent the ploughing: squares plough E, circles plough F, and diamonds plough G, while line styles indicate whether

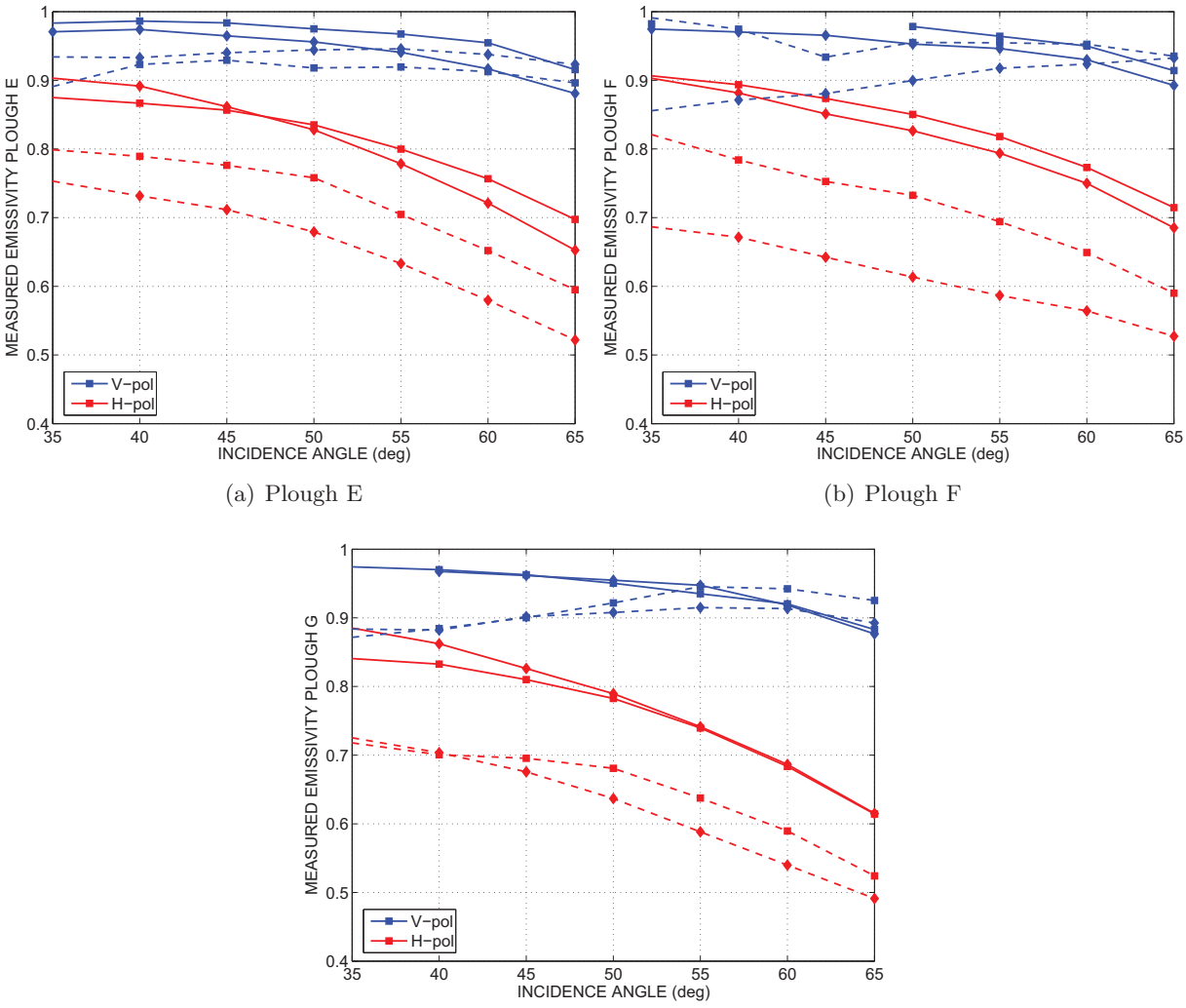

(a) Plough E

(b) Plough F

(c) Plough G

Fig. 6.4: Variation of the emissivity measured during the T-REX 2004 as a function of the incidence angle. Line style distinguishes between dry soil (solid line) and wet soil (dashed lines). Icons distinguish between two plots with the same ploughing.

the soil was dry (solid line) or wet (dashed-line). The increment in soil moisture between both days of experiment is in the order of 7% for all ploughs. Despite of this, the offset between dry and wet soil measurements at H-pol is rather different, being ∼0.3 for the smoothest plot (G) and 0.15 for the other two ploughing.

On the other hand, the variation of the emissivity measured during the T-REX 2006 experiment as a function of the incidence angle is shown in Fig. 6.6. Colours indicate the polarisation: H-pol (red) and V-pol (blue). Error bars indicate the standard deviation of measurements for the whole experiment, while lines indicate the mean value at each incidence angle. The trend is similar to that from T-REX 2004 dry soil measurements. While soil emission at H-pol decreases almost linearly with increasing incidence angle (and the trend is more significative at θ above 55°), the emission at V-pol slightly decreases with incidence angle until an inflexion point at θ = 55° , when it begins decreasing.

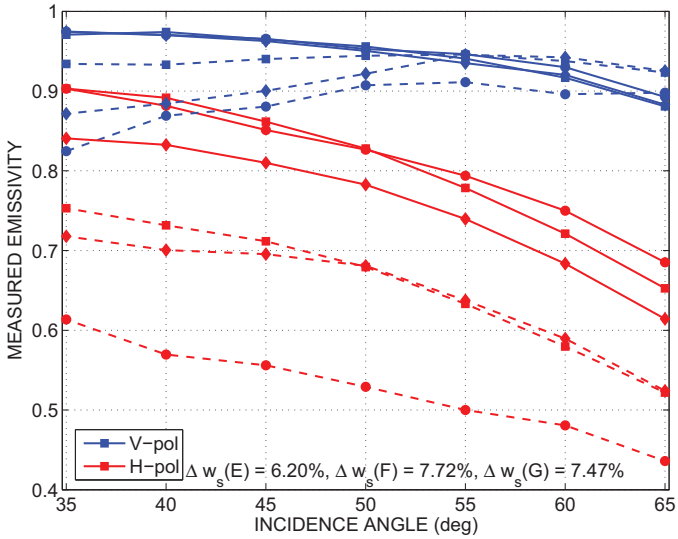

Fig. 6.5: Variation of the emissivity measured during the T-REX 2004 as a function of the incidence angle for the three ploughs. Colours indicate the polarisation: H- (red) and V-polarisation (blue). Line style distinguishes between dry soil (solid line) and wet soil (dashed lines). Icons represent the ploughing: squares plough E, circles plough F, and diamonds plough G.

The roughness effect is also shown in Fig. 6.7. In this case, line style and icons distinguish different plots with the same plough. Ploughs C and D, which correspond to the smoother and rougher plots in the site, have the highest (lowest) difference between V- and H-polarisation emissivities, respectively.

6.5 Comparison between measurements and simulations

6.5.1 Comparison with IEM predictions

In this section, radiometric measurements are compared to numerical simulations obtained with a numerical approach by means of the integral equation method (IEM, Fung [1994]). This work was performed during a stage at the Università Tor Vergata of Rome, Italy, in collaboration with the group of Prof. P. Ferrazzoli. Simulations were performed assuming three possible cases: Gaussian profile, exponential profile, and only coherent components of the soil emission. Inputs to the model are the soil moisture and temperature, the frequency of measurements, and the l_c and σ_s indicated in Table 6.1.

Figure 6.8 shows the variation of the emissivity measured during the T-REX 2004 experiment with the incidence angle. LAURA measurements (black icons) have been represented together with IEM simulations. Line style indicates V-pol (solid line) or H-pol (dashed-dotted line). The root mean squared error in emissivity between IEM predictions and LAURA's measurements for every plough and IEM configuration is summarised in Table 6.3.

IEM predicts an increase of the vertical emission with incidence angle, but this is only true for wet soils (right-hand side plots), since, as was pointed out in the previous section, dry soil measurements ($w_s < 10\%$, right-hand side plots) at V-pol decrease almost linearly with increasing incidence angle. T-REX 2004 measurements at H-pol decrease with incidence angle

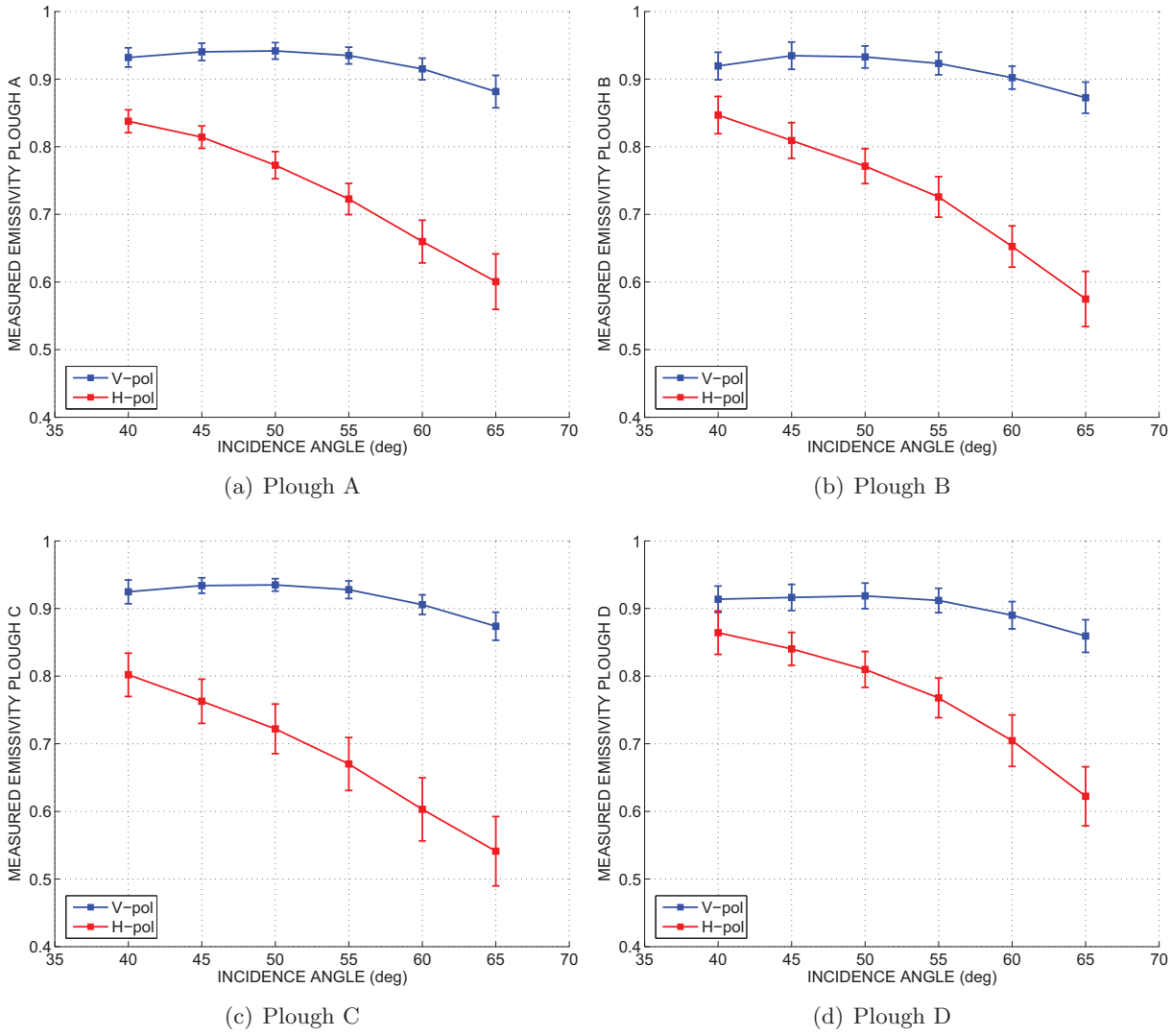

(a) Plough A

(b) Plough B

(c) Plough C

(d) Plough D

Fig. 6.6: Variation of the emissivity measured during the T-REX 2006 experiment as a function of the incidence angle. One plot per ploughing type has been included. Colours indicate the polarisation: H-pol (red) and V-pol (blue). Error bars indicate the standard deviation of measurements for the whole experiment at each incidence angle, while lines indicate the mean value.

as predicted by IEM, but they do it more slowly than predictions say, both for dry and wet soils. From Fig. 6.8 and Table 6.3 it is seen that the impact of choosing an exponential or gaussian height probability density function is minimum, and that the incoherent term of the reflectivity must be considered for rough soils.

Results for T-REX 2006 are represented in Fig. 6.9. Icons stand for the mean value of LAURA measurements while error bars indicate their standard deviation during the whole experiment. The root mean squared error in emissivity between IEM predictions and the mean value of LAURA's measurements for every plough and IEM configuration is summarised in Table 6.4.

In this case, comments regarding the vertical polarisation are the same as in T-REX 2004, but a good matching between simulations and measurements is observed at horizontal polarisa-

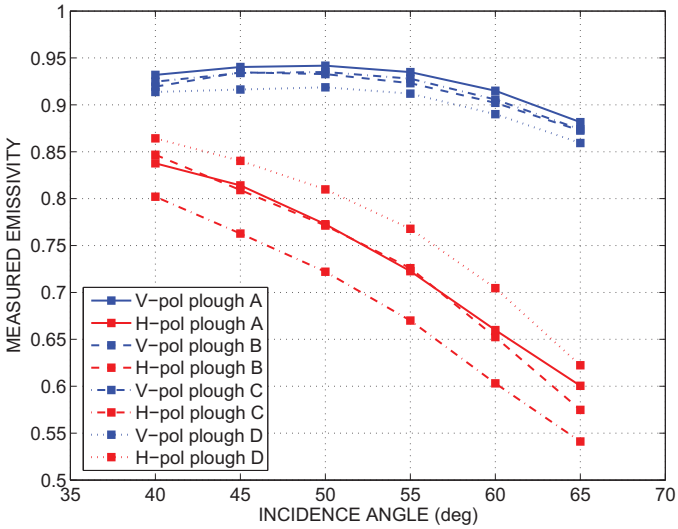

Fig. 6.7: Variation of the emissivity measured during the T-REX 2006 as a function of the incidence angle for the four ploughs. Colours indicate the polarisation: H-pol (red) and V-pol (blue). Line style and icons distinguish different plots with the same plough.

Table 6.3: RMSE in emissivity between TREX 2004 measurements and IEM simulations

IEM — plough	V-pol			H-pol		
	E	F	G	E	F	G
Gaussian	0.1	0.06	0.06	0.06	0.09	0.05
Exponential	0.09	0.04	0.05	0.06	0.1	0.04
Coherent only	0.05	0.06	0.03	0.1	0.12	0.1

tion. Moreover, the effects of taking into account the incoherent component are more relevant, specially in the case of plough D.

Table 6.4: RMSE in emissivity between TREX 2006 measurements and IEM simulations

IEM — plough	V-pol				H-pol			
	A	B	C	D	A	B	C	D
Gaussian	0.028	0.028	0.029	0.044	0.030	0.034	0.059	0.049
Exponential	0.019	0.018	0.029	0.020	0.025	0.029	0.056	0.035
Coherent only	0.027	0.028	0.021	0.036	0.041	0.028	0.033	0.127

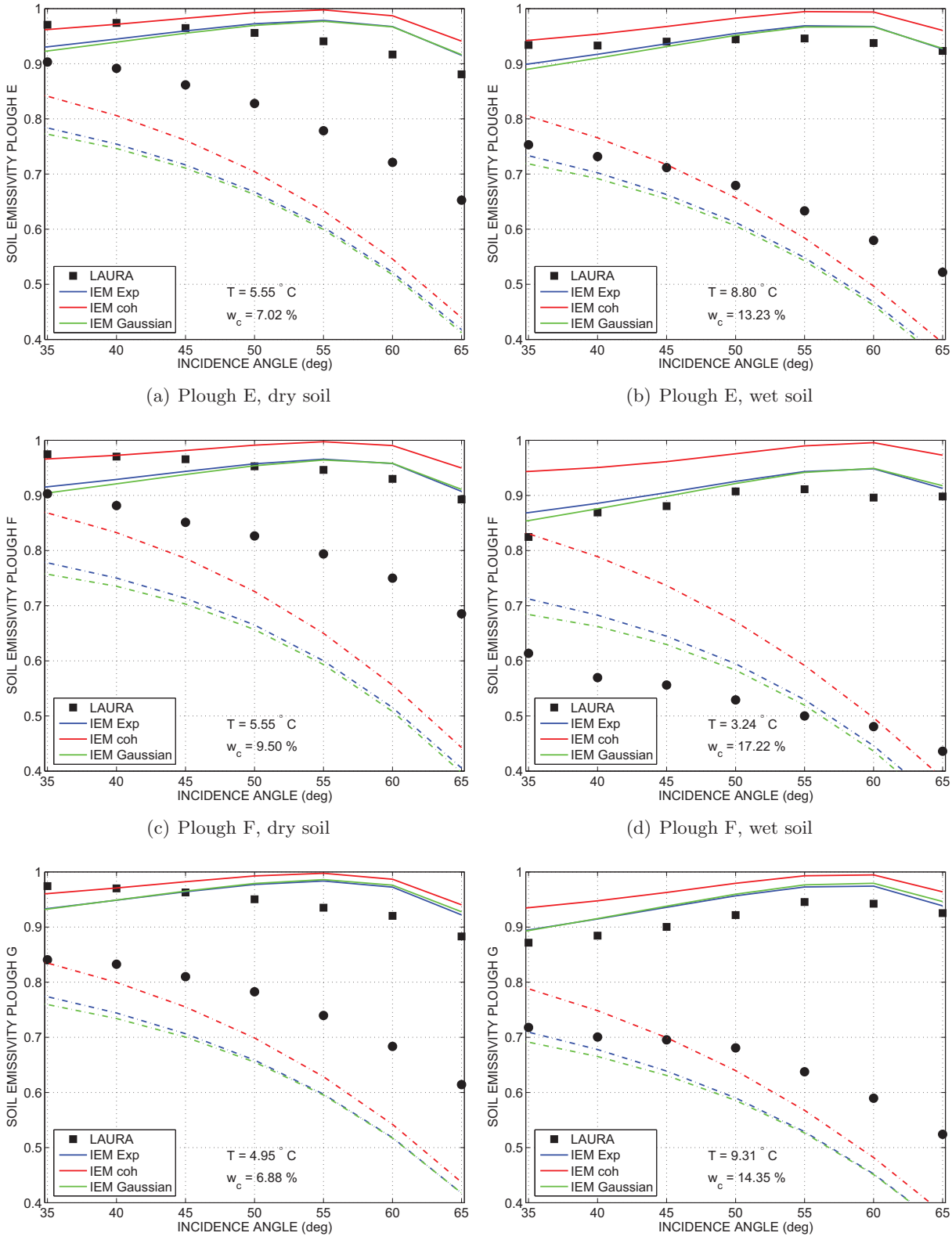

(a) Plough E, dry soil

(b) Plough E, wet soil

(c) Plough F, dry soil

(d) Plough F, wet soil

(e) Plough G, dry soil

(f) Plough G, wet soil

Fig. 6.8: Variation of the emissivity measured during the T-REX 2004 experiment with the incidence angle. LAURA measurements (black icons) have been represented together with IEM simulations. Line style indicates V-pol (solid line) or H-pol (dashed-dotted line).

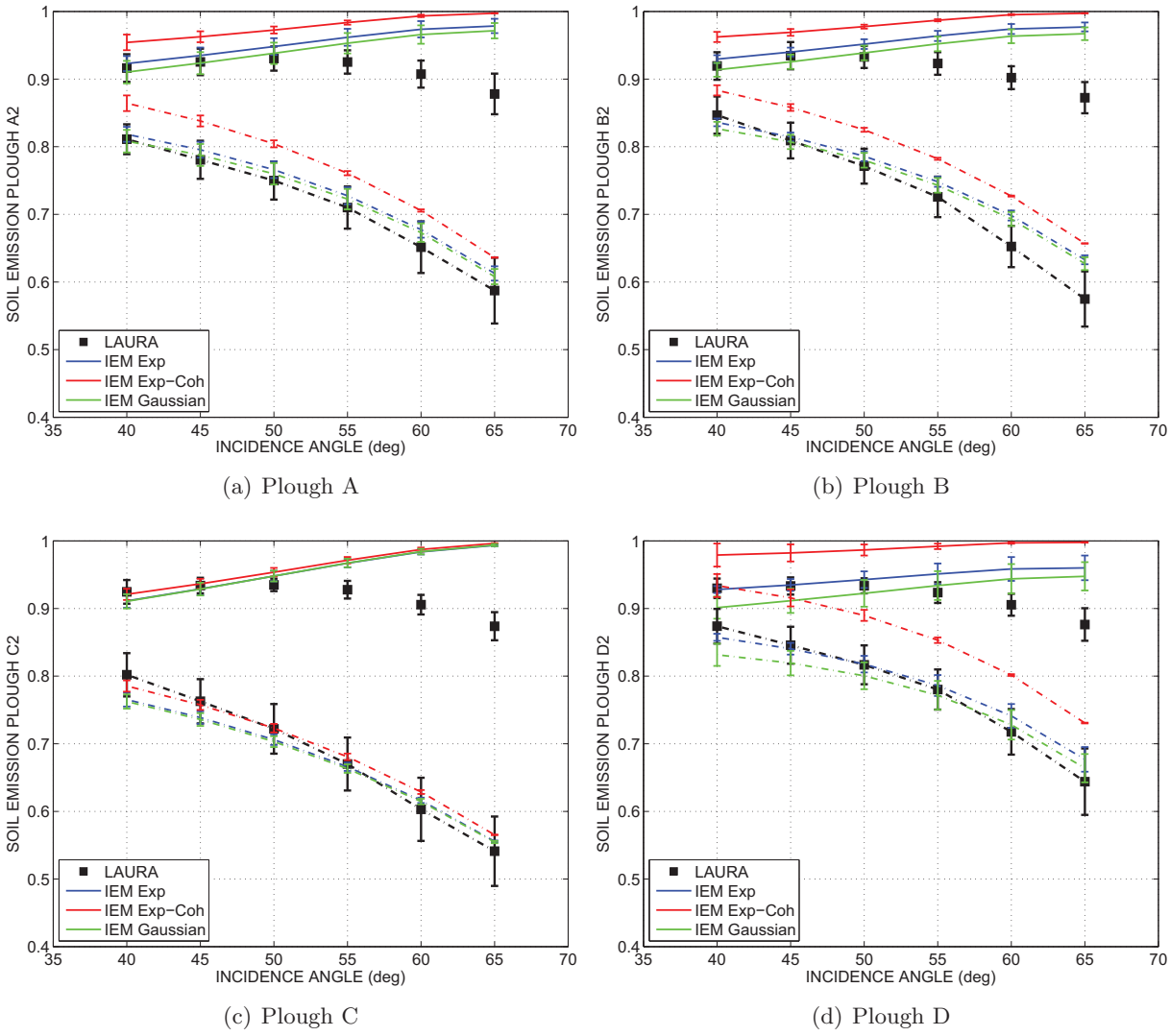

(a) Plough A (b) Plough B

(c) Plough C (d) Plough D

Fig. 6.9: Variation with time of the emissivity measured during the T-REX 2006 experiment as a function of the incidence angle. The mean value of LAURA measurements (black icons) and their standard deviation during the whole experiment have been represented together with IEM simulations.

6.5.2 Comparison with semi-empirical models predictions

In this section, T-REX measurements are compared to semi-empirical soil reflectivity models such as the ones in Wang & Choudhury [1981], Mo & Schmugge [1987], Escorihuela *et al.* [2007], and the air-to-soil transition model proposed in Schneeberger *et al.* [2004] which takes also into account the model proposed in Shi *et al.* [2002]. These models propose different expressions for the effective roughness parameter h_s. Their formulation has been summarised in Table 6.2.

Results for the T-REX 2004 experiment at horizontal polarisation are shown in Fig. 6.10, and at vertical polarisation in Fig. 6.11. Left-hand side plots correspond to dry soils, while right-hand side plots correspond to wet soils. Colours indicate the soil reflectivity model, while line types indicate whether the l_c and σ_s of the height profile (solid lines) or their equivalents taking into account the λ-windowing (dashed lines) have been used. The RMSE in emissivity at each incidence angle and for the whole experiment is represented in Fig. 6.12.

All models follow the trend of the dry soil radiometric measurements at H-pol, whereas discrepancies exist for wet soils. On the contrary, neither of these semi-empirical models nor the IEM describe the trend of the V-pol measurements. The RMSE at this polarisation increases with incidence angle. On the other hand, the lowest RMSE for H-pol is obtained using the simple model in Wang & Choudhury [1981], but with the λ-windowing soil roughness characteristics.

Results for the T-REX 2006 experiment are shown in Fig. 6.13. Upper plots correspond to vertical polarisation while bottom plots correspond to horizontal polarisation. Colours indicate the soil reflectivity model, while line types indicate whether the l_c and σ_s of the height profile (solid lines) or their equivalents taking into account the λ-windowing (dashed lines) have been used. The RMSE in emissivity at each incidence angle and for the whole experiment is represented in Fig. 6.14.

In this experiment, where a wider range of roughness conditions were available and soil moisture was kept almost constant, both the model in Wang & Choudhury [1981] using as inputs the λ-windowing soil roughness characteristics, and the air-to-soil transition model from Schneeberger *et al.* [2004] show similar RMSE. This may be due to the fact that inhomogeneities in soil moisture, or the presence of dew make it difficult to properly characterise the upper soil layer, which is needed for the air-to-soil transition model.

6.6 Conclusions

The Terrain-Roughness Experiments were carried out in Agramunt, Spain, with the aim of characterising the emission of bare rough soils.

Soil roughness has a strong impact on land brightness temperature. This effect is more noticeable in the case of dry soils. Data from bare soils with a standard deviation of height varying from 8 mm to 33 mm was acquired during the T-REX experiments, and was compared to predictions from numerical and semi-empirical soil emission models. The goodness of these models is of key importance for an accurate soil moisture estimation from SMOS data.

As expected, dry soil emissivity at H-pol decreased almost linearly with increasing incidence angle, being the decrement inversely proportional to soil roughness. Although similar emission was measured at H-pol for all plough at low incidence angles, it was noted that emission decreases slowly for rough soils than for smooth soils. Above $\theta = 50^\circ$, the decreasing slope of H-pol emission was higher for all plough.

The sensitivity of V-pol to roughness is lower than that of H-pol. The trend of V-pol emission was found to be different depending on whether the soil was wet or dry. When the soil is wet the emission increased with the incidence angle, which is in accordance with most model predictions. However, the trend for dry soils is decreasing with increasing incidence angle and roughness. This may suggest the existence of a relationship between soil moisture and the effective roughness.

The integral equation method (IEM) predicts an increase in V-pol emission with incidence angle, which is not in accordance with measurements of dry soils. On the other hand, the descending predicted descending trend at H-pol with increasing incidence angle is in accordance

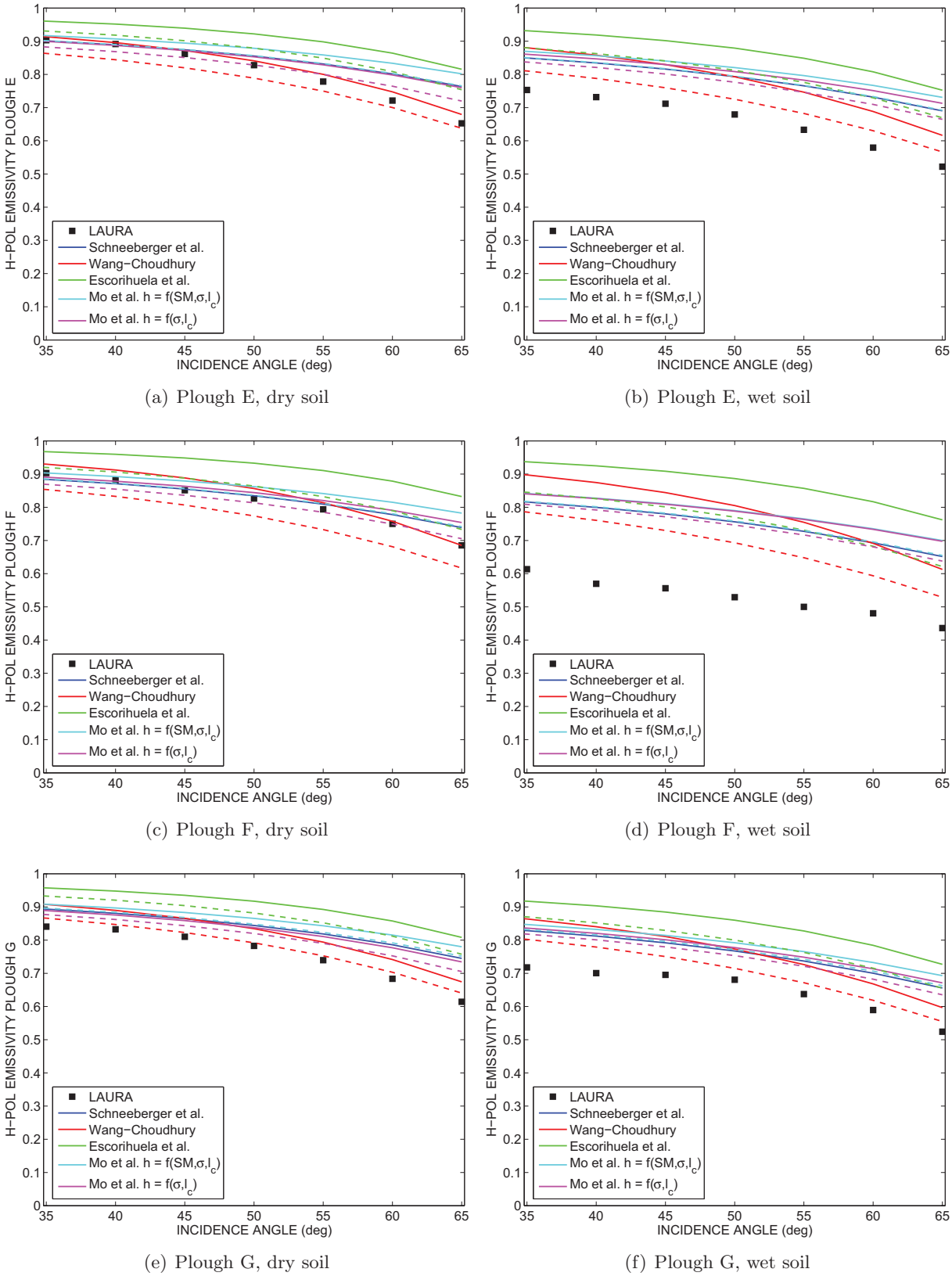

(a) Plough E, dry soil

(b) Plough E, wet soil

(c) Plough F, dry soil

(d) Plough F, wet soil

(e) Plough G, dry soil

(f) Plough G, wet soil

Fig. 6.10: Comparison between T-REX 2004 measurements at horizontal polarisation (black icons) and the models in Wang & Choudhury [1981], Mätzler [2006, section 4.7], Mo & Schmugge [1987], and Escorihuela *et al.* [2007]. Solid lines indicate results using the standard deviation of the surface height profile while dashed lines indicates results using the λ-average standard deviation of height

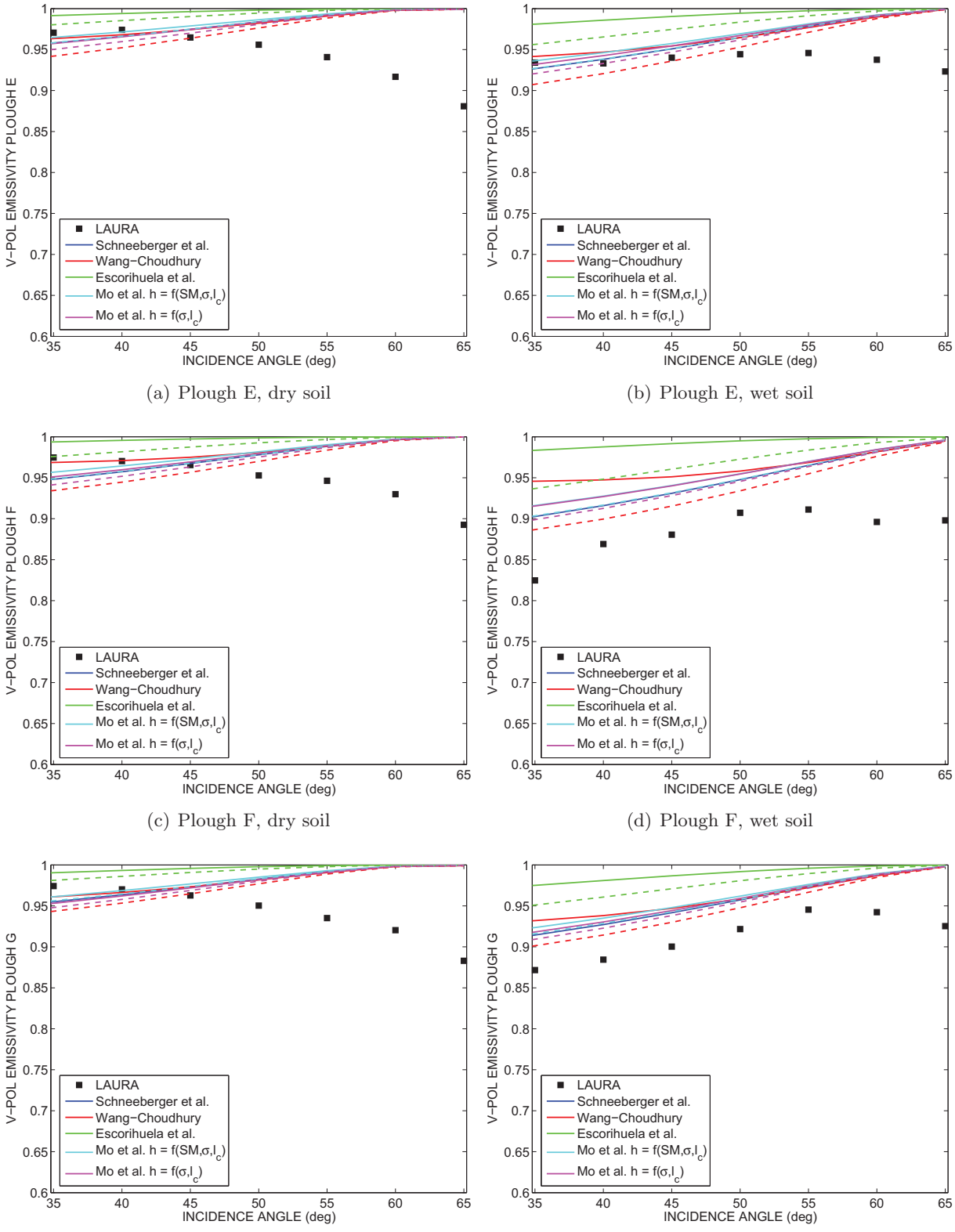

(a) Plough E, dry soil

(b) Plough E, wet soil

(c) Plough F, dry soil

(d) Plough F, wet soil

(e) Plough G, dry soil

(f) Plough G, wet soil

Fig. 6.11: Comparison between T-REX 2004 measurements at vertical polarisation (black icons) and the models in Wang & Choudhury [1981], Mätzler [2006, section 4.7], Mo & Schmugge [1987], and Escorihuela *et al.* [2007]. Solid lines indicate results using the standard deviation of the surface height profile while dashed lines indicates results using the λ-average standard deviation of height

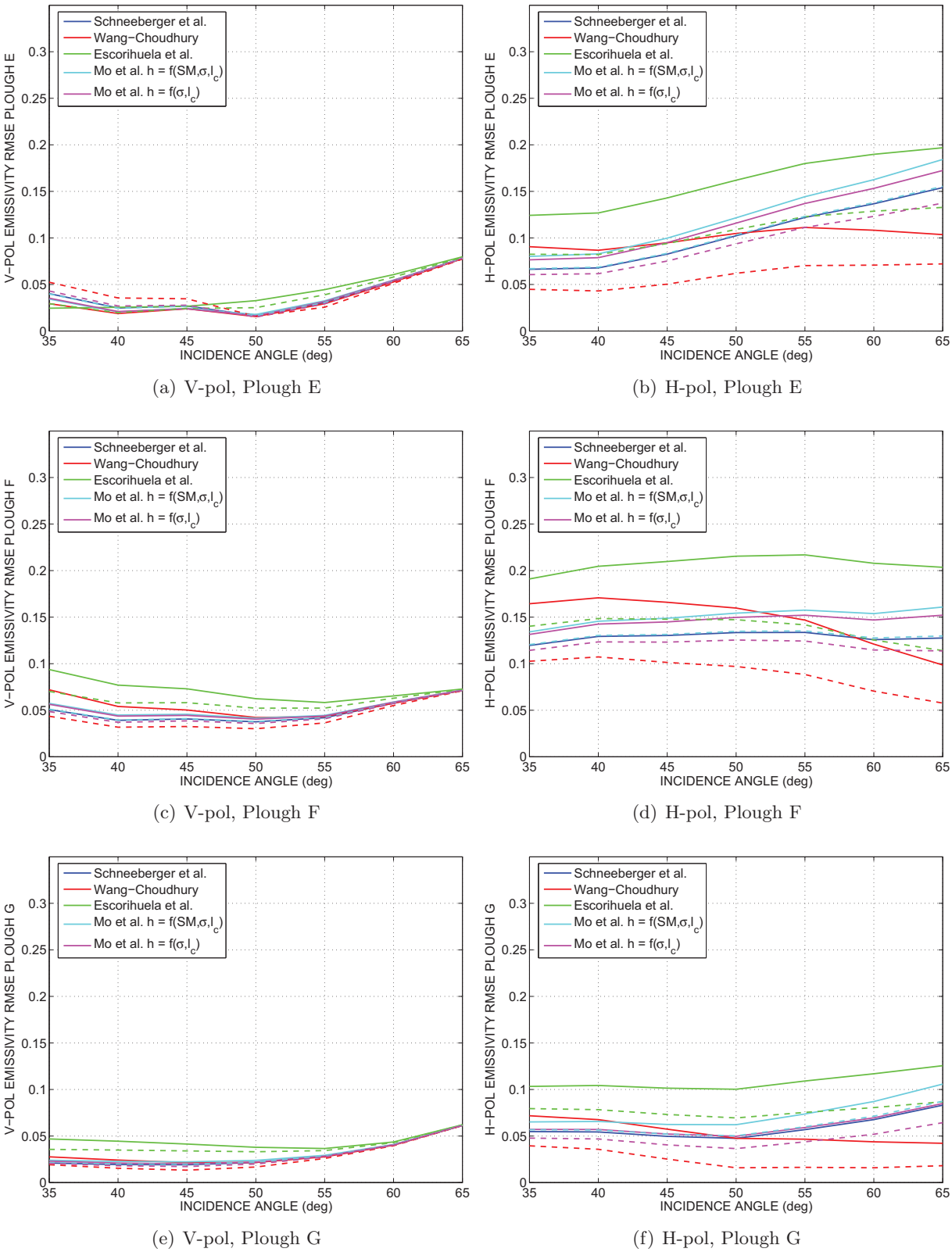

(a) V-pol, Plough E

(b) H-pol, Plough E

(c) V-pol, Plough F

(d) H-pol, Plough F

(e) V-pol, Plough G

(f) H-pol, Plough G

Fig. 6.12: RMSE in emissivity between T-REX 2004 measurements. Solid lines indicate results using the standard deviation of the surface height profile while dashed lines indicates results using the λ-average standard deviation of height

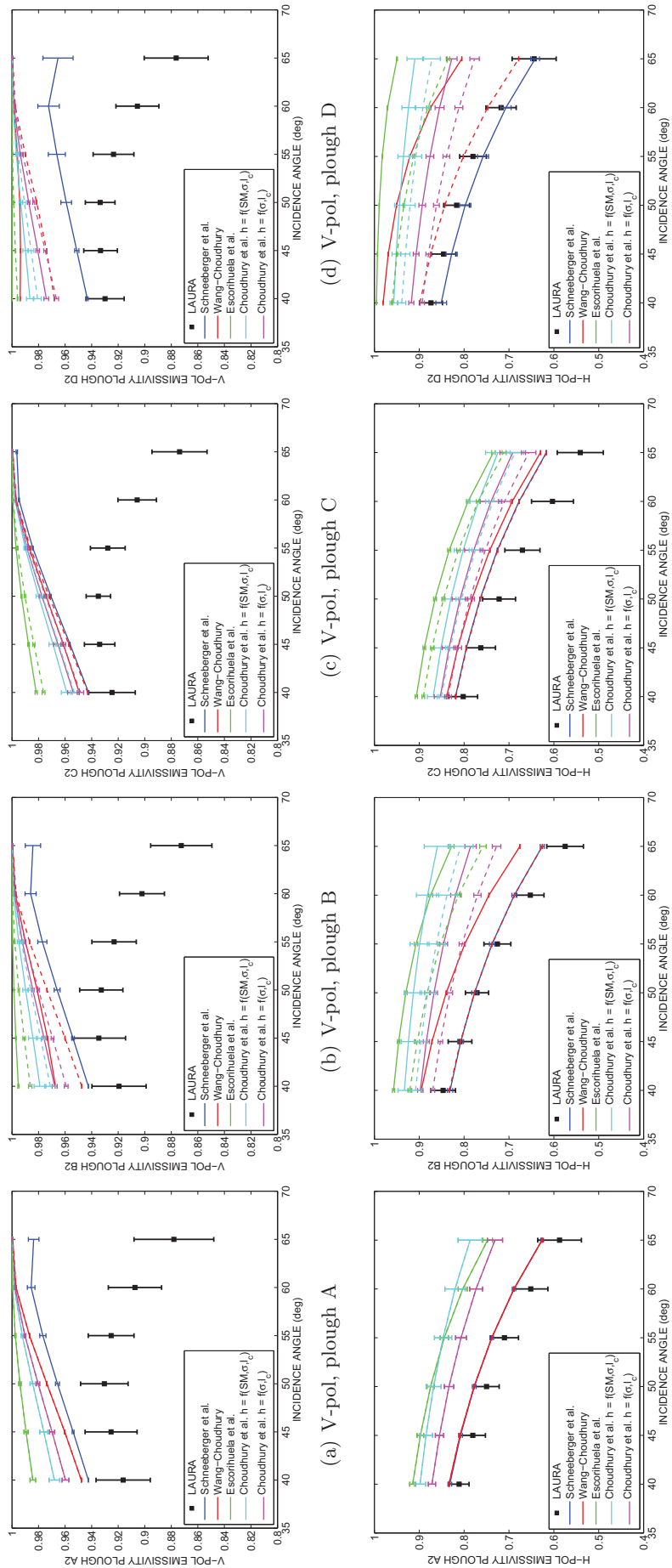

(a) V-pol, plough A (b) V-pol, plough B (c) V-pol, plough C (d) V-pol, plough D

(e) H-pol, plough A (f) H-pol, plough B (g) H-pol, plough C (h) H-pol, plough D

Fig. 6.13: Comparison between T-REX 2006 measurements (black icons) and the models in Wang & Choudhury [1981], Mätzler [2006, section 4.7], Mo & Schmugge [1987], and Escorihuela *et al.* [2007]. Solid lines indicate results using the standard deviation of the surface height profile while dashed lines indicates results using the λ-average standard deviation of height

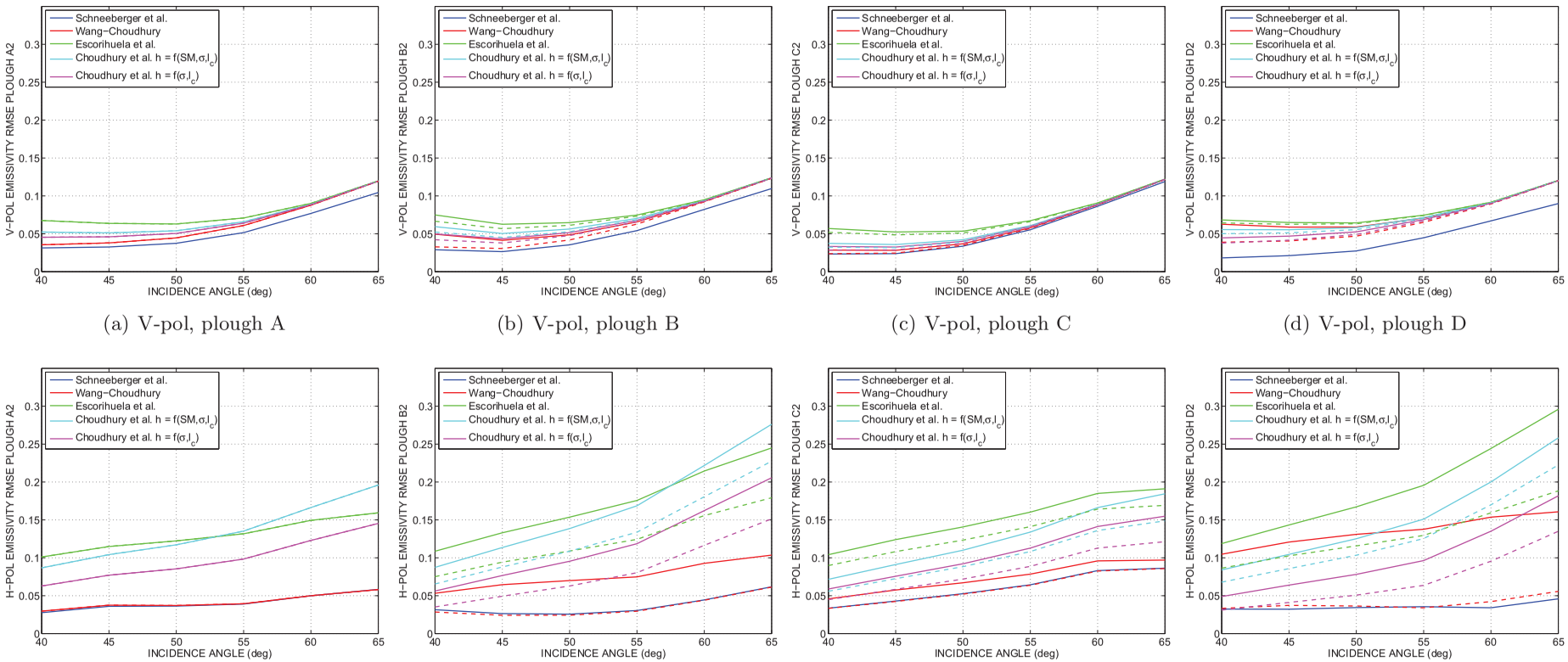

(a) V-pol, plough A (b) V-pol, plough B (c) V-pol, plough C (d) V-pol, plough D

(e) H-pol, plough A (f) H-pol, plough B (g) H-pol, plough C (h) H-pol, plough D

Fig. 6.14: RMSE in emissivity between T-REX measurements and the models in Choudhury *et al.* [1979], Mätzler [2006, section 4.7], Mo & Schmugge [1987], and Escorihuela *et al.* [2007]. Solid lines indicate results using the standard deviation of the surface height profile while dashed lines indicates results using the λ-average standard deviation of height

to measurements, although IEM underestimates the soil emission both for dry and wet soils. In a randomly ploughed field, without a significant tillage direction, the impact of choosing an exponential or gaussian height probability density function in the IEM model is minimum, whereas it was noted that the incoherent term of the reflectivity must be considered for rough soils.

In general, all semi-empirical land emission models follow the trend of dry soils measurements at H-pol, whereas discrepancies exist for wet soils. Neither the semi-empirical models nor the IEM describe the trend of dry soils V-pol measurements, being the error at this polarisation larger as the incidence angle increases. The lowest error between predictions and measurements for H-pol was obtained using the Wang & Choudhury [1981] model, but with the λ-windowing standard deviation of height instead of the standard deviation calculated from the height profile. The dependence on the incidence angle proposed by Wang & Choudhury (a squared cosine) had been discussed by other authors which considered it to be too much strong at L-band. However, this simple formulation has been tested with T-REX data with good results if the "averaged" standard deviation in λ transects is used.

Chapter 7

Radiometric observations of vineyards: Effects of vines and rock fraction

The presence of a vegetation layer above the soil influences the radiometric signal, since it not only attenuates the soil emission, but also adds its own contribution. This effect becomes more significant under wet conditions. Existing experimental data have shown that vegetation reduces the brightness temperature sensitivity to soil moisture content, and that it depends on the wavelength of observation and the type of vegetation. Although vines cover large areas in the Mediterranean Region, no measurements over vineyards were reported in literature before 2003. This fact, together with the possibility that the Valencia Anchor Station (VAS) could become a CalVal site for SMOS (as it later was confirmed) encouraged the UPC Passive Remote Sensing Group to perform, together with the Department of Physics of the Earth and Thermodynamics of the Universitat de València, Spain, two ground-based field experiments at the VAS to study the variations on the emissivity due to vines development. Results of the so called SMOS REFLEX 2003/2006 experiments are presented in this chapter.

7.1 Experimental research on emission from vegetation canopies

Several papers are available that present experimental studies of brightness temperatures from vegetation canopies. Jackson & Schmugge [1991], Jackson *et al.* [1982] noted that attenuation of the soil signal caused by the presence of a vegetation layer is related to the vegetation water content (VWC). Besides brightness temperature is also influenced by the geometrical structure of the vegetation [Mätlzler, 1990]. Wigneron *et al.* [2004] and de Griend & Wigneron [2004] focused the attention on the b-parameter, which relates the VWC to attenuation caused by the vegetation layer τ (see Chapter 3). Measurements over crops were used to assess the dependence of the b-parameter on polarisation, crop type, and incidence angle. It was found to be dependent on the crop type, which was related to plants structure of stems and branches, and almost independent on incidence angle at H polarisation, and on time (except for early

stages of plants growth). Jackson & Schmugge [1991], Saleh *et al.* [2006a] and Escorihuela *et al.* [2009] evidenced that plant debris, roots, and organic matter, which constitutes the vegetation litter, might also influence the canopy emission especially when wet. This fact would eventually explain the low sensitivity to surface moisture of forests found in Grant *et al.* [2007]. Simulations of forests are presented in Ferrazzoli *et al.* [2002], who noted that the main contribution to the emission from forests at L-band comes from the branches. Della Vecchia *et al.* [2006] and Saleh *et al.* [2005] presented a combination of modelling and measurements of forests.

A look at the field experiments conducted during the past decades over vegetated sites shows how they focused their attention on crops such as alfalfa, wheat corn, or soybean [Burke & Schmugge, 1982, Jackson *et al.*, 1982, 1997, Wigneron *et al.*, 1993a,b, Wang *et al.*, 1982, Bindlish *et al.*, 2008, Pardé *et al.*, 2003], on grass [de Rosnay *et al.*, 2006, Saleh *et al.*, 2006a, 2007a, Escorihuela *et al.*, 2009], on forests [Kirdiashev *et al.*, 1979, Saleh *et al.*, 2003, Grant *et al.*, 2007], and on bushes [Cano *et al.*, 2007], but few studies had been conducted over vineyards. In this context, two ground-based field experiments were performed to study the variations on the emissivity due to vines development. Results of the so called SMOS REFLEX 2003/2006 experiments are presented in the next sections.

7.2 SMOS REFLEX experiments overview

The SMOS REFerence pixel L-band EXperiments (REFLEX) were carried out in July 2003 and then again from July to November 2006 at two vineyards within the València Anchor Station (VAS; [López-Baeza *et al.*, 2001]), Spain. The location of the sites and the perimeter of the VAS are shown in Fig. 7.1. The VAS has been selected as a SMOS Cal/Val site because of its almost homogeneous land cover (vineyards) and its size, which is approximately that of a SMOS pixel. The goal of the SMOS REFLEX experiments was to assess the impact of grapevines on the radiometric emission and on the sensitivity of the sensor to soil moisture.

Fig. 7.1: Google-Earth view of the SMOS REFLEX experiment sites. The perimeter of the Valencia Anchor Station is indicated by a red rectangle.

During SMOS REFLEX 2003 radiometric measurements were acquired from DoY 181 to 191

at nine incidence angles (from 25° to 65° in 5° steps) and seven azimuth angles. Varying the incidence angle implied an increasing percentage of the field-of-view (FOV) occupied by vegetation, so its impact on the emission was expected to be more noticeable. Pictures at every look direction were taken to estimate the percentage of FOV covered by plants. The site was irrigated until saturation on DoY 182 and 185, and then was let to dry out. Volumetric soil moisture, soil temperature, and soil roughness were measured, and plants were fully characterised.

The experiment was then repeated from DoY 184 to 314 of year 2006 to monitor changes in the L-band emission of vines during part of their phenological cycle. In this case the soil was covered by rocks which were kept in half the vineyard (from 40% to 80% of surface rock fraction), and were partially removed in the other half (from 6% to 30% of surface rock fraction). Automatic observations were continuously acquired at incidence angles from 40° to 65° in 5° steps. The scan in incidence angles was performed at two azimuth angles φ which were selected so that the rocks-side was observed at φ_1, and the few-rocks-side was observed at φ_2. Ground-truth soil moisture and temperature ground-truth data were registered every 15 minutes at 0, 5, 10, 15, 20, and 40 cm depth. Apart from trickle irrigations, various rainfall events were registered during the experiment, so a wide range of soil moisture conditions was measured. The soil surface height profile was measured every 5 mm along a 1.5 m transect using a Leica Disto4a laser. The correlation length and standard deviation of the roughness profiles before (after) harvest are 10.1 cm (8.7 cm) and 1.2 cm (1.3 cm), respectively. Pictures at every look direction were taken to estimate the percentage of FOV covered by plants. At incidence angles lower than 55° the percentage of FOV occupied by bare soil is up to 40%, so the contribution of soil to the measured radiation might be important. For a detailed description of these experiments please refer to Chapter 4.

7.3 REFLEX 2003: L-band emissivity of fully developed grapevines

7.3.1 Ground-truth measurements of soil moisture and temperature

Ground measurements of soil moisture w_s were acquired using Delta-T ThetaProbe sensors at 396 points selected as follows: one sample under each grapevine, and five samples between vines from row to row. Figure 7.2 shows a w_s map of the vineyard for every day of experiment. At the beginning of the experiment, soil was completely dry because neither rain nor irrigation had moistened the field for weeks (see Fig. 7.2(a)). The site was irrigated until saturation on DoY 182 and then again on DoY 185. As shown in Fig. 7.2(b) and Fig. 7.2(e) even though the field was irrigated until saturation, different w_s values were measured depending on the location of the test point within the vineyard. This is most probably because of surface inhomogeneities and variations on the compactness of the terrain due to plough and roots distribution. This large spatial variability in soil moisture, which in this case varies from 3% up to 35% in a 20 m $\times$ 20 m area, is one of the main problems soil moisture retrieval algorithms must face since it complicates the comparison between ground-truth and estimated w_s at the plot scale. The soil moisture map of the vineyard for every radiometer observation position taking into account the averaging due to LAURA's antenna pattern has been represented in Fig. 7.3. These are the w_s

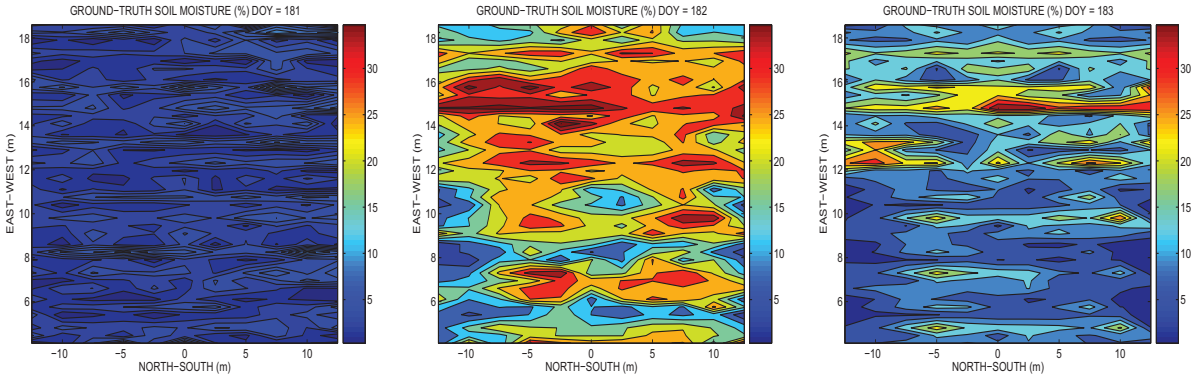

(a) DoY = 181, dry soil (b) DoY = 182, irrigation (c) DoY = 183

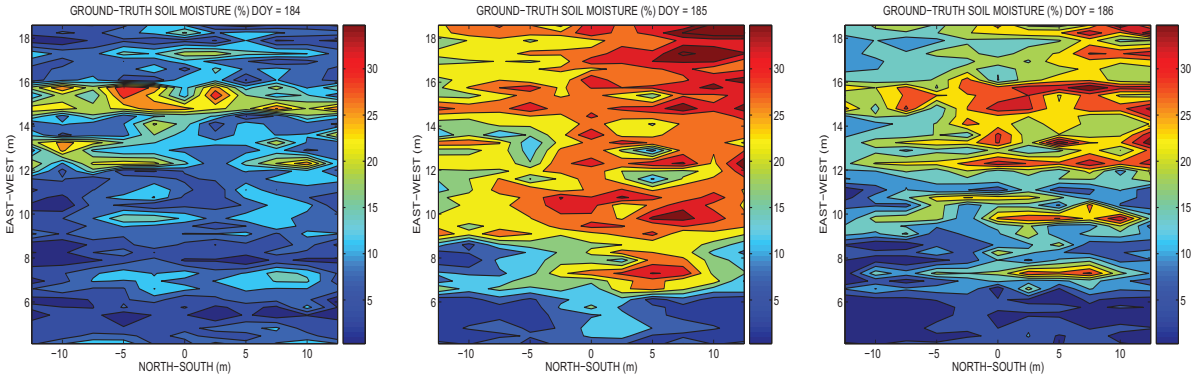

(d) DoY = 184 (e) DoY = 185, irrigation (f) DoY = 186

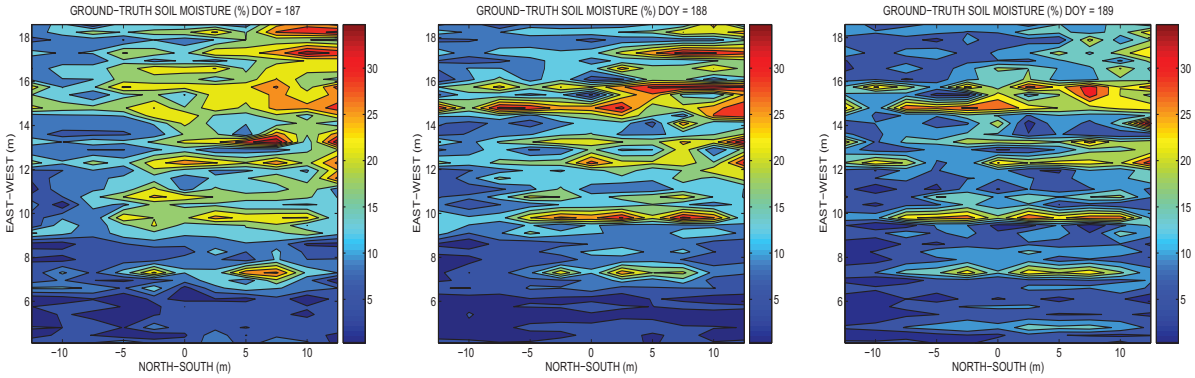

(g) DoY = 187 (h) DoY = 188 (i) DoY = 189

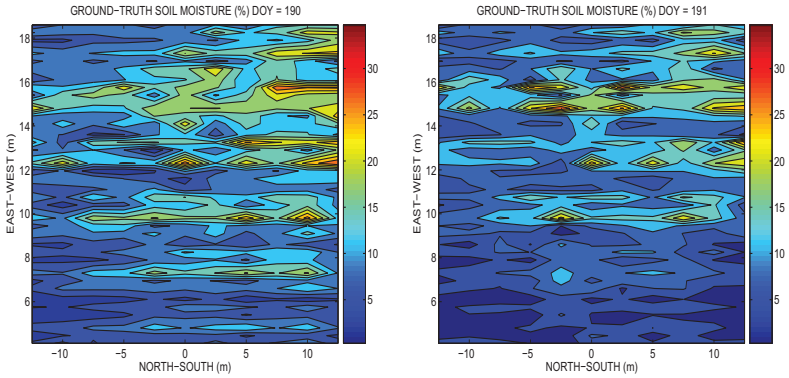

(j) DoY = 190 (k) DoY = 191

Fig. 7.2: Ground-truth soil moisture map (in %) measured during SMOS REFLEX 2003. Measurements at at each of the 36 × 11 test-points have been represented.

values which have been used as ground-truth data for comparison with w_s estimations at every look position.

Figure 7.4 shows the evolution of the atmospheric temperature at 2 m, and of the soil temperature acquired in the period between irrigations. Large atmospheric temperature gradients are registered in this area and for this time of the year. This fact was especially noticeable during DoY 182 when the atmospheric temperature reached 38 °C during daytime and 14 °C at night. As expected, differences between atmospheric and soil surface temperatures was larger for wet soils (up to 3 °C during radiometric measurements) than for dry soils. Soil temperature at 20 cm to 40 cm varies less than 3 °C during the whole experiment. The effective soil temperature has been computed taking into account the formulation by Choudhury *et al.* [1982].

7.3.2 Variation of the emissivity with the incidence angle

In Fig. 7.5, the measured and simulated emissivity of the vineyard at vertical (blue) and horizontal (red) polarisations, and the mean measured soil moisture (green lines) as a function of the incidence angle and for a fixed azimuth angle have been plotted. Since plants development did not significantly change during SMOS REFLEX 2003, two days of experiment have been selected as representative according to the measured soil moisture:

- DoY 181, the first day of experiment, completely dry soil ($w_s = 2\%$), and
- DoY 185, the second day in which the vineyard was irrigated until saturation ($w_s = 7\%$ to 25% depending on the position within the vineyard).

Icons in Fig. 7.5 indicate LAURA measurements -DoY 181 (squares) and DoY 185 (circles)-, while lines indicate the emissivity of bare soil simulated using (3.24) and the soil water content, temperature, and roughness ground-truth measurements for DoY 181 (dashed-dotted line) and DoY 185 (solid line) as inputs. The difference between LAURA measurements and simulated bare soil emissivity as a function of the incidence angle and for every azimuth position has been represented in Fig. 7.6. Icons indicate DoY 181 (squares), and DoY 185 (circles), while colours indicate the polarisation and azimuth angle: (V-pol, -φ) in blue, (V-pol, +φ) in green, (H-pol, -φ) in red, and (H-pol, +φ) in magenta.

The first day of experiment, DoY 181, has the advantage of soil being dry, which implies no soil moisture gradients within the site as shown in Fig. 7.2(a) and Fig. 7.3(a). Since measurements were performed at night, the soil temperature did not significantly change during measurements either (± 2 °C at most), which implies an homogeneous soil dielectric constant in the whole experiment site. The range of measured emissivity at vertical polarisation during DoY 181, blue squares, is rather low, taking values between 0.96 and 0.94 (∼5 K variation in brightness temperature for a typical soil temperature of 290 K). No apparent dependence on the incidence angle is observed. When V-pol measurements are compared to the simulated emission of a bare soil, both trends match, specially for $\theta < 50°$. The difference between measurements of the vineyard and the theoretical emission of the soil without plants shown in Fig. 7.6 is lower than 0.025 for dry soils (8 K). On the other hand, the measured emissivity at H-pol has an

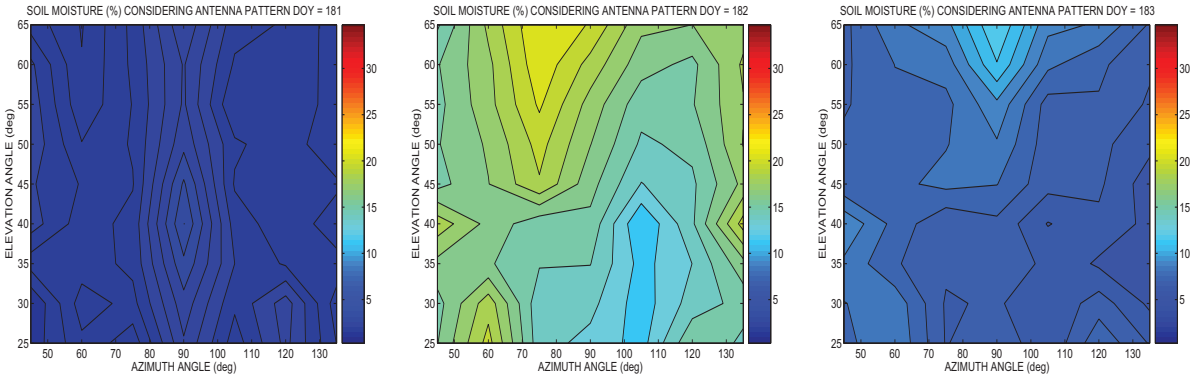

(a) DoY = 181, dry soil (b) DoY = 182, irrigation (c) DoY = 183

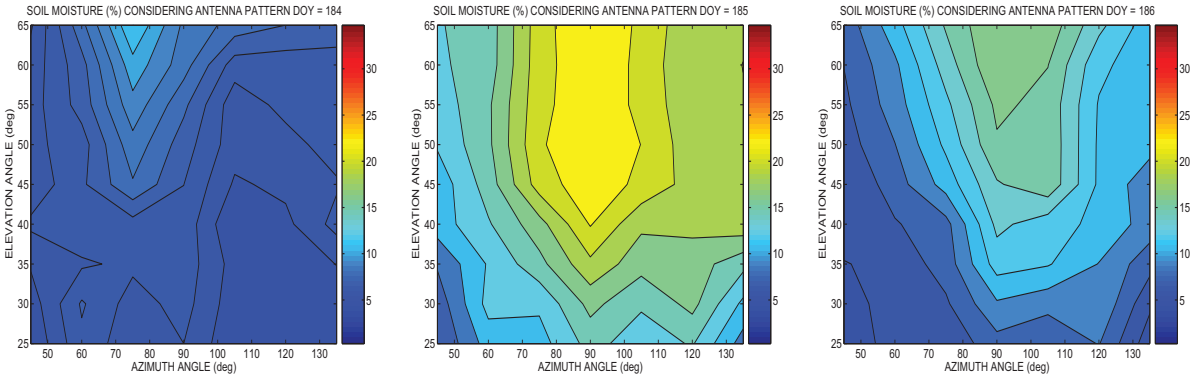

(d) DoY = 184 (e) DoY = 185, irrigation (f) DoY = 186

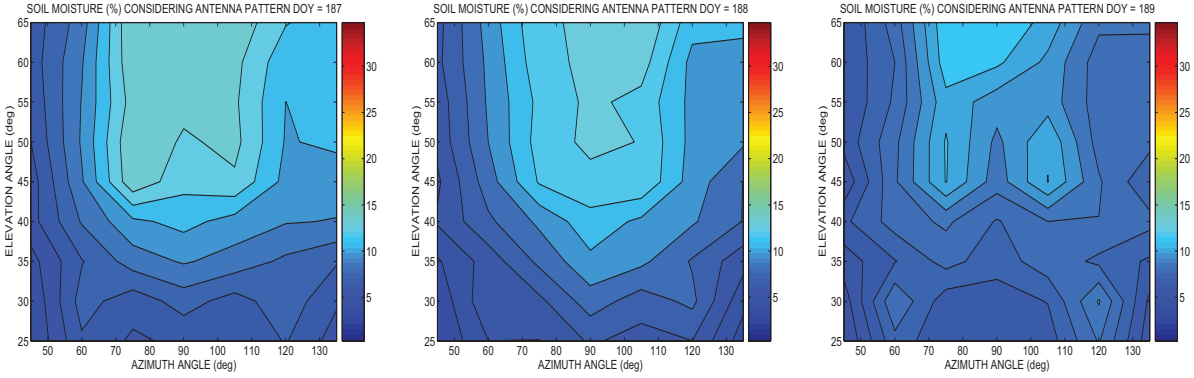

(g) DoY = 187 (h) DoY = 188 (i) DoY = 189

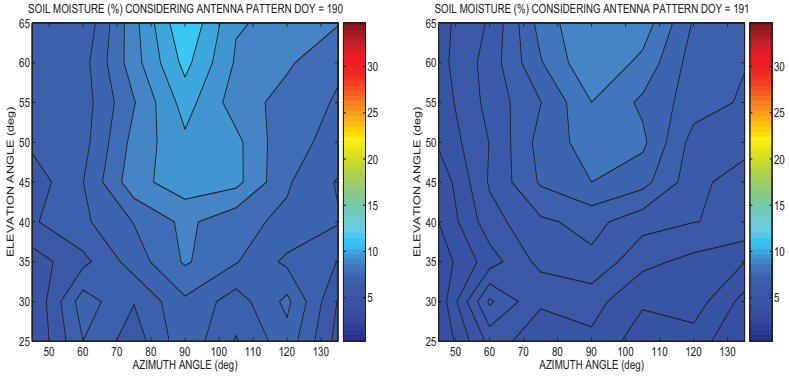

(j) DoY = 190 (k) DoY = 191

Fig. 7.3: Averaged soil moisture map of the vineyard for every radiometer observation position taking into account the radiometer antenna pattern.

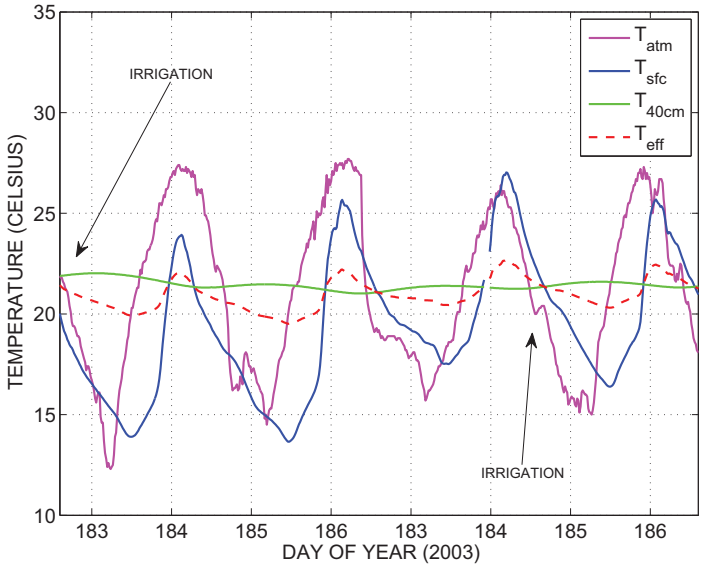

Fig. 7.4: Measured atmospheric temperature at 2 m, and soil temperature at surface level and at 40 cm depth, and estimated soil effective temperature [Choudhury *et al.*, 1982] between irrigations.

almost constant value around 0.82 for all observation positions whereas, in the case of a field without plants, the emission would have decrease with increasing incidence angle, from 0.93 to 0.81 (35 K range of variation).

The highest values of soil moisture were measured during DoY 185 as shown Fig. 7.2(e) and Fig. 7.3(e). On the contrary to DoY 181, in this case strong soil moisture gradients, up to 16%, were present within the vineyard. At the highest azimuth angles, $\varphi = \pm 45^\circ$, emissivity measurements at vertical polarisation, which are represented with blue circles, slowly increase from 0.9 at $\theta = 25^\circ$ to 0.925 at $\theta = 55^\circ$, and then keep this value until $\theta = 65^\circ$. The trend is similar for other φ but with lower V-pol emissivity, which varies from 0.86 to 0.89 at $\varphi = \pm 30^\circ$ and from 0.85 to 0.88 at $\varphi = \pm 15^\circ$ and 0° . No important differences on the measured V-pol emissivity between two similar azimuth with different w_s are observed. However, in this case there are differences between V-pol measurements acquired during DoY 185 simulated bare soil emissivity, which are higher ($\Delta e_v = 0.03$ to 0.05) at $\theta = 40^\circ$ and 45° . On the other hand, measured emissivity at H-pol has a descending trend with increasing incidence angle. As it should be expected tacking into account that the soil is wet, H-pol measurements have lower values than those from DoY 181. The mean H-pol value is lower for lower φ. Although the soil contribution to the scenario emission is more noticeable now, it is seen from Fig. 7.6 that vines introduce up to 0.12 ($\approx$ 35 K) differences with respect to a bare soils scenario. The lowest the azimuth angle, the lowest the measured emissivity for a wet soil vineyard, probably due to the increasing percentage of FOV occupied by soil as φ decreases.

These facts suggest that vines have a stronger impact on the H-pol, in opposition to plants with a predominant vertical structure such as wheat which seem to have a predominant effect over V-pol [Pardé *et al.*, 2003].

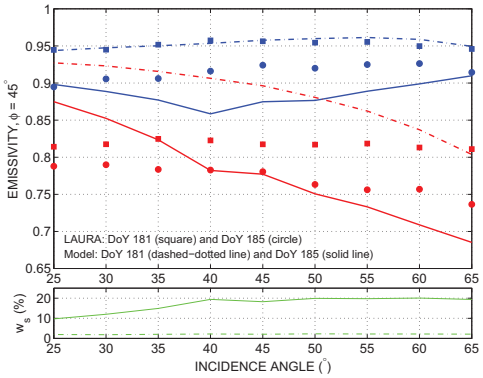

(a) $\varphi = 45°$

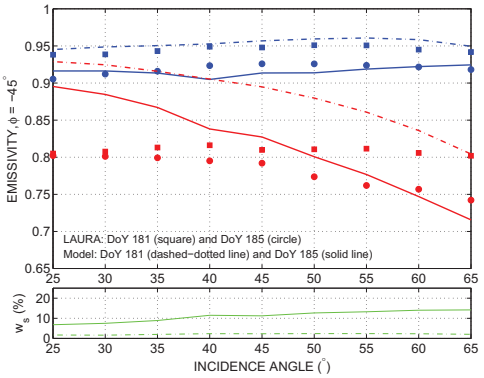

(b) $\varphi = -45°$

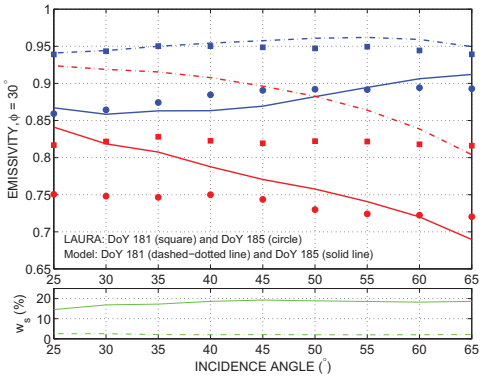

(c) $\varphi = 30°$

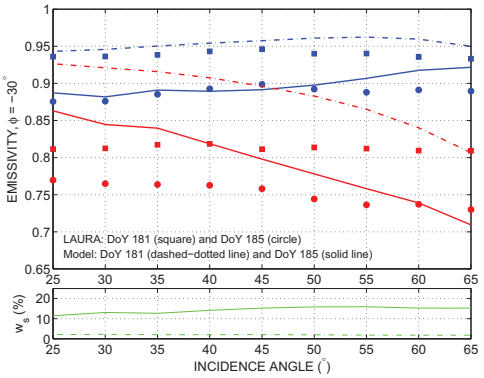

(d) $\varphi = -30°$

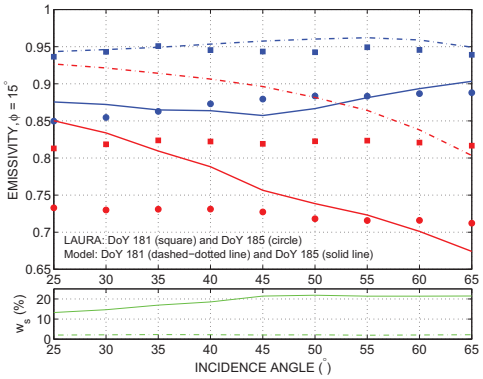

(e) $\varphi = 15°$

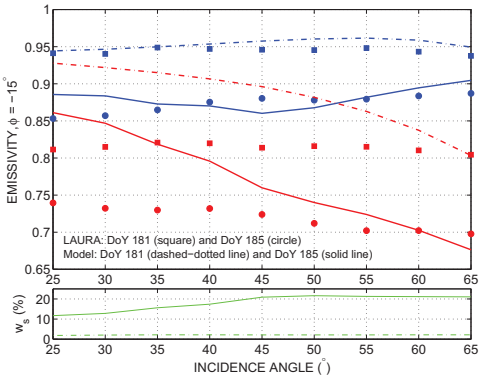

(f) $\varphi = -15°$

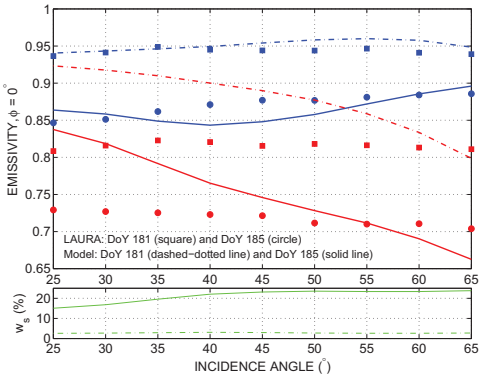

(g) $\varphi = 0°$

Fig. 7.5: Emissivity for vertical (blue) and horizontal (red) polarisations as a function of the incidence angle for every azimuth position. Icons indicate LAURA measurements for DoY 181 (squares), and DoY 185 (circles), while lines indicate the bare soil emissivity simulated for DoY 181 (dashed-dotted) and DoY 185 (solid). The averaged soil moisture at each observation position has been included (green lines).

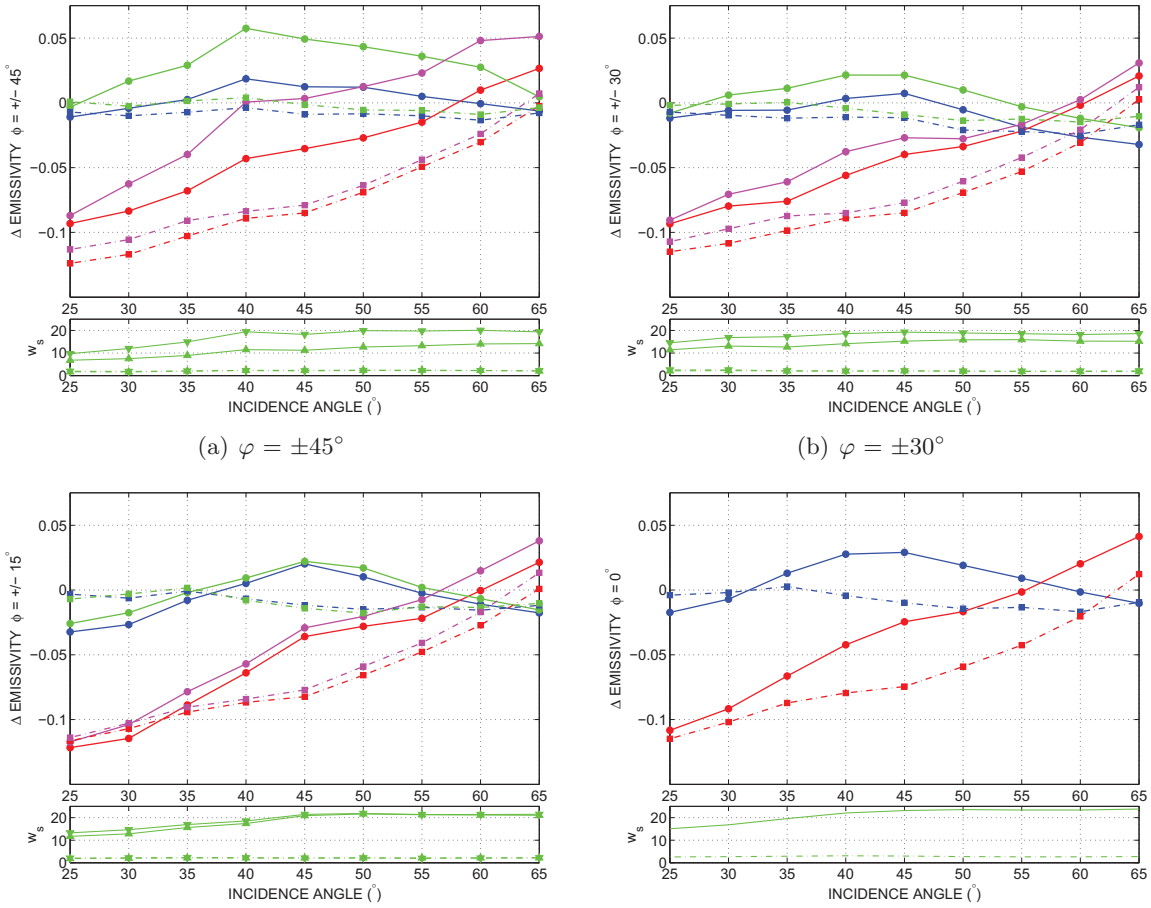

(a) $\varphi = \pm 45°$ (b) $\varphi = \pm 30°$

(c) $\varphi = \pm 15°$ (d) $\varphi = 0°$

Fig. 7.6: Difference between LAURA measurements of the vineyard and simulated bare soil emissivity for vertical and horizontal polarisations as a function of the incidence angle for every azimuth position. Icons indicate DoY 181 (squares), and DoY 185 (circles), while colours indicate the polarisation and azimuth position (V-pol: blue and green, and H-pol: red and magenta). The averaged soil moisture at each observation position has been included (green lines).

Figure 7.7 represents the mean value and standard deviation of the emissivity and of the ground-truth soil moisture as a function of the incidence angle and for all azimuth angles. Measurements from DoY 185 (solid line) and DoY 181 (dashed-dotted line) have been represented. A remarkable fact is that the mean value of both polarisations seem independent of incidence angle for completely dry soils, which is the case of DoY 181, being the std. of measurements lower than 0.005 (0.01) in emissivity - 1.5 K (3 K) in brightness temperature- for vertical (horizontal) polarisations. In contrast, for wet soil an ascending trend is observed for V-pol emissivity up to $\theta = 45°$, when V-pol emissivity seems to saturate, while H-pol emissivity decreases as incidence angle increases. The std. of measurements for wet soils is 0.025 (0.03) for vertical (horizontal) polarisations.

Finally, Fig. 7.8 represents the mean value and standard deviation of the emissivity measured during the whole SMOS REFLEX 2003 as a function of the incidence angle and for all azimuth angles. Blue and red indicate vertical and horizontal polarisations, respectively. The range of variation of the mean emissivity with respect to the incidence angle at V- (H-pol) is rather

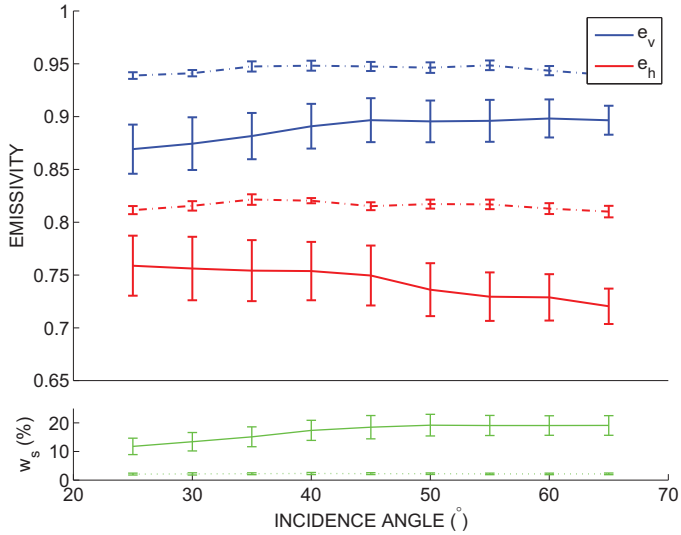

Fig. 7.7: Mean value and standard deviation of the emissivity and of the ground-truth soil moisture as a function of the incidence angle and for all azimuth angles. DoY 185 (solid line) and DoY 181 (dashed-dotted line) have been represented. Blue and red indicate vertical and horizontal polarisations, respectively.

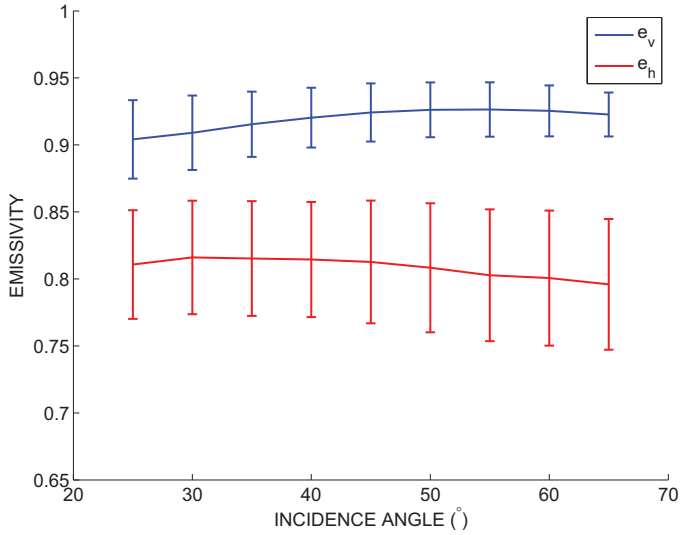

Fig. 7.8: Mean value and standard deviation of the emissivity as a function of the incidence angle angle, for all azimuth angles and days of experiment. Blue and red indicate vertical and horizontal polarisations, respectively.

low, 0.02 (6 K), whereas the standard deviation of measurements goes from 0.03 down to 0.015 (9–4 K) at V-pol, and from 0.04 up to 0.05 (11–15 K) at H-pol. most probably due to gradients in soil moisture depending on the azimuth angle.

7.3.3 Variation of the emissivity with the azimuth angle

For a given incidence angle, a not negligible standard deviation of the emissivity was observed in Fig. 7.7 and Fig. 7.8 when measurements for all azimuth angles were averaged. To assess whether these variations are related to gradients in soil moisture, the measured and simulated

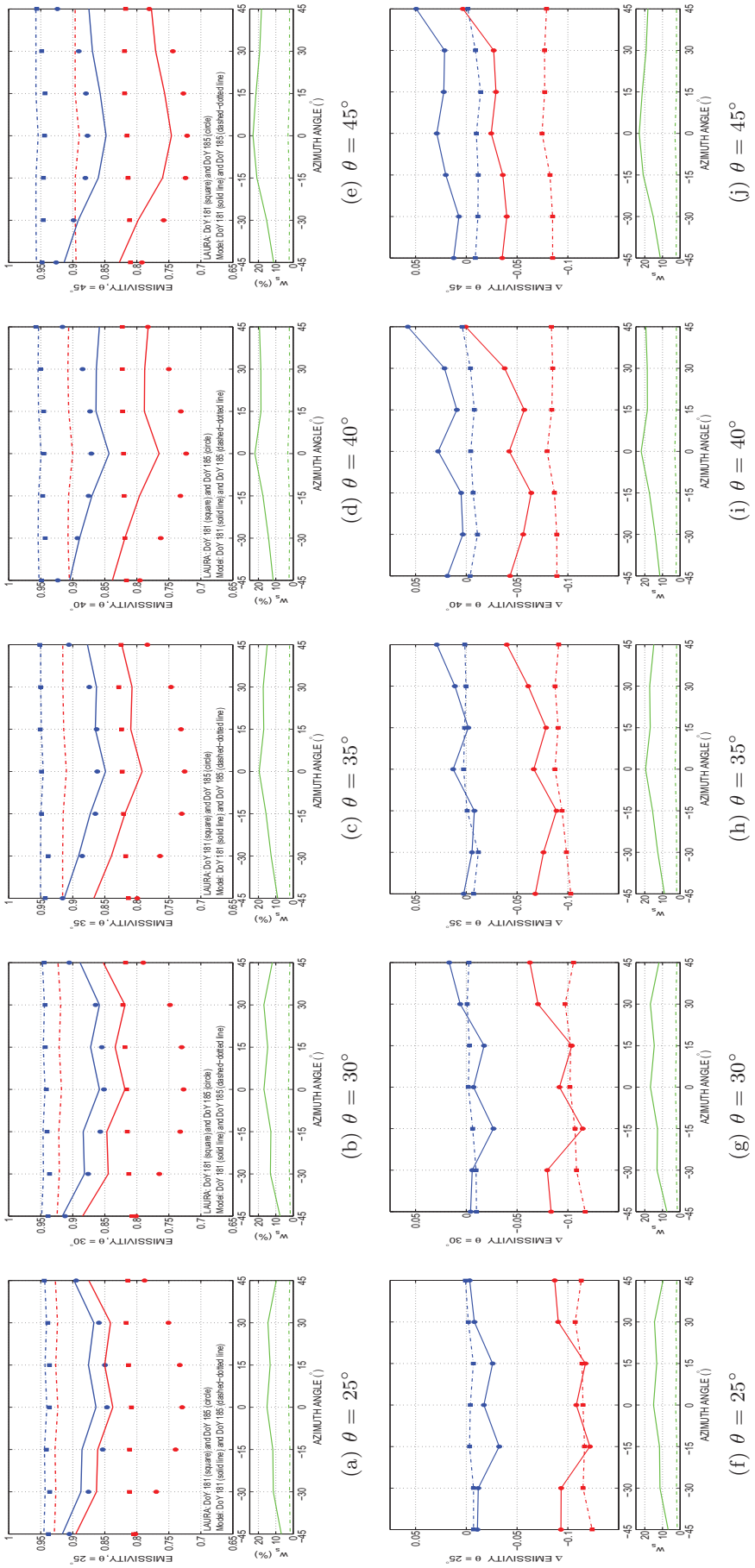

Fig. 7.9: [top] Emissivity for vertical (blue) and horizontal (red) polarisations as a function of the azimuth angle for incidence angles between 25° and 45° in 5° steps. [bottom] Difference between LAURA measurements of the vineyard and simulated bare soil emissivity for vertical and horizontal polarisations. In both cases, icons indicate LAURA measurements for DoY 181 (squares), and DoY 185 (circles), while lines indicate the bare soil emissivity simulated for DoY 181 (dashed-dotted) and DoY 185 (solid). The averaged soil moisture at each observation position has been included (green lines).

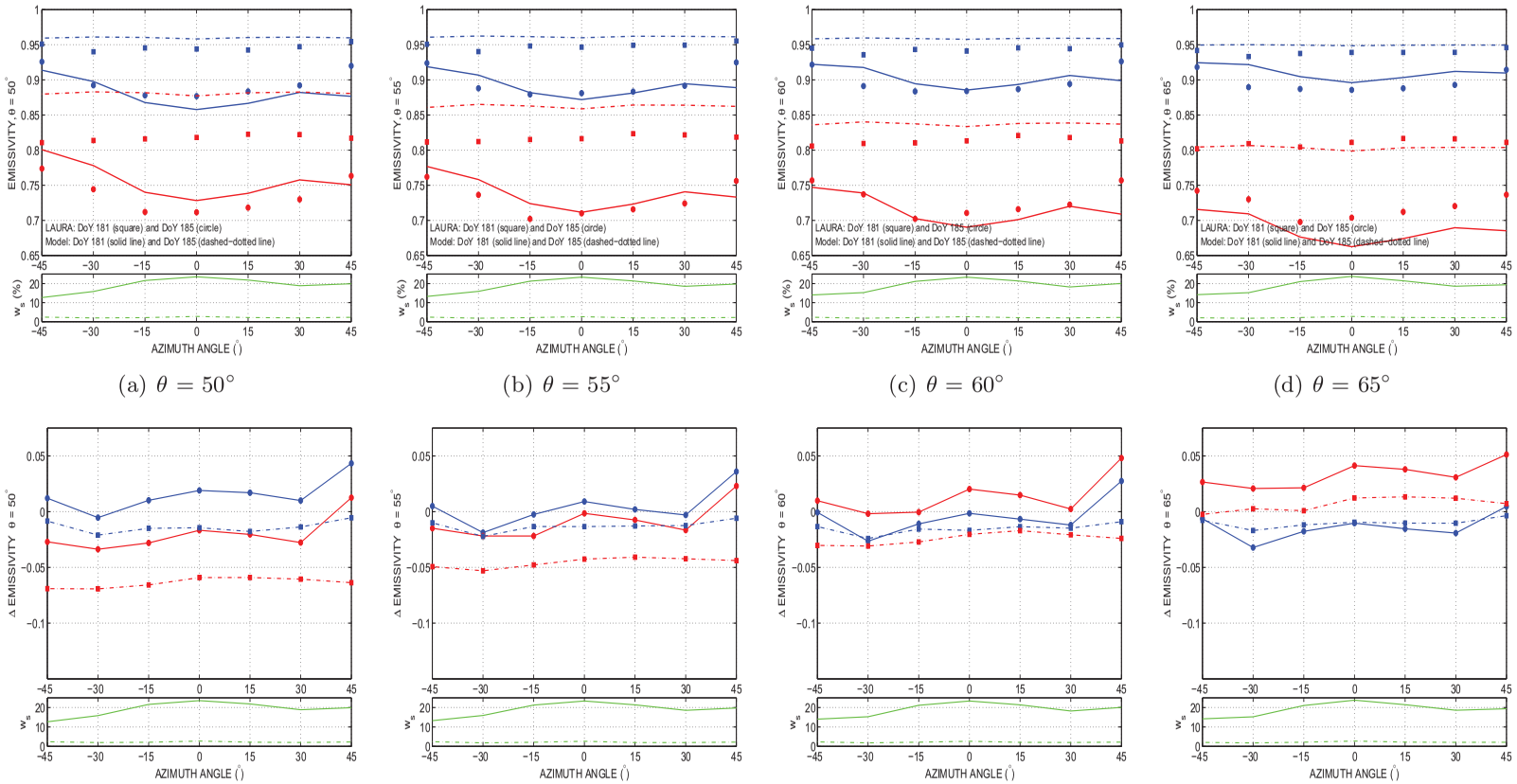

(a) $\theta = 50°$ (b) $\theta = 55°$ (c) $\theta = 60°$ (d) $\theta = 65°$

(e) $\theta = 50°$ (f) $\theta = 55°$ (g) $\theta = 60°$ (h) $\theta = 65°$

Fig. 7.10: [top] Emissivity for vertical (blue) and horizontal (red) polarisations as a function of the azimuth angle for incidence angles between 50° and 65° in 5° steps. [bottom] Difference between LAURA measurements of the vineyard and simulated bare soil emissivity for vertical and horizontal polarisations. In both cases, icons indicate LAURA measurements for DoY 181 (squares), and DoY 185 (circles), while lines indicate the bare soil emissivity simulated for DoY 181 (dashed-dotted) and DoY 185 (solid). The averaged soil moisture at each observation position has been included (green lines).

emissivity of the vineyard at vertical (blue) and horizontal (red) polarisations, and the mean measured soil moisture (green lines) as a function of the azimuth angle and for a fixed incidence angle have been represented at the top of Fig. 7.9 and Fig. 7.10. Icons indicate LAURA measurements -DoY 181 (squares) and DoY 185 (circles)-, while lines indicate the emissivity of bare soil simulated using Eq. (3.25) with inputs the soil water content, temperature, and roughness ground-truth measurements for DoY 181 (dashed-dotted) and DoY 185 (solid). During these two days of experiment the highest and the lowest w_s was measured.

Again, emissivity at vertical polarisation during DoY 181, blue squares, has a constant value independently of the azimuth angle. A good agreement is found between measurements of the vineyard and the theoretical emission of the soil without plants which is lower than 0.015 for $\theta < 50^\circ$. On the other hand, the measured emissivity at H-pol has an almost constant value around 0.82 for all observation positions whereas simulations of a bare field scenario overestimate the H-pol emission in all cases. A look at the bottom plots in Fig. 7.9 and Fig. 7.10 shows that this overestimation is larger for $\theta = 25^\circ$, 0.125 (35 K), and decreases down to almost 0 as the incidence angle increases.

In the case of wet soil, emissivity at both polarisations has a U-shape, with the minimum at φ=0° . The range of V-pol measurements, blue bullets, goes from 0.05 at $\theta = 25^\circ$ to 0.03 at $\theta = 65^\circ$. On the other hand, measurements at H-pol, red bullets, are more sensitive to changes in the azimuth angle, and the range of emission is higher than for V-pol: from 0.07 at $\theta = 25^\circ$ to 0.02 at $\theta = 65^\circ$. As expected, the mean value of the emissivity increases with incidence angle at V-pol and decreases for H-pol. Figure 7.9 and Fig. 7.10 show the decrease in emission due to vines, which is larger at H-pol than at V-pol, for $\theta < 50^\circ$.

The mean value and standard deviation of the emissivity from DoY 181 and DoY 185 as a function of the azimuth angle and for all incidence angles is represented in Fig. 7.11. For dry soils no dependence on the azimuth angle is observed, being the standard deviation of measurements lower than 1.5 K at both polarisations. In the case of wet soils, and since the contribution from vines is supposed to be the same for at $\pm\varphi$, the inhomogeneity in soil moisture content, which is higher for positive azimuth angles, leads to an asymmetry in the emission measurements of DoY 185 (solid lines), which as expected are higher for the lowest w_s. For a given azimuth angle, the standard deviation of the measured emissivity at V-pol goes from 0.014 (∼4 K) at φ=0° down to 0.008 (∼2 K) at φ=65° , whereas the largest standard deviation at H-pol goes from 0.007 (∼2.6 K) at φ=0° up to 0.022 (∼7 K) at φ=65° .

Finally, Fig. 7.12 shows the mean value and standard deviation of the emissivity as a function of the azimuth angle and for all incidence angles and days of experiment. The difference between the mean values of e_v and e_h is of the order of 0.11 (∼32 K) for all azimuth positions. The standard deviation of measurements goes from 0.023 down to 0.021 (∼7–6 K) at V-pol, and from 0.036 up to 0.05 (∼10–15 K) at H-pol. Since the lowest std. dev. corresponds to negative azimuths (left side of the vineyard from LAURA's position) where the lowest soil moisture content was measured, differences are most probably due to gradients in soil moisture.

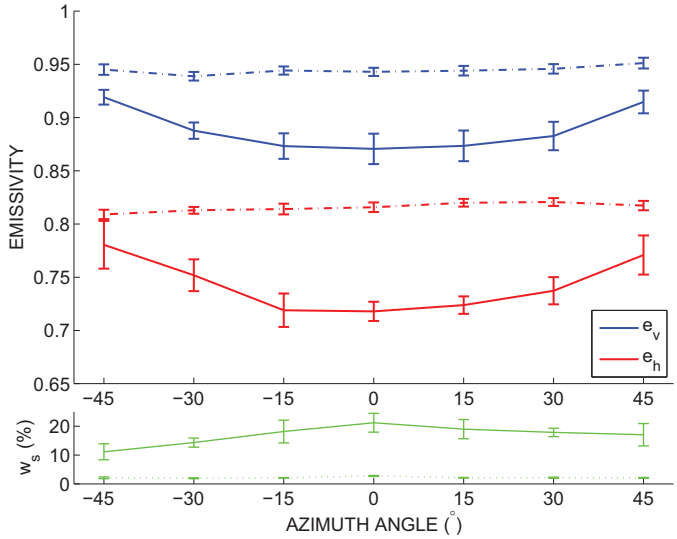

Fig. 7.11: Mean value and standard deviation of the emissivity as a function of the azimuth angle, for all incidence angles. Blue and red indicate vertical and horizontal polarisations, respectively. Values for two representative days of experiment have been represented: DoY 185 (solid line), and 181 (dash-dotted line). The averaged soil moisture at each observation position has been included (green lines)

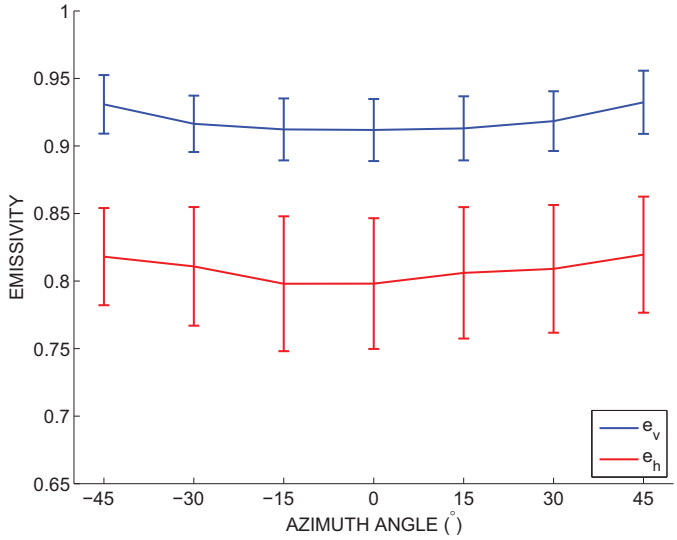

Fig. 7.12: Mean value and standard deviation of the emissivity as a function of the azimuth angle angle, for all incidence angles and days of experiment. Blue and red indicate vertical and horizontal polarisations, respectively.

7.3.4 Variation of the emissivity with ground-truth soil moisture

The dependence of the vineyard emissivity measurements at vertical (blue circles) and horizontal (red circles) polarisations with respect to ground-truth soil moisture for a single incidence angle and all azimuth angles has been represented in Fig. 7.13 and Fig. 7.14. Although the presence of a vine canopy above the soil, with vines in full maturity and with a VWC of 9 kg/m^2, the measured emission at both polarisations decreases as moisture increases. As has already been commented in the previous sections, H-pol is more sensitive to changes in w_s than V-pol. Scatter in the data is due to different radiometer observation positions.

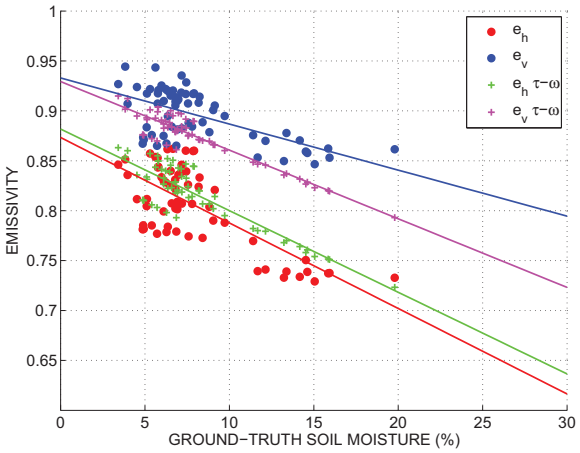

(a) $\theta = 25°$

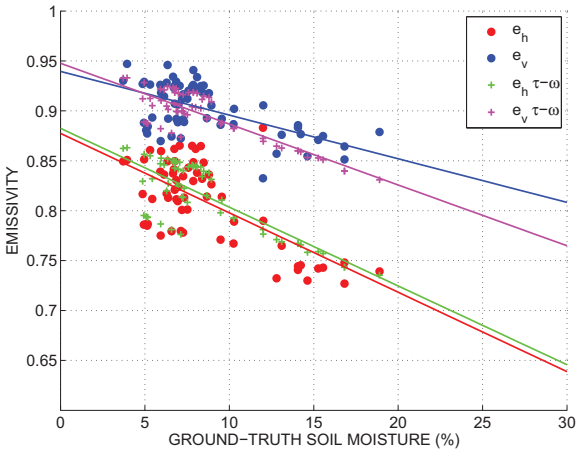

(b) $\theta = 30°$

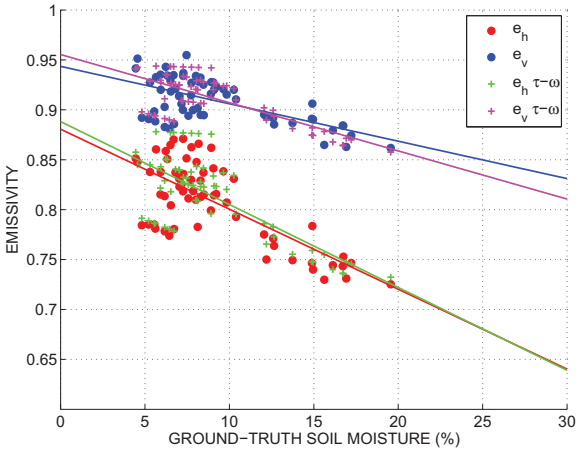

(c) $\theta = 35°$

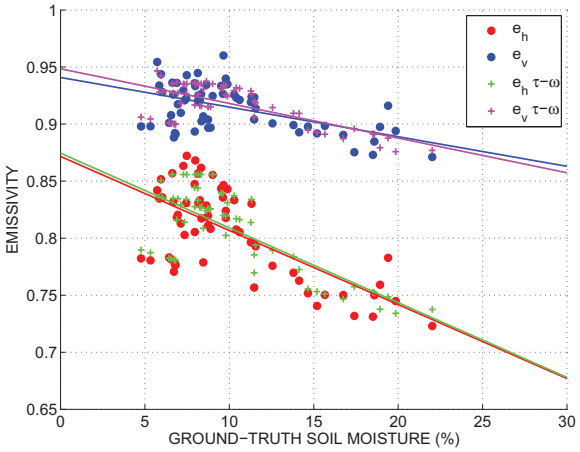

(d) $\theta = 40°$

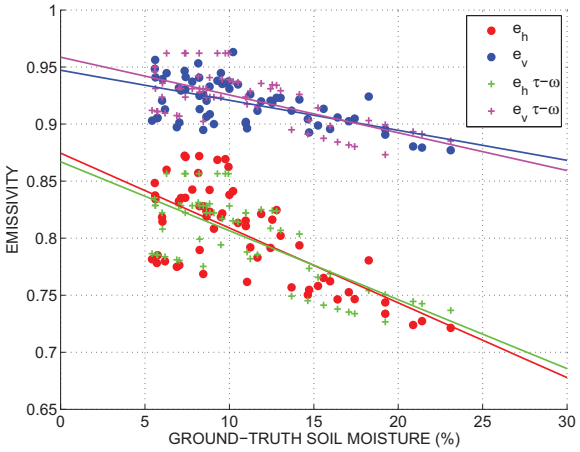

(e) $\theta = 45°$

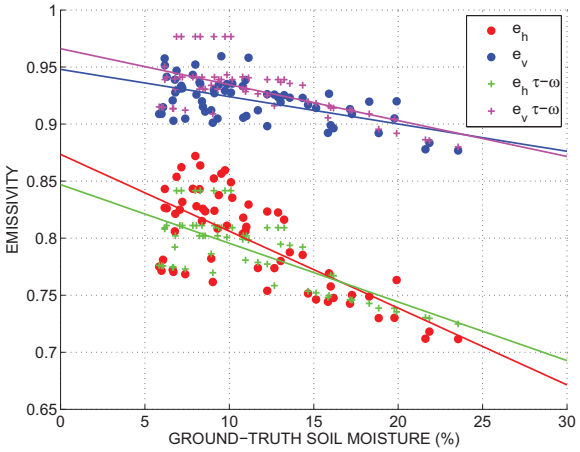

(f) $\theta = 50°$

Fig. 7.13: Emissivity for vertical and horizontal polarisations vs. measured soil moisture. Comparison between emissivity obtained with LAURA measurements (circles) and the one computed with the $\tau-\omega$ model (crosses). Each plot corresponds to a different incidence angle: (a) $\theta = 25°$, (b) $\theta = 30°$, (c) $\theta = 35°$, (d) $\theta = 40°$, (e) $\theta = 45°$, and (f) $\theta = 50°$. Values for the seven azimuth angles (-45° to 45°) are represented.

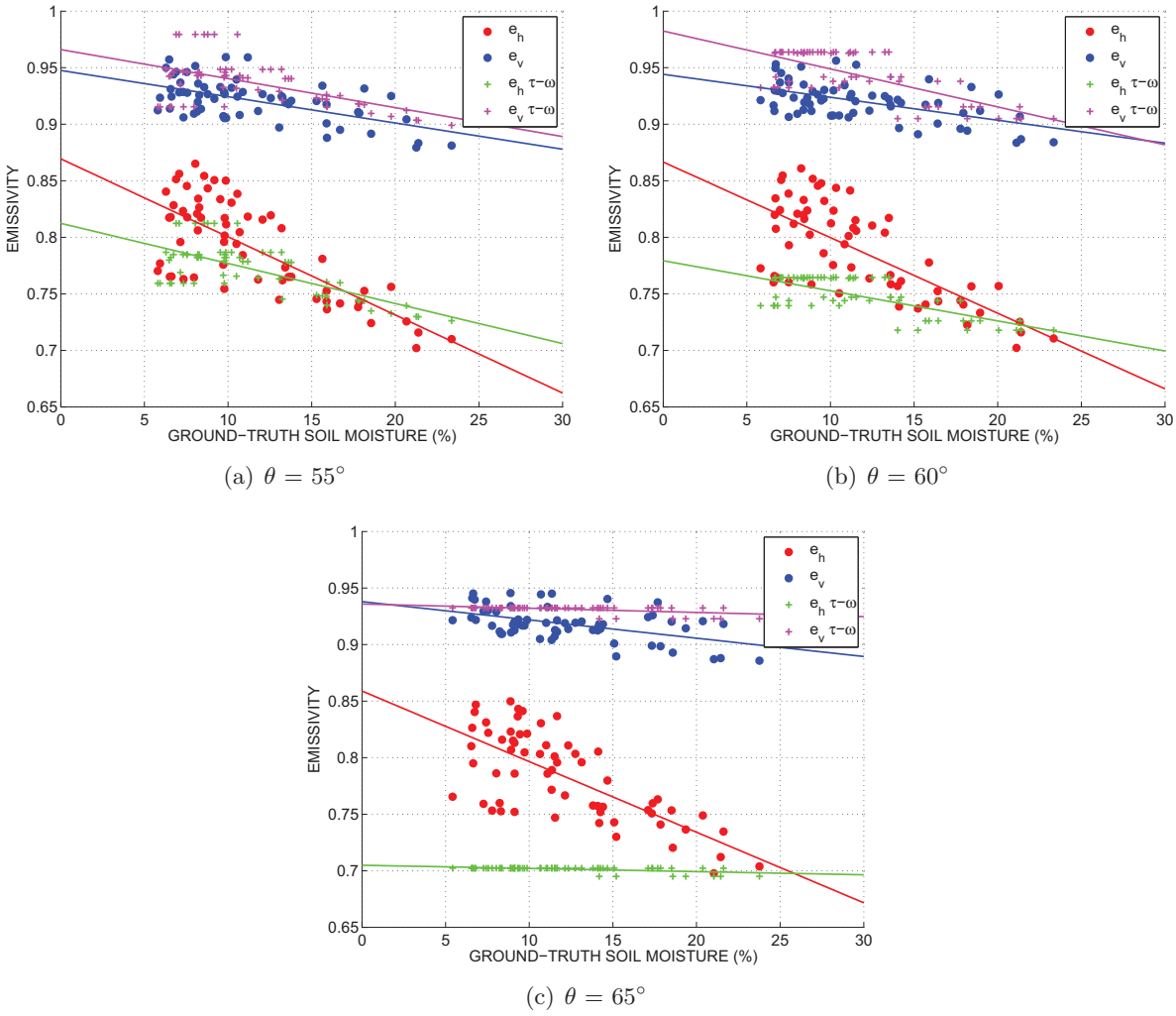

(a) $\theta = 55°$ (b) $\theta = 60°$

(c) $\theta = 65°$

Fig. 7.14: Emissivity for vertical and horizontal polarisations vs. measured soil moisture. Comparison between emissivity obtained with LAURA measurements (circles) and the one computed with the $\tau-\omega$ model (crosses). Each plot corresponds to a different incidence angle: (a) $\theta = 55°$, (b) $\theta = 60°$, and (c) $\theta = 65°$. Values for the seven azimuth angles (-45° to 45°) are represented.

7.3.5 Evolution of the polarisation index

The polarisation index (PI) is defined as two times the ratio between the difference and the sum of the measured brightness temperatures at vertical and horizontal polarisation, T_{Bv} and T_{Bh}:

$$\mathrm{PI} = 2\frac{T_{Bv} - T_{Bh}}{T_{Bv} + T_{Bh}} \tag{7.1}$$

Figure 7.15 shows the dependence of the polarisation index on the ground-truth soil moisture during the REFLEX 2003 experiment. The PI for all observation positions has been represented. Blue circles indicate the PI estimated from measurements, while green $*$ indicate the linear fit using soil moisture and incidence angle, and red solid line indicates the linear fit considering

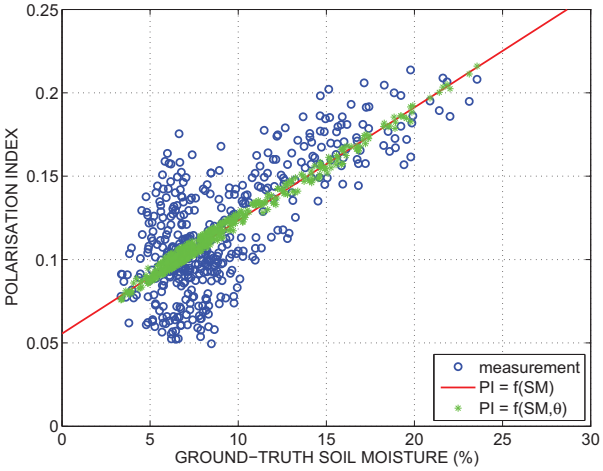

Fig. 7.15: Dependence of the polarisation index on the ground-truth soil moisture during the REFLEX 2003 experiment. The PI for all observation positions has been represented. Blue circles indicate experimental results, green $*$ stand for the fitting using soil moisture and incidence angle, and the red solid line is the linear fitting considering only soil moisture as input.

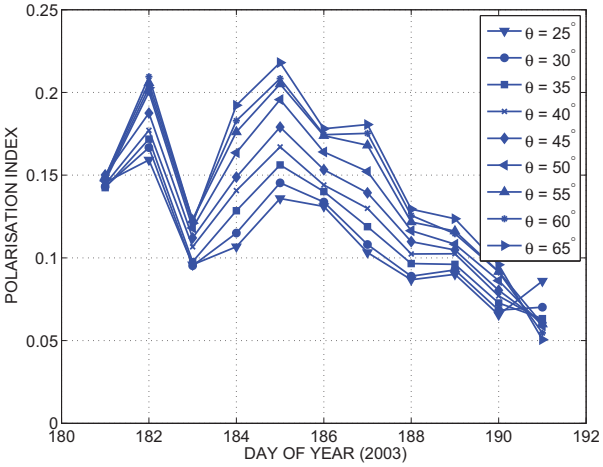

Fig. 7.16: Dependence of the polarisation index on the incidence angle. The mean values for all azimuth angles and days of year have been represented.

only soil moisture as input. The best fit equations for these two cases are the following:

$$\mathrm{PI} = \begin{cases} 0.007 \cdot \mathrm{SM}(\%) + 0.055, R^2 = 0.56 \\ 0.045 + 0.0065 \cdot \mathrm{SM}(\%) + 0.0004\theta(^\circ), R^2 = 0.55 \end{cases} . \tag{7.2}$$

The correlation coefficient R^2 is rather low in both cases, and the introduction of the incidence angle in the regression does not improve it, which suggest that other parameters other than w_s are affecting the PI.

On the other hand, the averaged PI for all azimuth angles as a function of the day of year and incidence angle is presented in Fig. 7.16. Paloscia & Pampaloni [1988] noted that the PI at C-band is related to the LAI and thus to plants development, which would be of interest to monitor changes in the vegetation. In the case of SMOS REFLEX 2003, where measurements were acquired at L-band, an increment of PI with incidence angle is appreciated. Furthermore,

this increase in PI is higher when the soil is irrigated and lower when the water has been absorbed by the plant and filtered to deeper soil layers. An increment of the vegetation water content produces a decrement of the polarisation index. Due to the presence of plants above the soil, the PI does not only depend on w_s and incidence angle, but also on the opacity and the albedo.

7.3.6 Soil moisture estimation from radiometric measurements

The emissivity of bare soils depends on soil surface roughness, soil temperature, and soil water content. If a vegetation layer is present above a soil, it will attenuate the soil emission and add its own contribution to the measured radiometric signal. The simple radiative transfer model $\tau - \omega$ has been used as forward model in the retrieval algorithms from SMOS REFLEX 2003 radiometric data. The contribution of vegetation is modelled by two parameters: the optical depth or opacity τ, and the single scattering albedo ω. More information on this model is given in Chapter 3.

The retrieval of w_s from measurements without constraints in any of the five parameters involved in the $\tau - \omega$ model led to erroneous results with no physical sense. Thus, the retrieval of w_s was approached in two steps:

- First, the vegetation parameters would be retrieved from measurements considering as known the soil temperature, roughness, and moisture,
- then, the estimated τ and ω would be used as a priory values in a constrained cost function in which the only non-constrained parameter would be w_s.

This approach is explained in the next sections.

Retrieval of vegetation albedo and opacity

Since the percentage of radiometer field of view occupied by vines was mainly dependent on the incidence angle, a value for both albedo and opacity was estimated from measurement for each incidence angle and day of experiment using a 2-parameters inverse model based on the least-square minimisation of the following cost function:

$$F(\theta, \mathrm{DoY}) = \sum_{i=1}^{7} \left[(T^*_{Bv} - T_{Bv})^2 + (T^*_{Bh} - T_{Bh})^2 \right]. \tag{7.3}$$

Subscript i indicates the sum of the error for all azimuth angles, T_{Bv} and T_{Bh} are the measured brightness temperature at vertical and horizontal polarisations, respectively, and T^*_{Bv} and T^*_{Bh} are brightness temperatures simulated using the $\tau - \omega$ forward model. From the five inputs to the model, three (ground-truth w_s, soil temperature, and roughness) have been constrained to the measured value, while τ and ω were let free.

Since some authors suggest that the vegetation parameters are dependent on the crop type and polarisation [Wigneron *et al.*, 2004], various dependencies for τ and ω have been analysed in this study. The best results were obtained when the albedo and the opacity were assumed to be independent on the polarisation, probably because vines do not present either a vertical or

a horizontal predominant structure. Only results from τ and ω estimations independent of the polarisation have been reported here.

Figure 7.17(a) shows the variation of the retrieved albedo with respect to the incidence angle for all azimuth angles. Icons indicate the day of experiment, while the solid line is the mean value of the whole experiment at each incidence angle. The albedo is smaller than 0.15, having its maximum for an incidence angle of 35° and then decreasing as the incidence angle increases. On the other hand, the opacity tends to increase with incidence angle as shown in Fig. 7.17(b), which is in accordance to the higher fraction of area covered by vegetation as the incidence angle increases. Figure 7.18 the temporal variation of the retrieved τ and ω, and of the measured soil moisture and the relative humidity have been indicated. Rather high values of relative humidity for a continental climate site were measured from DoY 184 to DoY 189. The opacity seems to increase with the water content in the plant: an opacity increase is appreciated the day of the first irrigation, which is more evident the day after, because of the water absorption by the plant. The same trend is observed after the second irrigation, DoY 185, which also translates to an increment of the opacity up to the same values as for the first case. No explanation has been found for the anomalies in DoY 190 and DoY 191, which predict and increase in opacity although no further irrigation nor rain had moistened plants and soil.

To assess how good the values in Fig. 7.17 fit the emissivity measurements, these have been compared to the emissivity estimated using as inputs to the $\tau - \omega$ model the ground-truth soil characteristics and the retrieved vegetation parameters. Results for $\theta \leq 50°$ have been represented as a function of soil moisture in Fig. 7.13, and those for $\theta = \{55° , 60° , 65° \}$ have been represented in Fig. 7.14. Blue (red) icons indicate measurements, while magenta (green) icons indicate estimations from the $\tau - \omega$ model at V- (H-) polarisation, respectively. Linear regressions for the two sets of values are also compared. Good agreement between measured and computed values is appreciated for incidence angles below 55° . For $\theta = 55°$ the algorithm does not always converge and at 60° and 65° , the convergence is rarely achieved, pointing out a problem in the emissivity model function for large incidence angles. This problem is clearly seen in Fig. 7.14 since estimations are far from measurements, specially at horizontal polarisation. This discrepancy can be due to the fact that as the incidence angle increases, the signal from the soil suffers from more attenuation and scattering in the canopy. The $\tau - \omega$ model is a valid and simple forward model to be used in optimal estimation approaches, but improvements are required if it is to be used at high incidence angles.

Estimation of soil moisture from radiometric measurements

In order to retrieve the soil water content from the LAURA's measurements, an iterative algorithm, based on the least squares minimisation procedure, was applied. A better performance was found out when the albedo, opacity and soil moisture were simultaneously retrieved, instead of retrieving the soil moisture and setting the other two parameters to the retrieved value. In the iterative algorithm the function to minimise is

$$F(\theta, \mathrm{DoY}) = (T^*_{Bv} - T_{Bv})^2 + (T^*_{Bh} - T_{Bh})^2 + \frac{(\tau - \tau_o)^2}{\sigma^2_\tau} + \frac{(\omega - \omega_o)^2}{\sigma^2_\omega}. \qquad (7.4)$$

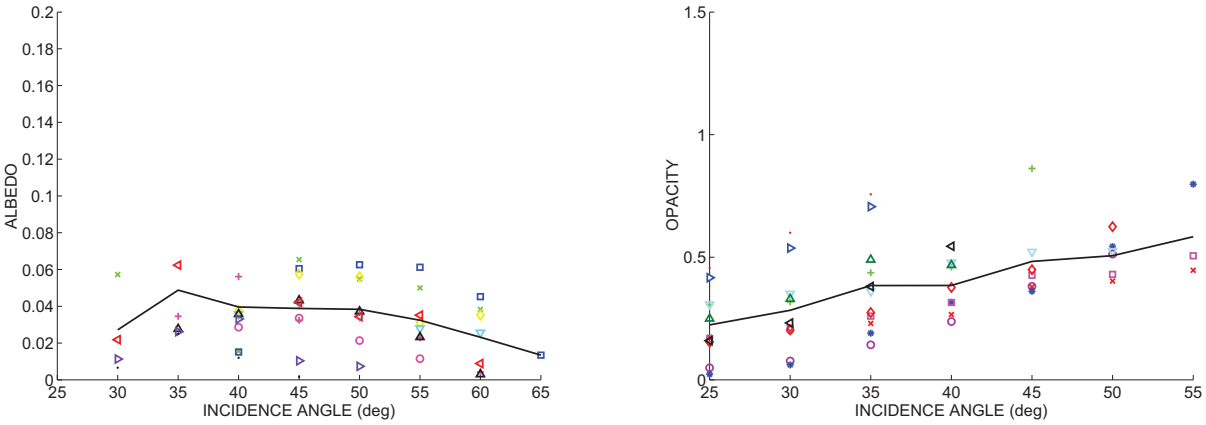

(a) (b)

Fig. 7.17: Dependence of the vegetation albedo (a), and opacity (b) on the incidence angle. Icons represent the value estimated from LAURA measurements for each day of experiment and all azimuth angles. The mean value is represented with a black solid line.

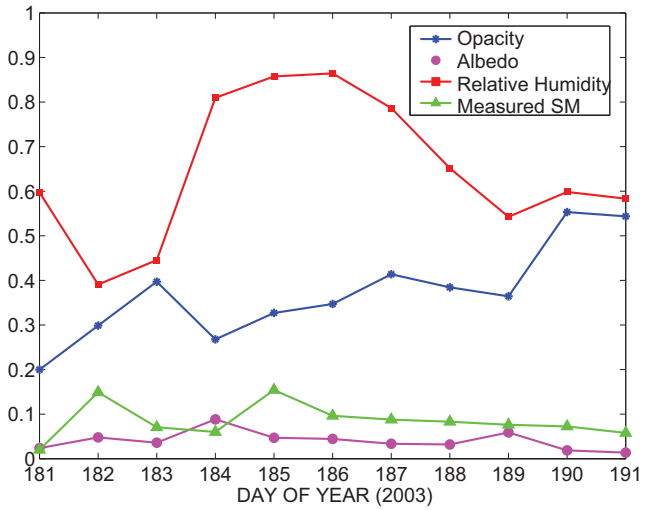

Fig. 7.18: Temporal variation of the measured soil moisture and relative humidity, and of the vegetation opacity and albedo estimated from LAURA measurements. The mean value for all incidence and azimuth angles has been plotted.

It includes two terms, one for the opacity and another one for the albedo. The first guesses for the opacity and the albedo (τ_o and ω_o) are the estimated values obtained in the iterative algorithm described in the previous section.

The algorithm converges for incidence angles equal to or smaller than 50° , only for some day of experiments at $\theta = 55°$, and rarely for $\theta = 60°$ or 65° due to the increasing discrepancy between the model and the data as the incidence angle increases, see Fig. 7.13 and Fig. 7.14. When the incidence angle increases, the canopy influence becomes more important (higher attenuation on the signal and higher scattering contribution), so a higher order approximation for the direct model becomes necessary. In Fig. 7.19, the retrieved and the measured w_s are

compared and a good agreement is appreciated: the slope of the computed linear regression is 0.9 (close to 1) and the ordinate at the origin is 0.29. The error between estimations and measurements is about 2.3%, which is smaller than the 4% accuracy required for SMOS.

7.3.7 Comparison between measurements and simulations using the EMISVEG tool

EMISVEG is a numerical model developed at the UPC to efficiently compute the complete modified Stokes emission vector (see Section 2.2.5) of vegetation-covered soils at low microwave frequencies over a wide range of incidence angles [Martínez-Vázquez *et al.*, 2002, Ledesma, 2003]. A brief description of the EMISVEG tool is given in Appendix A. The SMOS REFLEX 2003 site was simulated using the EMISVEG tool and results were compared to measured data. This study has not been performed by the author of this Ph.D. Thesis but results have been included here for completeness.

Figure 7.20(a) presents the estimated single-scattering albedo of a vineyard and of the individual contributions of its components (fruits, stems, leaves and branches). The predicted albedo is very similar at both polarisations, and is mostly due to the contribution from branches. Predictions match pretty well the albedo retrieved from measurements in the previous section, although retrievals slightly decrease at higher incidence angle, whereas simulations are almost constant. On the other hand, Fig. 7.20(b) represents the total transmissivity of the vegetation and the individual contributions of the different components of plants. Predictions at nadir agree well with the value retrieved from measurements, but at incidence angles larger than 55° the model seems to underestimate it. However, as pointed out in the previous section, the matching of the radiometric data to the $\tau-\omega$ model was only possible for incidence angles lower than 50° , in some cases at 55° , and never above 60° . Therefore, the inter-comparison of the predicted values has to be restricted to incidence angles lower than 50° . Figure 7.20(b) shows that the main contribution to the extinction coefficient comes from branches and leaves at H-pol, and from branches at V-pol. Vegetation attenuation was found to be almost independent on the VWC. Attenuation was dominated by the water content in the branches, while grapes exhibit a scattering behaviour [Ferrazzoli *et al.*, 2002].

Figure 7.21(a) shows the measured emissivity for an average soil moisture of 9%. Solid lines represent the mean value for all azimuth angles, whereas bars indicate the associated standard deviation of measurements. Figure 7.21(b) shows the bare soil emission computed using the $\tau-\omega$ model (dash-dot line) and the radiative transfer equation for soil and vines (solid line). The agreement is quite good at V-pol. At H-pol, however, the model is not able to reproduce the weak dependence of the measured emissivity with the incidence angle. This fact reinforces the need of more complex and accurate models for densely vegetated soils.

Finally, Fig. 7.22 represents the third parameter of the Stokes modified emission vector U as a function of the azimuth angle. Solid lines correspond to SMOS REFLEX 2003 measurements, while dashed lines are simulated values using EMISVEG scaled by a factor equal to 1/30. This empirical factor corresponds to the inverse of the approximate number of grapes per bunch, as if the whole bunch was a single scatterer and not an ensemble of smaller scatterers. The third element of the Stokes vector seems to be dominated by the scattering in the bunches of grapes,

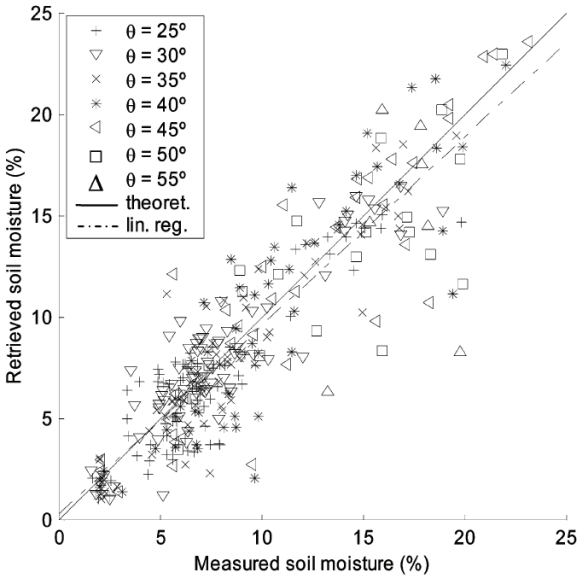

Fig. 7.19: Ground truth soil moisture vs. estimates from radiometric measurements.

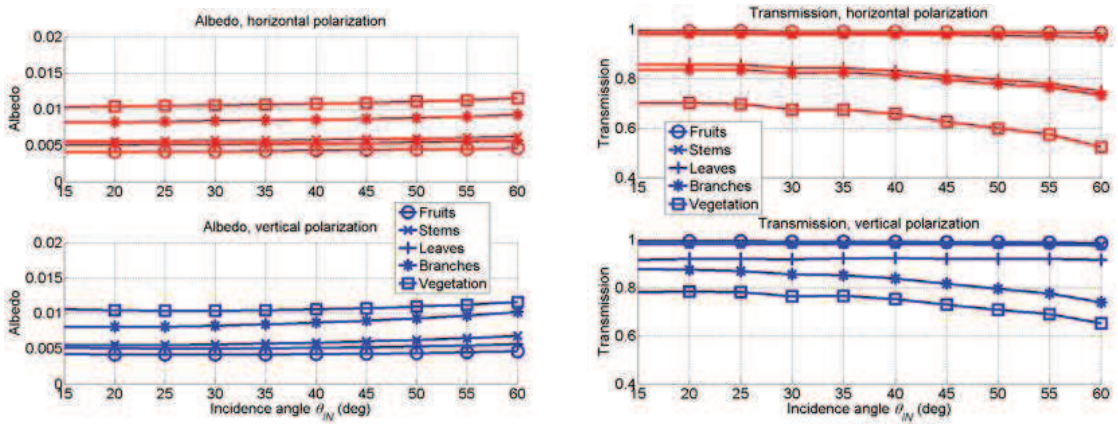

(a) (b)

Fig. 7.20: Computed albedo and transmissivity for the different components of the vegetation layer (fruits, stems, leaves and branches) and total value (vegetation). From Martínez-Vázquez *et al.* [2009]

and a clustering factor is needed to account for the random distribution of grapes used in the model. Fluctuations of U are due to the plants pattern in the vineyard, and both data and simulations show that U is not very sensitive to soil moisture content. The magnitude of the measured and simulated fourth Stokes parameter (not shown) is negligible, since there were no elements that induce a significant phase shift between the electric fields at H- and V-pol.

7.4 SMOS REFLEX 2006: temporal variation of vines emission and rock fraction effects

The SMOS Reference Pixel L-band Experiment (SMOS REFLEX) 2006 was planned to monitor changes in the L-band emission of vineyards during part of their phenological cycle.

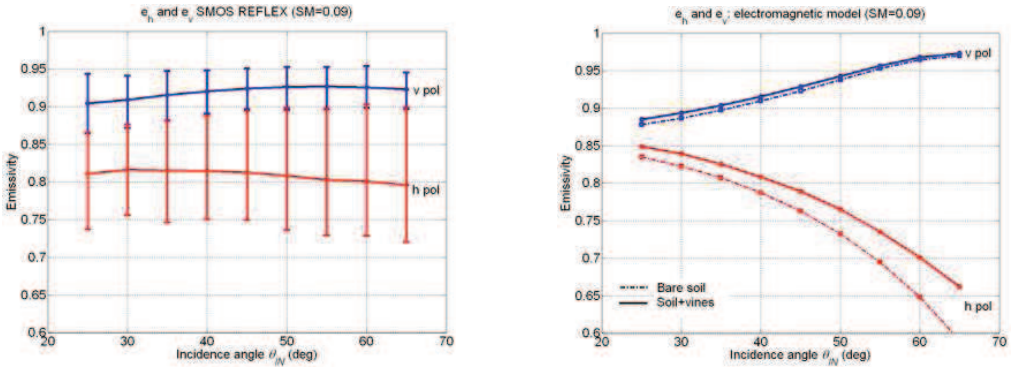

(a) (b)

Fig. 7.21: Emissivity at vertical and horizontal polarisations as a function of the incidence angle. (a) SMOS REFLEX 2003 measurements. Mean value (solid line) and standard deviation due to different azimuth angles. (b) Bare soil emission model (dash-dot line) and radiative transfer model computed from equations in Appendix A for soil and vines (solid line). From Martínez-Vázquez *et al.* [2009]

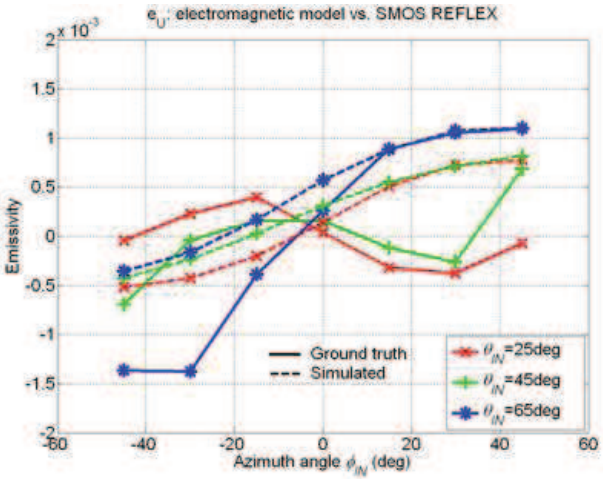

Fig. 7.22: Third parameter of the Stokes emission vector (U) as a function of the azimuth angle and for three incidence angle (25° , 45° and 65°). Experimental data (solid lines) and radiative transfer model computed from equations in Appendix A (dashed lines) scaled by a 1/30 factor to account for near field effects between grapes. The fourth parameter (V) was equal to zero. From Martínez-Vázquez *et al.* [2009]

The experiment was carried out from July 3 to November 10, 2006, which correspond to DoY 184 to 314. The experiment site was a vineyard at the Valencia Anchor Station, Spain (VAS, 39.6° N lat, 1.25° W long, 780 m altitude), located close to a wine cellar so that power for the instrumentation was available all the time and instrumentation could be left unattended. Figure 7.23 shows a picture of the site the first and last day of experiment. The site had a sandy clay loam soil with a 63% sand and 22% clay in volume. Rocks were kept in half the vineyard (from 40% to 80% of surface rock fraction, Fig. 7.23(c)) and were partially removed in the other half (from 6% to 30% of surface rock fraction, Fig. 7.23(d)). Since rocks have a low and constant dielectric permittivity, their presence masks the soil dielectric increase due to soil moisture. This leads to an almost constant relationship between the measured emission and ground-truth soil moisture and, thus, to a subestimation of the soil moisture by the retrieval algorithms: i.e. the

soil appears drier to the radiometer than it actually is.

7.4.1 Ground-truth measurements of soil moisture and temperature

The temporal evolution of the atmospheric temperature at 2 m and of the soil temperature at surface level and at 5 cm depth is shown in Fig. 7.24. The site has a continental weather, with warm summers and cold winters. During the first weeks of experiment, in the months of July and August, soil temperature gradients up to 20 °C were measured during a day.

Figure 7.25 represents the ground-truth measurements of soil moisture for the rocks (top) and few rocks (middle) halves of the vineyard. Colours indicate the location of the sensors: under vines (blue), between two vines of a row (red), and between rows of vines (green). The daily precipitation has also been represented in the bottom plot. Periodic increments in w_s correspond to trickle irrigations. A heavy rain event was registered in the area during DoY 251, and other rain events occurred during autumn, increasing the w_s significantly since, as the vineyard was not irrigated by saturation, the soil between vines was generally dry.

7.4.2 Variation of the vineyard emission with time

Diurnal variation

Figure 7.26 shows the diurnal emissivity of the vineyard for an incidence angle of 50° and six days of experiment. Figures 7.26(a)–7.26(c) correspond to measurements before harvest while Fig. 7.26(d)–7.26(f) correspond to measurements after harvest. Colours indicate whether measurements are from the rocks (green) or from the few-rocks side of the vineyard (magenta), icons indicate the polarisation (dots for V-pol and asterisks for H-pol), and solid lines are the mean value of the daily emissivity. The mean soil moisture in the 0–5 cm layer acquired by the sensors installed in the bare soil areas (between rows of vines) is also indicated. The range of emissivity and the difference between the p-polarised emissivity at both sides of the vineyard referred to plots in Fig. 7.26 are given in Table 7.1. The emissivity oscillates within a day, having its maximum around noon if no rain is registered, and a peak-to-peak variation up to 0.05, ∼15 K in brightness temperature. This highlights the importance of having concurrent SMOS and ground-truth data during the CalVal phase.

Measurements of the emissivity at V-pol at both halves of the site are quite similar to each other during the whole experiment, having a mean value around 0.95 and shifting down when soil moisture increases due to rain. On its part, H-pol is more sensitive to changes in plants and soil moisture. Figure 7.26(b) and Fig. 7.26(c) correspond to measurements of vines in full maturity acquired with four days of difference but in Fig. 7.26(c) the mean value of the emissivity has shifted down, and the ratio between the emissivity range of the rocks side and the few rocks side has decreased from 0.91 to 0.48. Since the vegetation water content remained constant, the emissivity decrease was due to an increase in the soil moisture content, which varies from 8.5% in DoY 248 to 26% in DoY 253 due to rain. Moreover, note that in Fig. 7.26(b) the difference between the H-pol emissivity at both halves of the site was 0.008, while in Fig. 7.26(c) it was of 0.04 due to rocks. The H-pol emissivity in the rocks side of the vineyard is not so sensible to

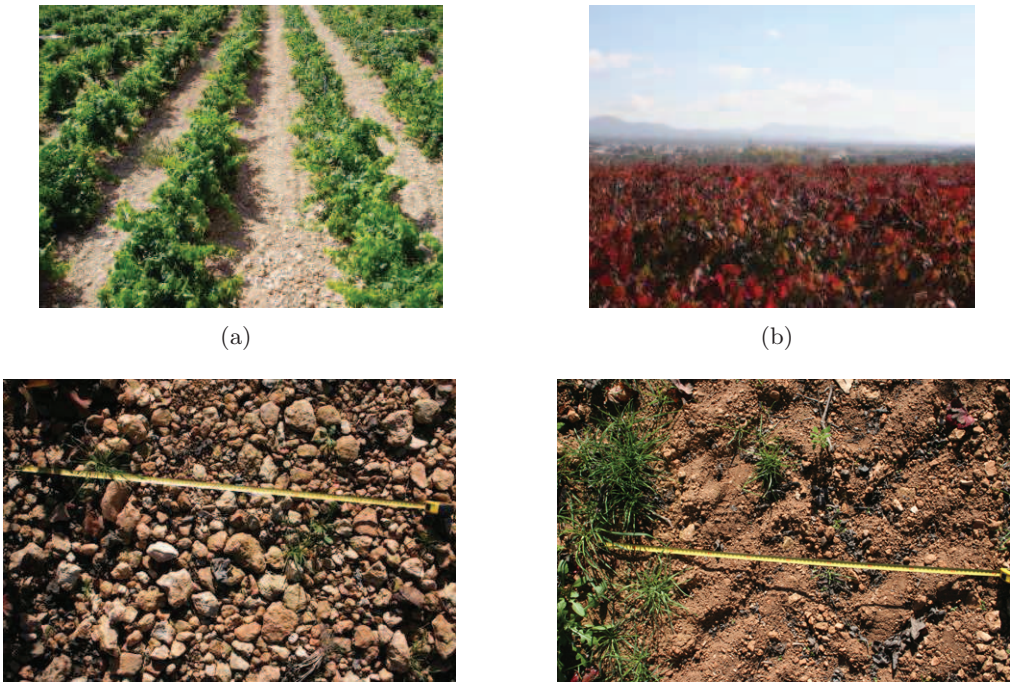

(a) (b)

(c) (d)

Fig. 7.23: Pictures of the experiment site. (a) DoY 184. Rocks cover a large percentage of the soil surface, and vines are fully developed. (b) DoY 310. Vines are withering, the soil surface is wet due to rain, and there is some vegetation litter. (c)-(d) Soil at the rocks side (c) and few rocks side (d) of the vineyard.

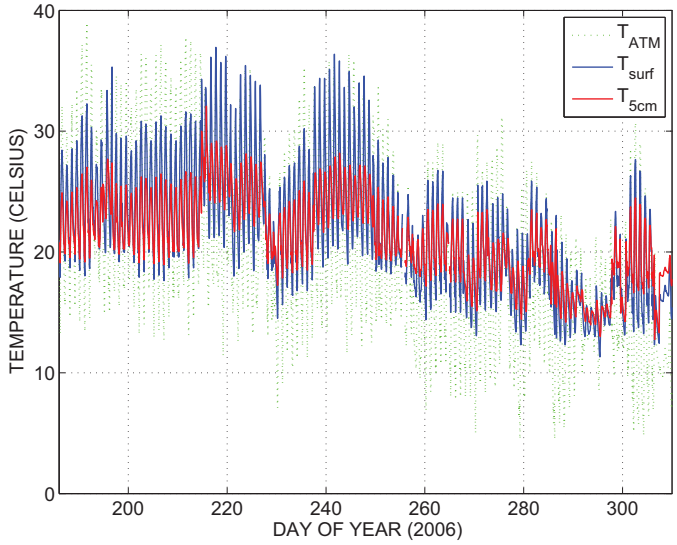

Fig. 7.24: Ground-truth measurements of atmospheric temperature at 2 m, and soil temperature at the surface and at 5 cm depth

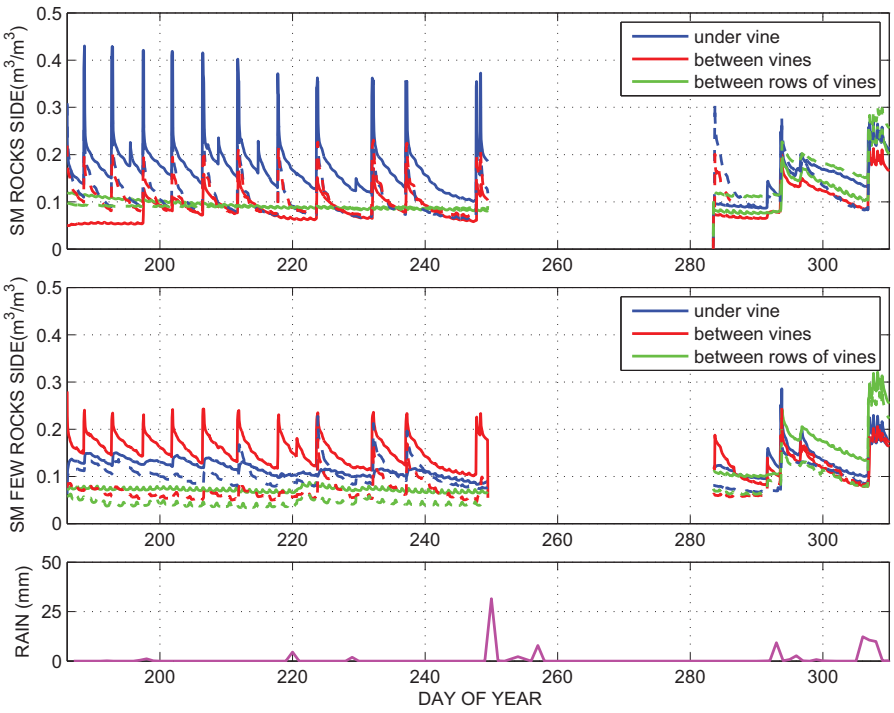

Fig. 7.25: Ground-truth measurements of soil moisture for the rocks (top) and few rocks (middle) halves of the vineyard. Colours indicate the location of the sensors: under vines (blue), between two vines of a row (red), and between rows of vines (green). The daily precipitation is represented in the bottom plot.

changes in the soil moisture since (i) the increase in the rock fraction increases the effective soil roughness, and (ii) the dielectric constant of rocks is lower than that of wet soils. These results are in accordance with remarks in Jackson *et al.* [1992].

Comparing the emissivity before harvest, Fig. 7.26(c), and after harvest, Fig. 7.26(d), there are no significant changes. This fact does not conclude that harvest has had no impact on the emissivity since roughness and soil moisture conditions also changed.

Figure 7.27 represents the measured emissivity at incidence angles of 50° and 65° from DoY 297 to DoY 301. This period corresponds to the site in Fig. 7.23(b), with withering standing vegetation, wild grass and plants litter in some areas, and no fruits in the vines. The contribution from soil to the emissivity increases as plants wither and is larger at θ =50° (Fig. 7.27(a)) than at θ =65° (Fig. 7.27(b)) since the fraction of soil within the FOV is larger for lower incidence angles. The ratio between the rocks and few rocks H-pol emissivity decreases down to 0.37 in Fig. 7.27(a) because of the contrast between the dielectric constant of rocks ($\varepsilon_{\text{rock}} \sim 5$) and wet soil ($\varepsilon_{\text{soil}}(W_c = 18\%) = 9 + 1.7j$) and the increase in the surface roughness. Note that although the soil moisture value is lower in Fig. 7.26(c) than in Fig. 7.27, the mean H-pol emissivity in the few rocks side is 0.05 higher since vegetation in the first DoY 253 is fully developed and, thus, shifts up the emissivity Jackson & Schmugge [1991]. Some studies suggest that the presence of litter increases the emissivity for dry and wet soils Jackson & Schmugge [1991], Saleh *et al.* [2006a]. This point has not been observed in this preliminary work, probably because the litter layer was not thick and was only present in isolated spots.

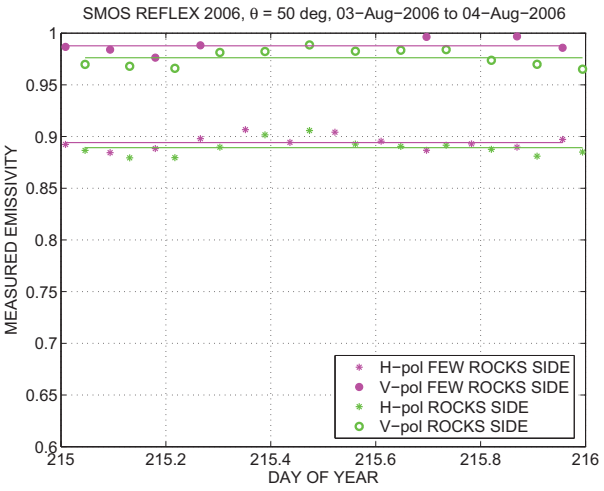

(a) DoY 215, $W_c = 9\%$ (5%), before harvest

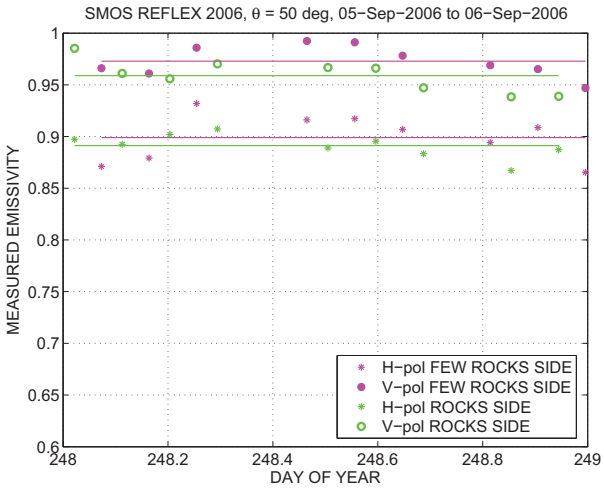

(b) DoY 248, $W_c = 8.5\%$ (5.5%), before harvest

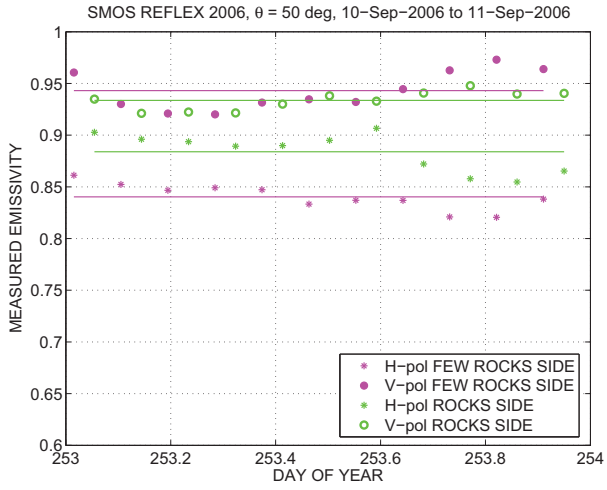

(c) DoY 253, $W_c = 26\%$ (21%), before harvest

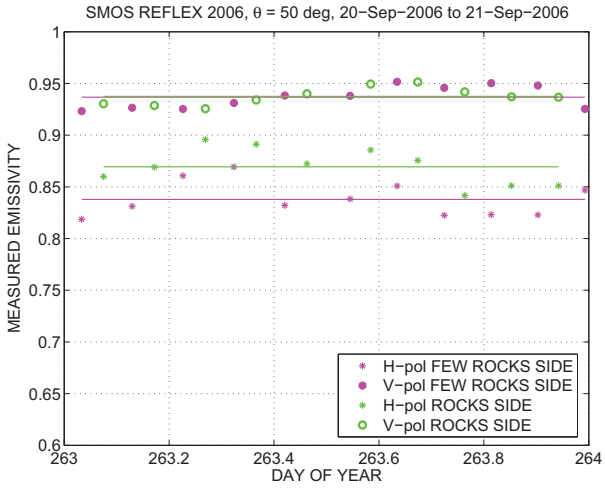

(d) DoY 263, $W_c = 15\%$ (11%), after harvest

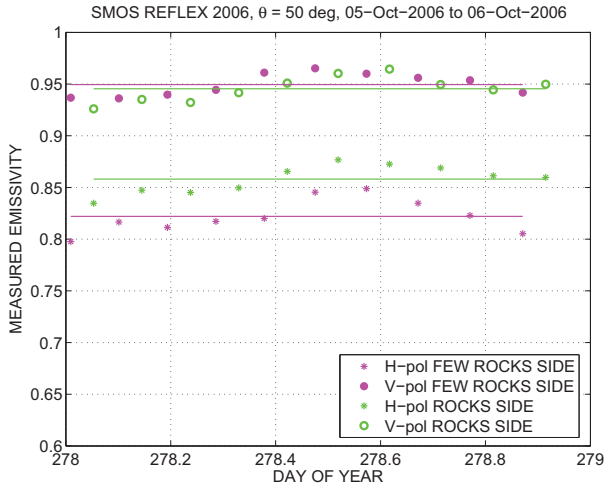

(e) DoY 278, $W_c = 12\%$ (9%), after harvest

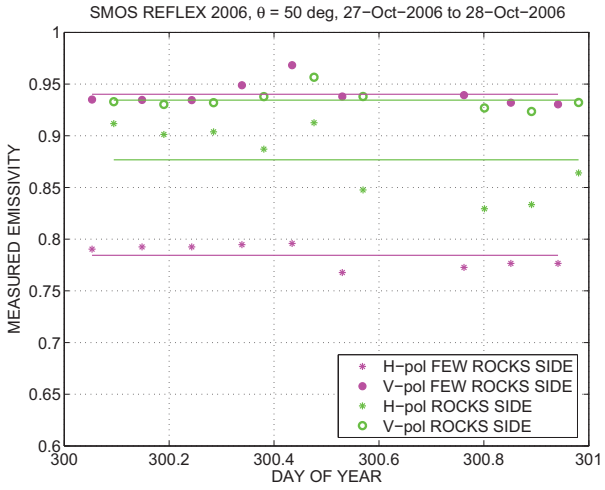

(f) DoY 300, $W_c = 18\%$ (14%), after harvest

Fig. 7.26: Diurnal variation of the emissivity measured at $\theta = 50°$ for six DoY, before harvest (a)-(c) and after harvest (d)-(f). Colours indicate the side of the experiment site: magenta for the few-rocks side, and green for the rocks side. Icons indicate the polarisation: dots for V-pol and asterisks for H-pol. Solid lines are the mean value of the emissivity. The mean value of the soil moisture W_c in the 0-5 cm layer for the rocks (few rocks) side is given.

Table 7.1: Diurnal Variation of the Emissivity for a 50° Incidence Angle and Six Days of Experiment. $|\bar{e}_v - \bar{e}_h|$ is the Mean Value of the Range of Emissivity, $\Delta\bar{e}_p$ is the Difference Between the Mean Value of the p-polarised Emission at both Sides of the Vineyard, and w_s is the Mean Soil Moisture in the 0-5 cm Layer. Values correspond to Plots in Fig. 7.26.

DoY	215	248	253	263	278	300
$\lvert\bar{e}_v - \bar{e}_h\rvert$ rocks	0.087	0.067	0.05	0.07	0.09	0.06
$\lvert\bar{e}_v - \bar{e}_h\rvert$ few rocks	0.094	0.073	0.1	0.1	0.12	0.15
$\Delta\bar{e}_v$	0.01	0.014	0.01	0	0.004	0.005
$\Delta\bar{e}_h$	0.005	0.008	0.04	0.03	0.04	0.1
w_s^{rocks}	9%	8.5%	26%	15%	12%	18%
$w_s^{\text{few rocks}}$	5%	5.5%	21%	11%	9%	14%

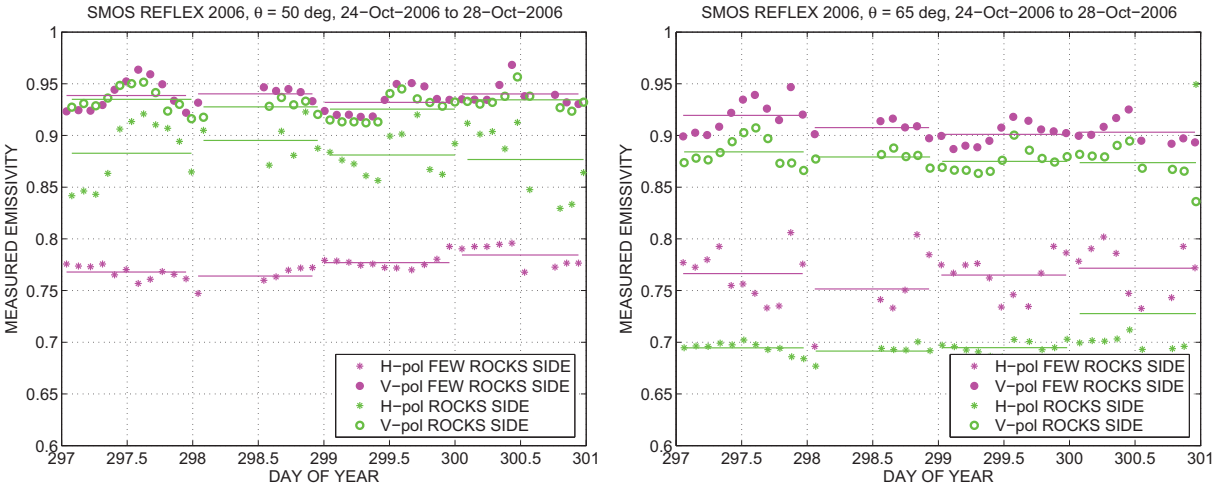

(a) $\theta = 50°$ (b) $\theta = 65°$

Fig. 7.27: Emissivity measured at $\theta = 50°$ and $\theta = 65°$ from DoY 297 to DoY 301. Colours indicate the side of the experiment site: magenta for the few-rocks side, and green for the rocks side. Icons indicate the polarisation: dots for V-pol and asterisks for H-pol. Solid lines are the mean value of the diurnal emissivity.

Time series

Figure 7.28 represents the temporal variation of the measured vineyard emission at the few rocks side for different incidence angles, for vertical (blue) and horizontal (red) polarisations. Ground-truth measurements of daily precipitation in litre(green line) and soil moisture in m^3/m^3 (blue lines) are also represented. The same plots but for the rocks half of the vineyard are shown in Fig. 7.29.

Measurements of the emissivity at V-pol at both halves of the site are quite similar to each other during the whole experiment, having a mean value around 0.95. On the other hand, measurements at H-pol show a different trend before and after harvest, which was done around

DoY 260. Before harvest, H-pol acquisitions are quite similar at both halves of the experiment site (~ 0.87) since the soil was dry (5% to 8% moisture content) and then the dielectric constants of soil and rocks were similar. After harvest, frequent precipitation events were registered at the experiment site as can be seen in Fig. 7.25. This fact, concurrently with vines withering, which increases the soil fraction on the radiometer field-of-view, highlights the impact of rocks: the increase in the dielectric constant of soil, which should lead to a decrease in the H-pol emission, is not so evident in the rocks side of the vine. The mean value of the emission at H-pol is 0.77 in the few-rocks side and 0.85 at the rocks side during the last days of experiment for a soil moisture of 26%. These behaviour of the emission is in accordance with remarks in Jackson *et al.* [1992].

7.4.3 Variation of the emissivity with ground-truth soil moisture

The dependence of the vineyard emission on the measured soil moisture at the few rocks side for different incidence angles is shown in Fig. 7.30, while Fig. 7.31 shows the same for the rocks half of the vineyard. The regression line and R^2 estimator have been included in the plots.

Since the V-pol emission range is small during the experiment, the trend of the emission as a function of ground-truth soil moisture is almost constant at both halves of the site. However, the regression line of the H-pol measurements has a different behaviour depending on the vineyard side: while at the rocks side the radiometric measurements do not sense changes on the soil moisture because of the presence of rocks (low R^2), the few-rocks side H-pol emission decreases as soil moisture increases, which is in accordance to theory due to the increase in the soil dielectric constant (high R^2). The maximum increment in soil moisture between two acquisitions at the few rocks side was 15% and induced a decrease of $\sim$26 K in the brightness temperature. On the rocks side, however, the maximum increment in soil moisture was 12%, but this only decreased the brightness temperature in $\sim$5 K. This fact will lead to a underestimation of the soil moisture content by the retrieval algorithms.

7.5 Conclusions

The SMOS REFLEX 2003/2006 experiments were both carried out at vineyards at the Valencia Anchor Station, a selected area for the SMOS cal/val. In the first experiment, fully developed vines were characterised during two weeks, while controlled irrigations moistened the field. The second experiment was planned to monitor changes in the L-band emission of vineyards during different stages of plants development. The vineyard had one side covered by rocks (from 40% to 80%) and other one with few rocks (less than 30%). In both cases, ground-truth soil moisture and temperature data were registered at different depths below the surface down to 40 cm.

During SMOS REFLEX 2003, plants opacity and albedo have been found to be independent on the polarisation. A simple radiative transfer model has been used as forward model in the iterative algorithm for the retrieval of soil moisture and vegetation parameters, with good results for incidence angles up to 55° . The error of the scattered points of data when the retrieved soil

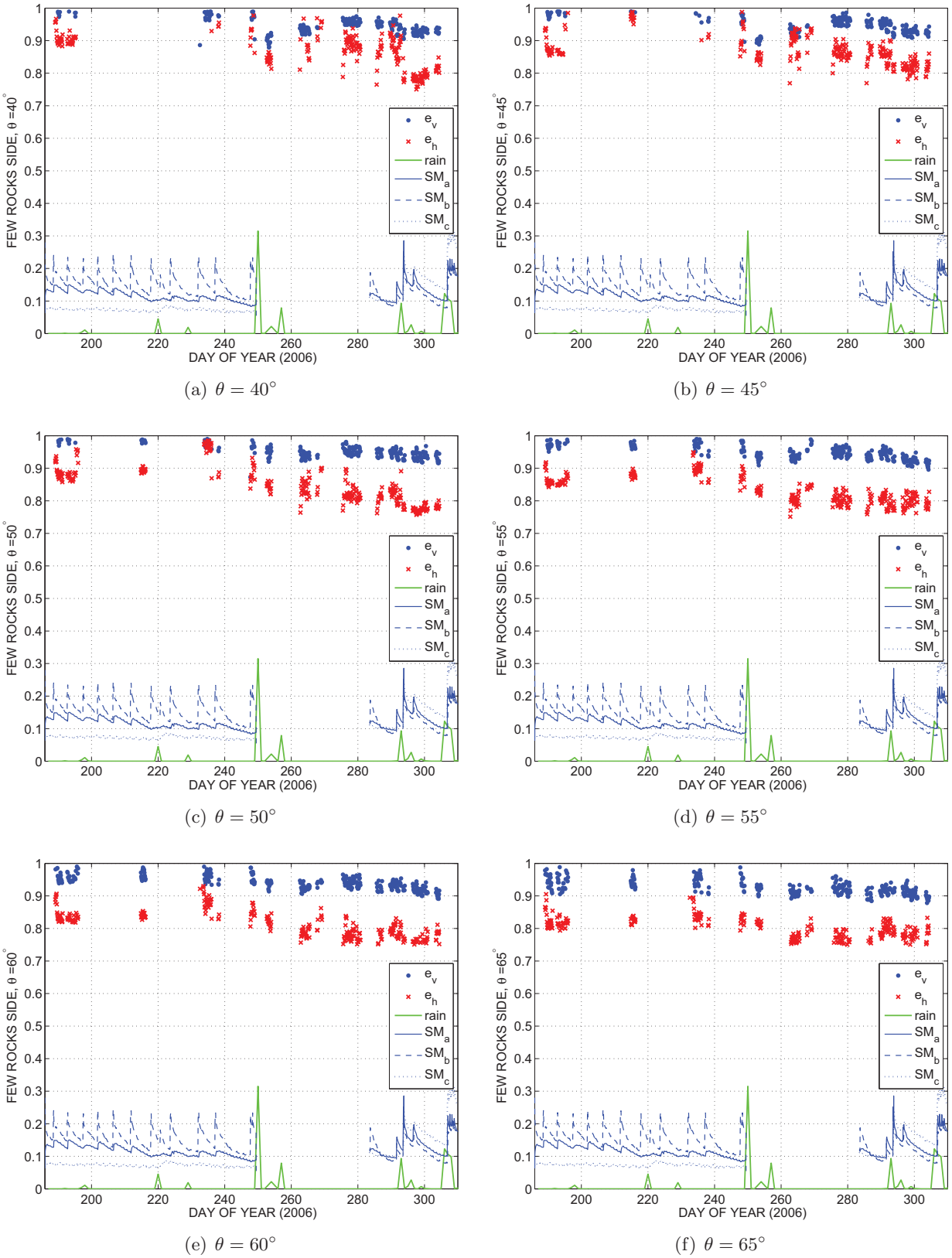

(a) $\theta = 40°$ (b) $\theta = 45°$

(c) $\theta = 50°$ (d) $\theta = 55°$

(e) $\theta = 60°$ (f) $\theta = 65°$

Fig. 7.28: Temporal variation of the measured vineyard emission at the few rocks side for different incidence angles, for vertical (blue) and horizontal (red) polarisations. Ground-truth measurements of daily precipitation in litre(green line) and soil moisture in m^3/m^3 (blue lines) are also represented. Blue line styles indicate the position of the soil moisture sensors: under vines (solid), between two vines in a row (dashed) and between rows of vines (dotted).

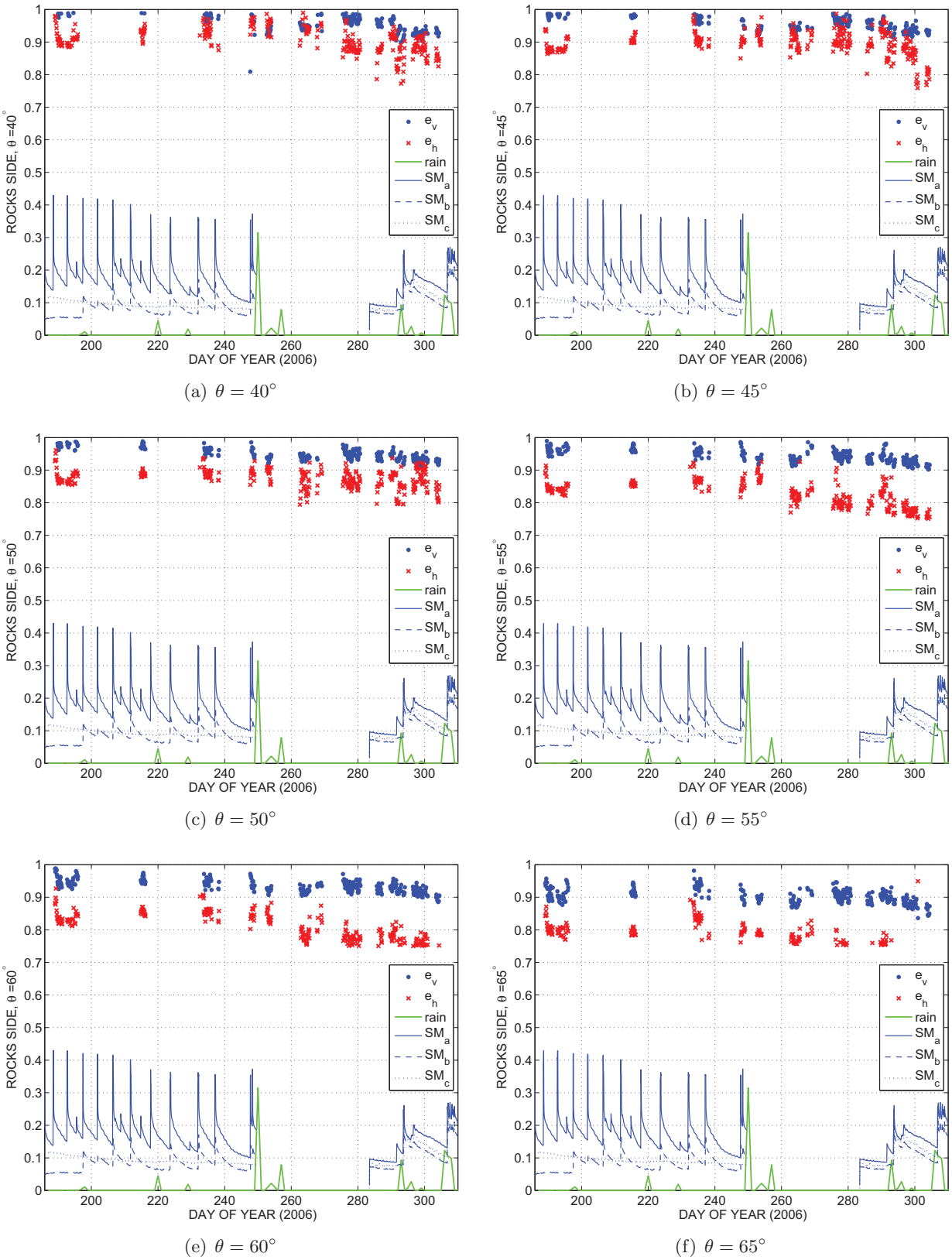

(a) $\theta = 40°$ (b) $\theta = 45°$

(c) $\theta = 50°$ (d) $\theta = 55°$

(e) $\theta = 60°$ (f) $\theta = 65°$

Fig. 7.29: Temporal variation of the measured vineyard emission at the rocks side for different incidence angles, for vertical (blue) and horizontal (red) polarisations. Ground-truth measurements of daily precipitation in litre(green line) and soil moisture in m^3/m^3 (blue lines) are also represented. Blue line styles indicate the position of the soil moisture sensors: under vines (solid), between two vines in a row (dashed) and between rows of vines (dotted).

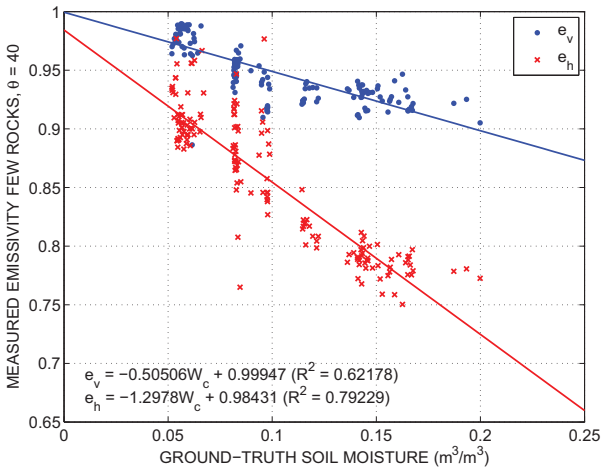

(a) $\theta = 40°$

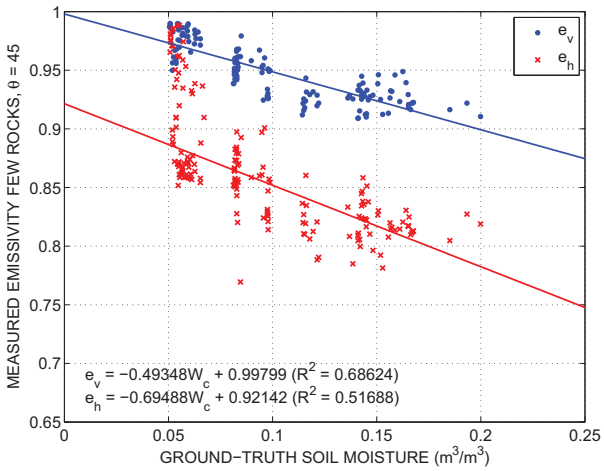

(b) $\theta = 45°$

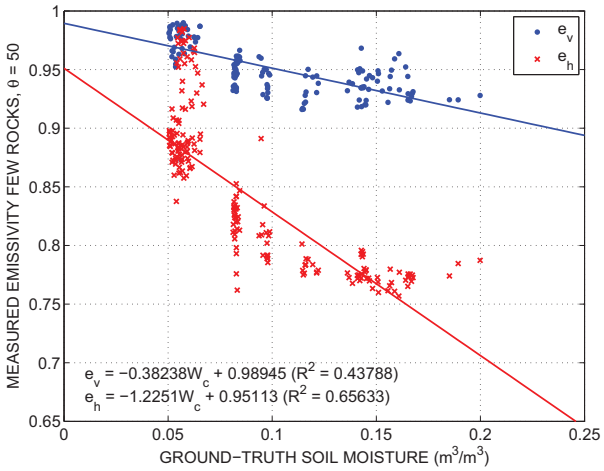

(c) $\theta = 50°$

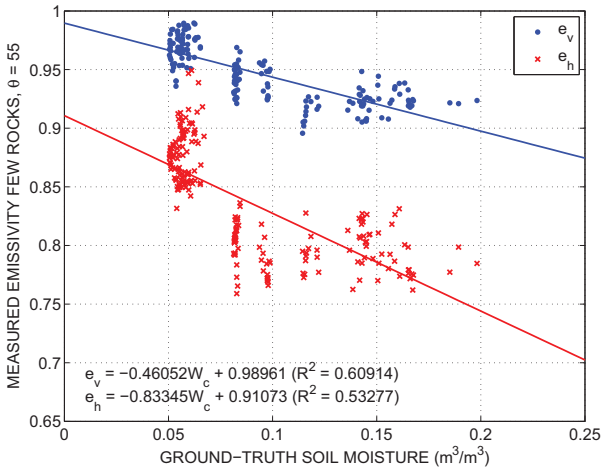

(d) $\theta = 55°$

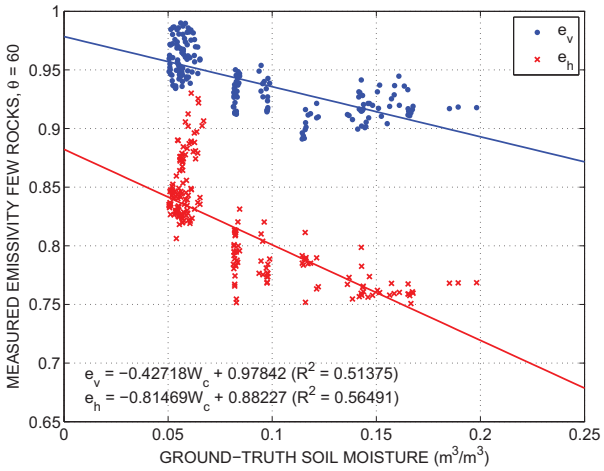

(e) $\theta = 60°$

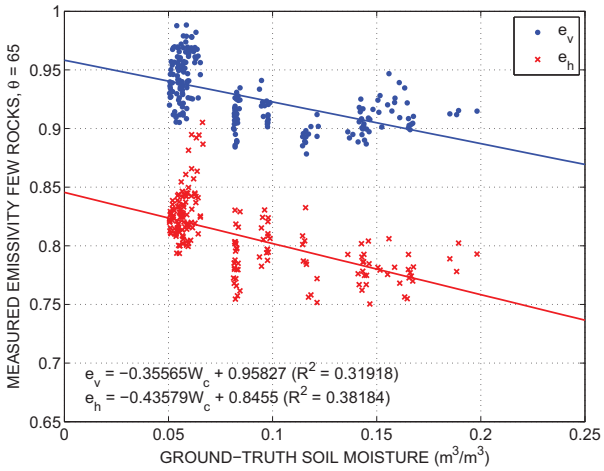

(f) $\theta = 65°$

Fig. 7.30: Dependence of the vineyard emission on the measured soil moisture at the few rocks side for different incidence angles, for vertical (blue) and horizontal (red) polarisations.

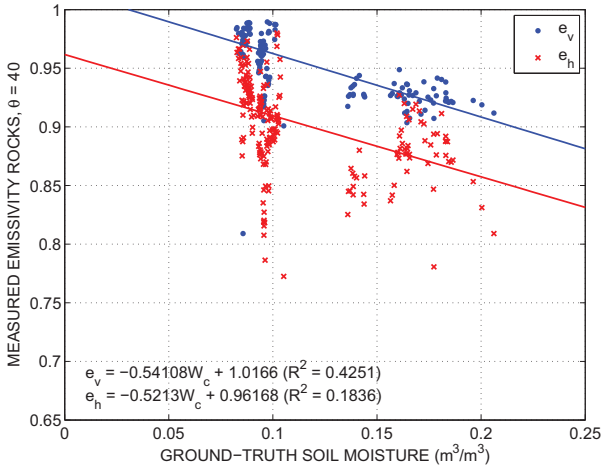

(a) $\theta = 40°$

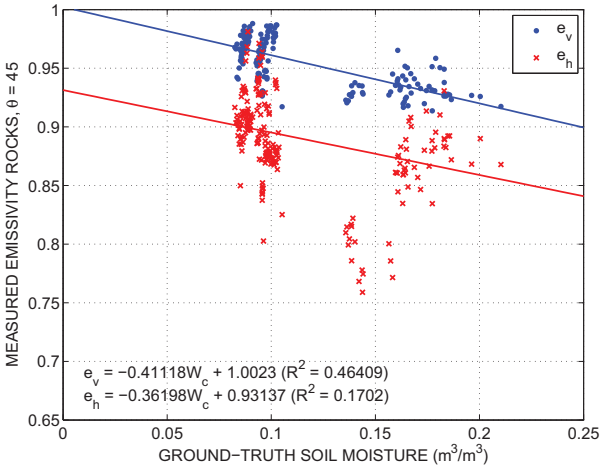

(b) $\theta = 45°$

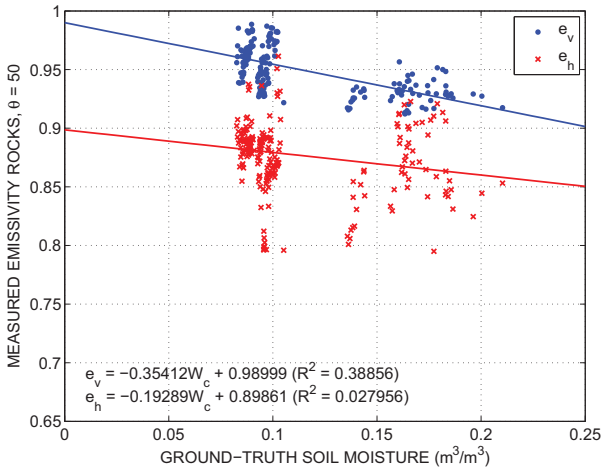

(c) $\theta = 50°$

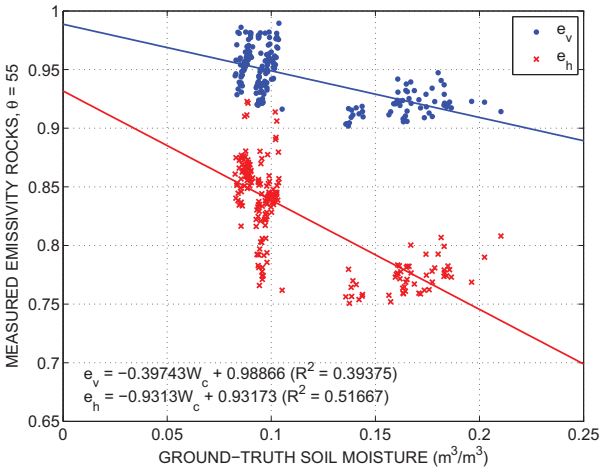

(d) $\theta = 55°$

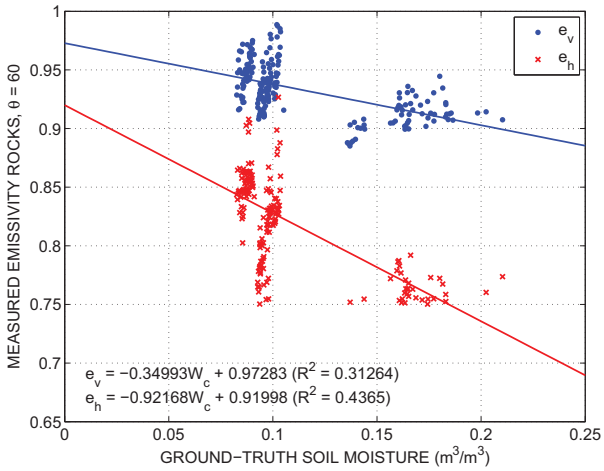

(e) $\theta = 60°$

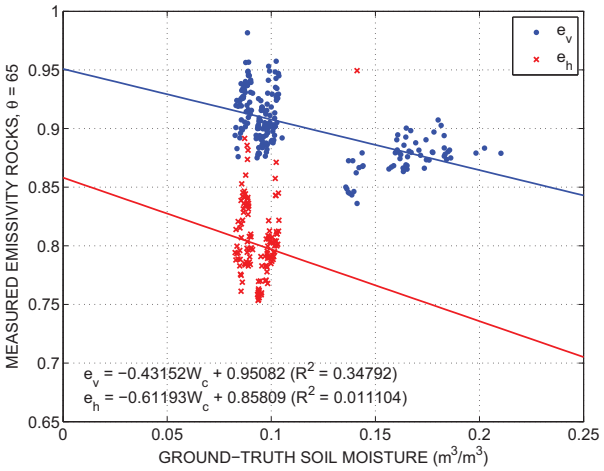

(f) $\theta = 65°$

Fig. 7.31: Dependence of the vineyard emission on the measured soil moisture at the rocks side for different incidence angles, for vertical (blue) and horizontal (red) polarisations.

moisture is plotted versus the measured one was 2.3%, better than the 4% required for SMOS. For incidence angles above 55° the convergence of the algorithm is rarely achieved. This could be due to the larger attenuation and scattering effect of the vegetation layer at large incidence angles, not accurately described by the simple model. Higher order models should be accounted for at these angles.

Data from SMOS REFLEX 2003 was compared to simulations using the EMISVEG tool. The impact of the canopy on the total emissivity was found to be dominated by the branch volume, whereas it was almost insensitive to the vegetation type and geometry. The agreement between measurements and simulations was satisfactory for the emissivity at V-pol, but it did not seem able to model the effects at H-pol, which reinforces the need for more accurate models for very dense canopies.

SMOS REFLEX 2006 measurements show a diurnal oscillation of the emissivity which has its maximum around noon (if no rain), and a peak-to-peak variation up to 0.05. This highlights the importance of having concurrent SMOS and ground-truth data during the cal/val activities. Measurements of the V-pol emissivity at both halves of the site are quite similar to each other during the whole experiment, having a mean value around 0.95 and shifting down when soil moisture increases due to rain. H-pol emissivity is more sensitive to changes in plants and soil moisture than V-pol. The ratio between the emissivity range of the rocks side and the few rocks side is smaller than one, and decreases to 0.37 for wet soils, and low VWC of the standing vegetation. However, H-pol emissivity in the rocks side of the vineyard is not so sensible to changes in the soil moisture since (i) the increase in the rock fraction increases the effective soil roughness, and (ii) the dielectric constant of rocks is lower than that of wet soils. The trend of the emission as a function of ground-truth soil moisture is almost constant at the rocks side, which show how the radiometric measurements do not sense changes on the soil emission because of rocks. This will lead to underestimation of the soil moisture content by the retrieval algorithms.

Although the radiometric behaviour varies from one canopy to the other, at a larger scale such as that of SMOS it is very likely that the vegetation types can be averaged over the footprint and that it is not necessary to account for an accurate distinction between canopies.